

Volumetric Manganese Enhanced Magnetic Resonance Imaging in mice

Sebastian F. Kaltwasser



München 2011

**Volumetric Manganese Enhanced
Magnetic Resonance Imaging
in mice (*mus musculus*)**

Sebastian F. Kaltwasser

Dissertation
der Fakultät für Biologie
der Ludwig-Maximilian-Universität
München

**vorgelegt von
Sebastian F. Kaltwasser**

München, den 03.05.2011

Erstgutachter: PD Dr. Carsten T. Wotjak
Zweitgutachter: Prof. Dr. Christian Leibold
Tag der mündlichen Prüfung: 16. Februar 2012

I would like to dedicate this thesis
to the loving memory of my father,
Tillmann Kaltwasser.

Table of contents

Abstract	VII
Zusammenfassung	XI
Abbreviations	XV
A. Introduction	1
1. The hippocampus	1
1.1. Function of the hippocampus	1
1.2. Hippocampal plasticity and related disorders	6
1.3. Methods to determine hippocampal morphology	13
2. Manganese enhanced magnetic resonance imaging (MEMRI)	16
2.1. Manganese	16
2.1.1. Occurrence in the environment and uses	16
2.1.2. Occurrence in the body	17
2.1.3. Absorption of manganese into the body	18
2.1.4. Manganese deficiency and toxicity	19
2.2. Magnetic resonance imaging (MRI)	21
2.3. Manganese as a contrast agent in MRI	23
3. Mice and animal models examined for hippocampal differences	26
3.1. Cyclin D2	26
3.2. Ibotenic acid	27
3.3. Posttraumatic stress disorder (PTSD)	27
4. Aims of the thesis	30
5. Structure of the thesis	30
6. Working hypothesis	31
6.1. Study 1: Manganese toxicity	31
6.2. Study 2: Validation of volumetric MEMRI (vMEMRI)	31
6.3. Study 3: Application of vMEMRI in a mouse model of PTSD	32

Table of contents

B. Methods	34
B.I. General Methods	34
1. Animals	34
2. Manganese chloride application	35
3. MEMRI	35
3.1. MRI measurements	35
3.2. MRI data processing	36
3.3. Regions of interest	37
3.4. Image presentation	38
4. Ultramicroscopy	39
5. Mouse model of PTSD	40
6. Acoustic Startle Response (ASR)	41
7. Conditioned odor avoidance (CODA) task	42
8. Behavioral scoring in viewing arena	43
9. Endocrine measurements	44
10. Telemetric measurements	44
11. Ibotenic acid	46
11.1. Solution	46
11.2. Surgery	46
12. Water cross-maze	47
12.1. Apparatus	47
12.2. General procedure for training	48
12.3. Learning protocols	49
12.3.1. Spatial learning protocol	49
12.3.2. Response learning protocol	50
12.3.3. Free choice learning protocol	50
12.4. Data presentation	51
13. Data presentation and statistics	51
B.II. Experimental design	53
1. Study 1: Manganese toxicity	53
1.1. Single application of manganese	53
1.2. Comparison of different fractionated application protocols of manganese	53

Table of contents

1.3.	Acute and long-term effects of manganese application on associative and specific hippocampus-dependent learning	56
1.3.1.	Effects of manganese application on associative learning	56
1.3.2.	Effects of manganese application on learning in the water cross-maze	57
2.	Study 2: Validation of vMEMRI	57
2.1.	Methodological validation of vMEMRI	57
2.1.1.	Image contrast of the different fractionated application protocols of manganese	59
2.1.2.	Bias correction	59
2.1.3.	Accuracy of manual determination of hippocampal volume	60
2.1.4.	Comparison of semi-automatic and manual determination of volume	61
2.1.4.1.	Brain volume	61
2.1.4.2.	Hippocampal volume	63
2.2.	Experimental validation of vMEMRI	64
2.2.1.	vMEMRI in cyclin D2 animals	65
2.2.2.	vMEMRI in ibotenic acid lesioned animals	65
3.	Study 3: Application of vMEMRI in a mouse model of PTSD	65
3.1.	Experiment 1: volumetric and behavioral changes after trauma and environmental enrichment (EE)	65
3.2.	Experiment 2: effects of pre- and post-shock EE on PTSD-like symptoms and hippocampal volume loss	66
C.	Results	68
1.	Study 1: Manganese toxicity	68
1.1.	Single application of manganese	68
1.2.	Comparison of different fractionated application protocols of manganese	69
1.2.1.	Visual image contrast of different fractionated application protocols of manganese	69
1.2.2.	Health assessment	70
1.2.3.	Telemetry	72
1.2.4.	Endocrine measurements	73
1.3.	Acute and long-term effects of manganese application on associative and specific hippocampus-dependent learning	75
1.3.1.	Effects of manganese application on associative learning	75
1.3.2.	Effects of manganese application on learning in the water cross-maze	78

Table of contents

2. Study 2: Validation of vMEMRI	80
2.1. Methodological validation of vMEMRI	80
2.1.1. Image contrast of the different fractionated application protocols of manganese	80
2.1.2. Bias correction	84
2.1.3. Accuracy of manual determination of hippocampal volume	88
2.1.4. Comparison of semi-automatic and manual determination of volume	89
2.1.4.1. Brain volume	89
2.1.4.2. Hippocampal volume	89
2.2. Experimental validation of vMEMRI	90
2.2.1. vMEMRI in cyclin D2 animals	90
2.2.2. vMEMRI in ibotenic acid lesioned animals	92
3. Study 3: Application of vMEMRI in a mouse model of PTSD	94
3.1. Experiment 1: volumetric and behavioral changes after trauma and EE	94
3.1.1. Trauma-related changes of PTSD-like symptoms and hippocampal volume	94
3.1.2. Impact of EE on PTSD-like symptoms and hippocampal volume	96
3.1.3. Trauma-related changes in other brain structures	99
3.2. Experiment 2: effects of pre- and post-shock EE on PTSD-like symptoms and hippocampal volume loss	100
D. Discussion	103
1. Study 1: Manganese toxicity	103
2. Study 2: Validation of vMEMRI	108
3. Study 3: Application of vMEMRI in a mouse model of PTSD	112
4. Conclusion and outlook	118
References	125
Appendix	145
Contributions	166
Acknowledgments	168
CV	

Abstract

The present doctoral thesis introduces a method for semi-automatic volumetric analysis of the hippocampus and other distinct brain regions in laboratory mice. The method of volumetric manganese enhanced magnetic resonance imaging (vMEMRI) makes use of the paramagnetic property of the manganese ion, Mn^{2+} , which results in a positive contrast enhancement of specific brain areas on the MR image and enables a more detailed image of brain morphology. The chemical similarity of Mn^{2+} to Calcium leads to an accumulation of Mn^{2+} in excited cells and consequentially an enhanced signal in certain brain regions in an activity dependent manner. However, one major drawback for vMEMRI is the toxicity of Mn^{2+} . Therefore, the aims of the thesis have been:

- (1) Establishment of a MEMRI protocol in mice
- (2) Optimization of a Mn^{2+} application procedure to reduce toxic side effects
- (3) Development of an automatized method to determine hippocampal volume
- (4) Validation of vMEMRI analysis
- (5) Application of volumetric analysis in mouse models of psychopathology

This thesis splits onto 3 studies. Study 1 deals with Mn^{2+} toxicity and introduces an application method that considerably reduces the toxic side effects of Mn^{2+} . Study 2 validates vMEMRI as a method to reliably determine hippocampal volume and explores its utilization it in animals with genetically and chemically modified hippocampi. Study 3 displays the application vMEMRI in a mouse model of a psychiatric disorder.

Study 1 shows that a single application of Mn^{2+} in dosages used in current MEMRI studies leads to considerable toxic side effects measurable with physiological, behavioral

Abstract

and endocrine markers. In contrast, a fractionated application of a low dose of Mn^{2+} is proposed as an alternative to a single injection of a high dose. Repeated application of low dosages of 30 mg/kg Mn^{2+} showed less toxic side effects compared to the application schemes with higher dosages of 60 mg/kg. Additionally, the best vMEMRI signal contrast was seen for an injection protocol of 30 mg/kg 8 times with an inter-injection interval of 24 h (8x30/24 protocol).

The impact of the 8x30/24 application protocol on longitudinal studies was tested by determining whether learning processes are disturbed. Mice were injected with the 8x30/24 protocol 2 weeks prior to receiving a single footshock. Manganese injected mice showed less contextual freezing to the shock context and a shock context reminder one month after shock application. Furthermore, mice showed increased hyperarousal and no avoidance of shock context related odors. This impairment in fear conditioning indicates a disturbed associative learning of Mn^{2+} injected mice. Therefore, it was investigated whether Mn^{2+} application shows a specific disturbance of hippocampus dependent learning. Mice were subjected to habitual and spatial learning protocols 12 h after each injection in a water cross-maze. There was no impairment in learning protocols which allowed for hippocampus-independent habitual learning. However, Mn^{2+} injected mice were specifically impaired in the hippocampus-dependent spatial learning protocol. Furthermore, it was shown that only mice with higher Mn^{2+} accumulation showed this impairment. Altogether, the results of this chapter argue for a fractionated application scheme such as 30 mg/kg every 24 h for 8 days to provide sufficient MEMRI signal contrast while minimizing toxic side effects. However, the treatment procedure has to be further improved to allow for an analysis of hippocampus-dependent learning processes as well. Because of the potential side effects, the vMEMRI method was applied as a final experiment in

chapters 2 and 3.

Study 2 introduces the method of vMEMRI, which allows, for the first time, an *in vivo* semi-automatic detection of hippocampal volume. Hippocampal volume of mice with genetically altered adult neurogenesis and those with chemically lesioned hippocampi could be analyzed with vMEMRI. Even the highly variable differences in hippocampal volume of these animals could be detected with vMEMRI. vMEMRI data correlated with manually obtained volumes and are in agreement with previously reported histological findings, indicating the high reliability of this method.

Study 3 investigates the ability of vMEMRI to detect even small differences in brain morphology by examining volumetric changes of the hippocampus and other brain structures in a mouse model of PTSD supplemented with enriched housing conditions. It was shown, that exposure to a brief inescapable foot shock led to a volume reduction in both the left hippocampus and right central amygdala two months later. Enriched housing decreased the intensity of trauma-associated contextual fear independently of whether it was provided before or after the shock. vMEMRI analysis revealed that enriched housing led to an increase in whole brain volume, including the lateral ventricles and the hippocampus. Furthermore, the enhancement of hippocampal volume through enriched housing was accompanied by the amelioration of trauma-associated PTSD-like symptoms. Hippocampal volume gain and loss was mirrored by *ex vivo* ultramicroscopic measurements of the hippocampus. Together, these data demonstrate that vMEMRI is able to detect small changes in hippocampal and central amygdalar volumes induced by a traumatic experience in mice.

In conclusion, vMEMRI proves to be very reliable and able to detect small volumetric differences in various brain regions in living mice. vMEMRI opens up a great

Abstract

number possibilities for future research determining neuroanatomical structure, volumes and activity *in vivo* as well as the ability to repeatedly determine such characteristics within each subject, given an improvement of the Mn^{2+} treatment protocols to minimize potential toxic side effects.

Zusammenfassung

Die vorliegende Doktorarbeit führt eine Methode zur halbautomatischen Bestimmung des Volumens des Hippokampus und verschiedener weiterer Gehirnregionen in Labormäusen ein. Die Methode der volumetrischen manganverstärkten Magnetresonanztomographie (vMEMRI) macht sich die paramagnetische Eigenschaft des Manganions Mn^{2+} zunutze. Diese führt in den Gehirnregionen in denen sich Mn^{2+} anlagert zu einer Verstärkung der Helligkeit auf dem durch Kernspintomographie erzeugten Bild. Somit kann ein detaillierteres, kontraststärkeres Bild der Morphologie des Gehirns erstellt werden. Die chemische Ähnlichkeit des Mn^{2+} -Ions zu Kalzium führt zu einer Akkumulation von Mn^{2+} in erregten Nervenzellen und somit zu einer aktivitätsabhängigen Verstärkung des Magnetresonanzsignals in spezifischen Gehirnregionen. Ein großer Nachteil der vMEMRI ist die Toxizität des Mn^{2+} -Ions. Demzufolge hatte die Doktorarbeit folgende Hauptziele:

- (1) Etablierung eines Applikationsprotokolls für die MEMRI in Mäusen
- (2) Optimierung des Mn^{2+} -Applikationsprotokolls zur Reduzierung toxischer Nebenwirkungen
- (3) Entwicklung einer automatischen Methode zur Bestimmung von hippokampalen Volumina
- (3) Validierung der vMEMRI Analysemethode
- (4) Applikation der vMEMRI Analysemethode in einem psychopathologischen Mausmodell

Die Arbeit gliedert sich in drei Studien. Studie 1 beschäftigt sich mit der Toxizität des Mn^{2+} -Ions und zeigt eine Methode, die die toxischen Nebenwirkungen erheblich verringert.

Zusammenfassung

Studie 2 etabliert vMEMRI als eine Methode, die zuverlässig die Bestimmung hippokampaler Volumina zulässt und untersucht weiterhin die Anwendung der Methode in Mäusen mit genetisch und chemisch modifizierten Hippokampi. Studie 3 zeigt die Anwendung der vMEMRI-Methode in einem Mausmodell einer psychiatrischen Erkrankung.

Studie 1 zeigt, dass eine Einmalgabe von Mn^{2+} in einer Dosis, die in derzeitigen MEMRI-Studien üblich ist, zu erheblichen toxischen Nebenwirkungen führt, die sich physiologisch, endokrinologisch und verhaltensbedingt messen lassen. Als Alternative zur Einmalgabe einer hohen Dosis wird eine fraktionierte Gabe vorgeschlagen. Im Vergleich zu einer hohen Dosis von 60 mg/kg, zeigt eine wiederholte Gabe geringer Dosen von 30 mg/kg verringerte toxische Nebenwirkungen. Darüber hinaus zeigt eine Gabe von 8 Dosen zu 30 mg/kg mit einer 24-stündigen Pause zwischen den Injektionen (8x30/24 Protokoll) den besten Bildkontrast.

In einer Langzeitstudie werden die Auswirkungen des 8x30/24 Protokolls auf Lernprozesse getestet. Die Mäuse wurden, zwei Wochen bevor sie einen elektrischen Fußreiz erhielten, mit dem 8x30/24 Protokoll injiziert. Die Tiere die Mangan erhielten, zeigen bei einer nochmaligen Exposition gegenüber der Umgebung in der sie den Fußreiz erfuhren und gegenüber einer neuen Umgebung, die das Gitter, mit dem sie den Reiz erhielten, beinhaltet, weniger kontextuelle Furcht. Des Weiteren zeigten diese Mäuse erhöhte Erregbarkeit und kein Meideverhalten in einer Umgebung, die einen Geruch enthielt, der mit der Umgebung, in der sie den Fußreiz erhielten, verknüpft ist. Deshalb wurde untersucht, ob die Verabreichung von Mn^{2+} zu einer spezifischen Beeinträchtigung von hippokampalen Lernen führt. Dafür wurden Mäuse, 12 Stunden nachdem sie eine Injektion mit Mn^{2+} erhielten in einem water-cross maze (Plus-förmiges Wasserlabyrinth)

Zusammenfassung

mit verschiedenen räumlichen und habituellen Lernprotokollen trainiert. Dabei zeigte sich, dass Hippokampus-unabhängiges, habituelles Lernen nicht durch die Gabe von Mn^{2+} beeinträchtigt wird, wohingegen Hippokampus-abhängiges, räumliches Lernen durch Mn^{2+} spezifisch beeinflusst wird. Des weiteren zeigen sich besonders Mäuse beeinträchtigt, die eine erhöhte Mn^{2+} -Akkumulation im Hippokampus aufwiesen. Zusammengenommen zeigen die Ergebnisse der Studie, dass eine fraktionierte Gabe von Mn^{2+} , wie z.B. mit dem 8x30/24 Protokoll, zu einer Verringerung der toxischen Nebenwirkungen führt und gleichzeitig ein zufriedenstellender Kontrast im Kernspintomografie Bild erreicht werden kann. Allerdings muss die Applikationsmethode verbessert werden um die Analyse von Hippokampus-abhängigen Lernprozessen zu ermöglichen. Da es durch die Anwendung der vMEMRI-Methode zu Nebenwirkungen kommen kann wird diese Methode in den Studien 2 und 3 als finales Experiment angesetzt.

Studie 2 etabliert die vMEMRI Methode, die zum ersten Mal eine halbautomatische Bestimmung hippokampaler Volumina im lebenden Tier zulässt. Es wird gezeigt, dass sie sehr unterschiedlichen hippokampalen Volumina von Mäusen mit genetisch und chemisch modifizierten Hippokampi mit vMEMRI zuverlässig bestimmt werden können. Die Werte, die mit vMEMRI erhalten werden korrelierten mit manuell bestimmten Volumina und stimmen mit veröffentlichten Werten, die mit histologischen Verfahren gewonnen wurden, überein.

Studie 3 untersucht, ob vMEMRI dazu in der Lage ist, selbst kleine strukturelle Unterschiede im Gehirn festzustellen. Dazu werden hippokampale Veränderungen und Veränderungen weiterer Bereiche des Gehirns in einem Mausmodell der posttraumatischen Belastungsstörung untersucht. Durch die teilweise Anreicherung der Umgebung der Behausung der Tiere soll die Gehirnstruktur noch weiter modifiziert

Zusammenfassung

werden. Es wird gezeigt, dass Mäuse zwei Monate nachdem sie einem kurzen elektrischen Fußreiz ausgesetzt wurden kleinere Volumina im linken Hippokampus und in der rechten Amygdala aufweisen. Eine Anreicherung der Umgebung führte zu einer Verminderung der Trauma-assoziierten kontextuellen Furcht, egal ob die Anreicherung vor oder nach dem Trauma stattfand. Die vMEMRI Analysemethode zeigt, dass es durch die Anreicherung der Umgebung zu einer Vergrößerung des Gesamthirnvolumens, eingeschlossen der Lateralventrikel und des Hippokampus, kommt. Weiterhin führt die Vergrößerung des hippokampalen Volumen zu einer Verminderung der Trauma assoziierten, Posttraumatischen Belastungsstörung-ähnlichen, Symptome. Die Vergrößerung bzw. Verkleinerung des hippokampalen Volumens wird auch durch ein ultramikroskopisches Verfahren bestätigt. Zusammengenommen zeigen die aufgeführten Daten, dass die vMEMRI-Methode dazu in der Lage ist, kleine volumetrische Veränderungen im Hippokampus und der Amygdala von Mäusen zu erkennen, die durch ein traumatisches Erlebnis verursacht werden.

Als Fazit zeigt sich die vMEMRI-Methode als sehr zuverlässig und im Stande dazu, kleine volumetrische Unterschiede im Gehirn von Mäusen festzustellen. Die vMEMRI-Methode ist vorstellbar in einer Reihe von möglichen Forschungsanwendungen durch die Ermöglichung von Untersuchungen von neuroanatomischen Strukturen und deren Volumina und neuronalen Aktivitätszuständen im lebendigen Tier. Durch eine Verbesserung des Mn^{2+} -Applikationsprotokolls, was zu einer Verminderung der toxischen Nebenwirkungen führen sollte, kann auch eine wiederholte Messung im selben Tier möglich gemacht werden.

Abbreviations

%	percent
A	ampere
ASR	acoustic startle response
cm	centimetre
d	day
dB(A)	decibel (A-weighting)
h	hours
FOV	field of view
HPA	hypothalamic-pituitary-adrenal
INT	intensity
I/O	input/outout
i.p.	Interperitoneally
kg	kilogram
kHz	kilohertz
ko	knockout
l	liter
mA	miliampere
MEMRI	manganese enhanced magnetic resonance imaging
mg	milligram
min	minutes
µm	microgram
MeSH	medical subject heading
mm	millimeter
mM	millimolar
Mn ²⁺	Manganese
MRI	magnetic resonance imaging
ms	milliseconds
NaCl	sodium chloride
ng	nanogram
ppm	parts per million
RI	relative intensity
ROI	region of interest

Abbreviations

RPM	rounds per minute
RV	relative volume
s	seconds
SPL	sound pressure level
T	tesla
T1w	T1 weighted
T2w	T2 weighted
tbrain	total brain without ventricles
vol%	volume percent

A. Introduction

This doctoral thesis presents a method in the field of magnetic resonance imaging (MRI) that can semi-automatically determine hippocampal volume in mice. The following will first introduce the basic characteristics of the hippocampus covering function, plasticity and relevance in psychological and neurological illnesses. Additionally an overview of the current dominant methods to determine hippocampal volume is given. Secondly the method of manganese enhanced MRI (MEMRI), on which the hereupon presented volumetric method is based, is introduced, dealing with the properties of the contrast agent manganese, introducing basic principles of MRI and displaying the application fields of MEMRI. Thirdly the mice and animal models in which hippocampal volume with the presented method of volumetric MEMRI (vMEMRI) is probed are introduced. Subsection four of the introduction defines the general aims of the thesis, followed by an outline of the structure of the thesis. Last, the working hypothesis for the three main studies are specified.

1. The hippocampus

1.1. Function of the hippocampus

The hippocampus, placed right underneath the inner edge of the cerebral cortex, accounts for approximately 5 % of the total brain volume in C57Bl6/N mice (unpublished data), whereas a normal human hippocampus only makes up 0.1 % of the total brain volume (Simić et al., 1997). Along the longitudinal axis in mice and rats, the hippocampus resembles two “bananas”, present in the right and left brain hemisphere and merging dorsally at the brain's midline (Figure 1A). Surprisingly few studies estimated neuronal numbers in the whole hippocampus of mice; in rats, total neuronal number assessments of

Introduction

the hippocampus are between 2×10^6 (Long Evans rats) and 3×10^6 (Male Wistar rats) cells (Rasmussen et al., 1996; Rapp and Gallagher, 1996). Based on ratios of cell numbers between hippocampal subregions in these rat studies and estimated neuronal numbers in hippocampal subregions in C57Bl6/N mice, a total neuronal number of 2×10^6 cells can be estimated (Calhoun et al., 1999) . In humans, the neuronal count in the hippocampus is estimated to be about 25 times higher at nearly 50×10^6 cells (Simić et al., 1997). The general layout of the hippocampus, although varying in shape, is preserved within the mammalian species. The basic neuroanatomical features of the hippocampus were described at the end of the 19th century (reviewed in Andersen et al., 2007). The Ammon's horn is a brain structure which is comprised of the hippocampus and parahippocampal subfields. Santiago Ramón Y Cajal distinguishes cells of different shape, neuronal pathways and projections of the hippocampal formation in his work on the Ammon's Horn in the beginning of the 20th century. He observed distinct regional differences in neuronal shape and composition in the Ammon's horn, with small (region superior, CA1) and large (CA2) pyramidal neurons. Large pyramidal neurons occur together with mossy fibers (region inferior, CA3), which project from the granule cell layer of the dentate gyrus (Figure 1B). Santiago Ramón Y Cajal described a basic circuit of the Ammon's horn which connects the entorhinal cortex with the dentate gyrus, CA3, CA1 and subiculum. Projection from the subiculum then connect back to the entorhinal cortex, which functions as the main output center connecting the hippocampal formation with the cerebral cortex, thalamus, hypothalamus and brainstem. These connections from the entorhinal cortex to all hippocampal subfields and the subiculum are what Cajal named the perforant pathway. Cajal also distinguished two different perforant pathways, the superior and inferior, located at the dorsal and ventral part of the hippocampus, respectively.

Introduction

In the first half of the 20th century major interest from neuroscientists was drawn to the hippocampus after it was proposed to be critically involved in the cortical control of emotion (Papez, 1937). Papez incorporated theoretical connections between the cortex and the mesencephalon into an observed projection loop which connected the cortex to the hippocampus and hypothalamus and projected back to the cortex. The cortical connections of this loop, which came to be known as the Papez circuit, were theorized to be the basis of emotion (Cannon, 1927; Bard, 1929). Paul MacLean and others extended the Papez circuit into the presently known limbic system (MacLean, 1949; Fulton, 1953). They included the hippocampus along with the amygdala, septum and the prefrontal cortex in the limbic system as key structures of emotional memory. The linkage of the hippocampus with the prefrontal cortex via subcortical fields has since been shown to be essential in anxiety and motivation (McNaughton and Gray, 2000; Bast, 2003; Cooper et al., 2006). Additionally, a close correlation between hippocampal function and stress was shown, as the hippocampus executes regulatory control of the hypothalamic-pituitary-adrenal (HPA) axis. Conversely, a long-term elevation of stress hormones leads to hippocampal dysfunction (McEwen, 1999; Dedovic et al., 2009). The relationship between the hippocampus and emotion and affect is demonstrated by numerous reports of compromised hippocampal integrity in affective disorders (Campbell et al., 2004; Frey et al., 2007; Woon et al., 2010).

The hippocampal formation has been associated with memory formation since the middle of the 20th century after neurologists observed the loss of the ability to form new memories in a patient with bilateral medial temporal lobe resection (Scoville, 1954; Scoville and Milner, 1957). Later scientists found a relationship between the firing pattern of certain neurons in the hippocampus, called place cells, and the spatial location of a rat, and

Introduction

proposed the hippocampus to be the neuronal substrate of a cognitive map (O'Keefe and Dostrovsky, 1971). The synchronous firing pattern of these hippocampal cells was found to be present not only during exploration, but also similarly during resting and sleep, additionally suggesting memory consolidation in these areas (Buzsáki, 1986; O'Neill et al., 2006). The neuronal mechanisms of spatial orientation and integration and episodic memory are believed to be similar as both processes deal with sequentially arranged information with a temporal context (Dragoi and Buzsáki, 2006). Incorporation of a variety of sensory information, critical for the processing of episodic and spatial memory, are obtained by the hippocampus through parahippocampal regions, especially the entorhinal cortex showing strong connections with the neocortex (Burwell, 2000). These findings suggest an involvement of the hippocampus in integrating the chronological storage of episodic and spatial information together with related visual, auditory and somatosensory experiences (Eichenbaum, 1997; Moser et al., 2008).

The differential distribution of hippocampal connections through the entorhinal cortex to the subcortical and cortical sites along the longitudinal axis which extends from the rostral-dorsal to the caudal-ventral pole was already observed by Santiago Ramón Y Cajal and has been confirmed and extended over the last century (Swanson and Cowan, 1977; Witter, 1986; Risold and Swanson, 1996). Numerous experimental evidence has shown, that this neuroanatomical dissociation also corresponds to a functional differentiation along the poles, with the dorsal part related to processing of environmental information and the ventral part to processing and expression of emotional and motivational information (Moser and Moser, 1998; Bannerman et al., 2004). Recent studies

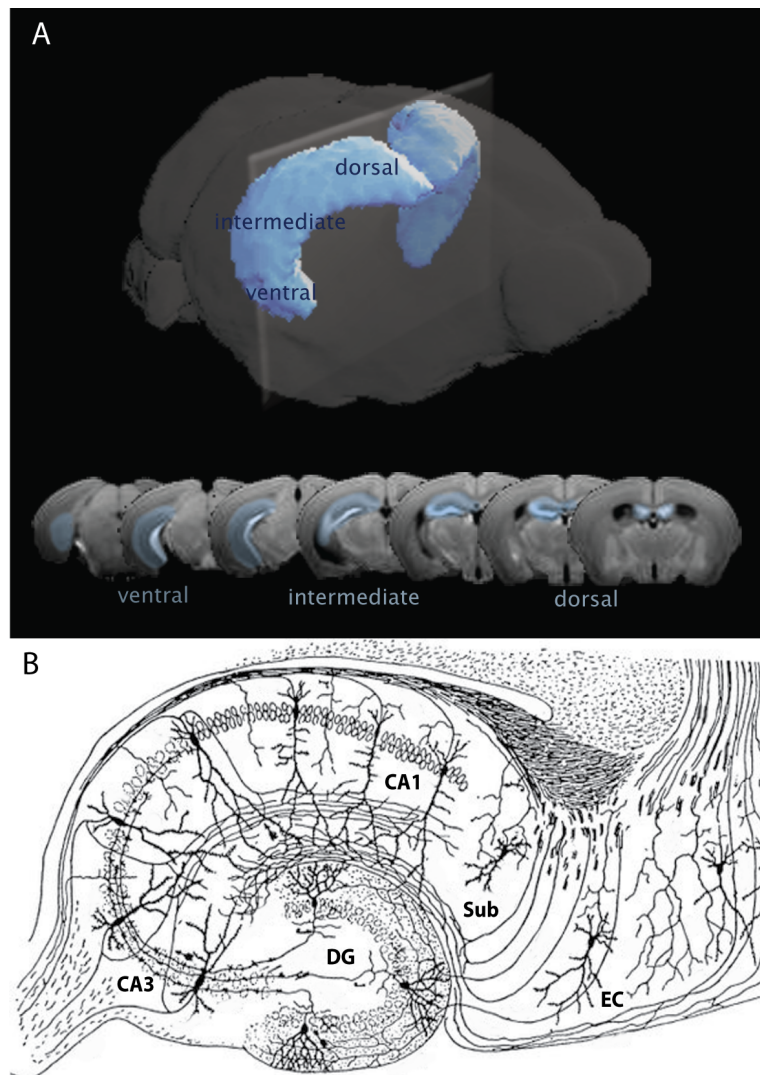


Figure 1: Anatomy of the hippocampus: (A) Spatial position of the hippocampus (blue) in the mouse brain (3D reconstruction of regions of interest; upper row). Section indicates orientation of the coronal slices (T1-weighted manganese enhanced MR images; lower row). The figure is produced from own data and observations of C57BL/6N mice. (B) Schematic drawing of the neuronal cell types in the hippocampus of a rat modified from Santiago Ramon y Cajal (1911). DG: dentate gyrus; Sub: subiculum; EC: entorhinal cortex.

on gene expression and function suggest a segregation of the hippocampus into a dorsal, intermediate and ventral part (cf. figure 1A; Fanselow and Dong, 2010). This differentiation is gradual and there are functional interactions between the poles, related to anatomical septo-temporal connections, which allow for functional integration between these regions (Amaral and Witter, 1989; Buckmaster and Schwartzkroin, 1995). This integrates of

Introduction

emotional, motivational and environmental information allows for the translation of learning into adaptive behavior. This translation was shown to be driven by strong neuroanatomical and functional connectivity with brain systems central to behavioral control, such as the prefrontal cortex, mediodorsal striatum and nucleus accumbens (Bast, 2007).

1.2. Hippocampal plasticity and related disorders

The hippocampus is a region of great plasticity, responding to aging, environmental factors and psychological state with morphological and functional modulation during development and in adult life (Sapolsky, 1996; van Praag et al., 1999; McEwen, 1999). Alteration and differences in hippocampal integrity have been associated with many neurological diseases and psychiatric disorders.

Although the discovery of adult neurogenesis occurred in the early 1960s, acceptance of this fact only started to occur after the 1980s, and great attention in the scientific world only increased shortly before the turn of the millenium (Altman, 1962; Bayer et al., 1982; Gross, 2000). Although tens of thousands of new neurons are produced everyday in the subgranular zone of the DG and the subventricular zone of the lateral ventricle, many of these newly generated cells die after a few days (Bayer, 1982; Biebl et al., 2000; Winner et al., 2002; Kempermann, 2003). Adult neurogenesis does not necessarily lead to increased volumes in these areas. The subventricular zone was shown to be increased with age, by the addition of new cells, whereas the subgranular zone did not show an increase of volume (Imayoshi et al., 2008). It has been shown that exposure of young adult rodents to a complex enriched environment or to a running wheel increases the number and survival rate of adult-born neurons in the DG (Kempermann et al., 1997; van Praag et al., 1999). Adult-born hippocampal neurons have been related to both

Introduction

reference memory (spatial memory) and associative memory, with experimental evidence showing hippocampal learning even enhancing adult neurogenesis itself. Nevertheless it should not be neglected that other studies have also shown no beneficial effects of enhanced neurogenesis on learning and memory (Gould et al., 1999; Shors et al., 2001; Meshi et al., 2006). *In vitro* studies show functional integration of newborn neurons into neuronal networks forming synapses and becoming electrically active (Song et al., 2002; Benninger et al., 2003). Whether this functional integration also affects hippocampal function *in vivo* is unclear, as ablation of neurogenesis led to hippocampal dysfunction in some hippocampus related tasks but not others (Shors et al., 2001; Shors et al., 2002).

The hippocampus can be damaged by stroke and head trauma; however, hormonal action was found to be one of the main factors leading to morphological restructuring of the hippocampus, leading to dendritic atrophy, lowering of synaptogenesis and suppression of adult neurogenesis in the DG (McEwen, 1999). Besides rapid, reversible effects of estrogen on hippocampal synaptogenesis and of thyroid hormones on hippocampal dendritic morphology, corticosteroids seem to have possibly long-term effects on hippocampal plasticity (Popov and Bocharova, 1992; Popov et al., 1992; Woolley et al., 1997; de Kloet, 2000). Glucocorticosteroids, namely cortisol (humans) or corticosterone (non-human), are regulated by the HPA axis and can bind hippocampal neurons via two types of adrenal steroid receptors, mineralocorticoid and glucocorticoid receptors. These receptors mediate glucocorticoid-induced effects on neuronal excitability, neurochemistry and structural plasticity (reviewed in de Kloet, 2000; Joëls, 2010). The profound effects of stress on endocrine levels, hippocampal plasticity and related learning and memory processes have been reviewed extensively and highlight the central, and plastic role of the hippocampus in stress and cognitive functions (Sapolsky, 1996; McEwen, 1999; 2001; Kim

Introduction

et al., 2006).

A decline in memory is one of the earliest diagnosed cognitive impairments that occurs in a normal aging human and occurs with steadily increasing prevalence with increasing age (Larrabee and Crook, 1989; Larrabee and Crook, 1994). It stands to reason, that a connection between memory impairment and functional and structural hippocampal impairment would exist. Studies on the human hippocampus report volume decreases of 10 % and loss of neurons of up to 23 % between the age of 30 and 80 (Simić et al., 1997). Increasing levels of glucocorticoids with age are thought to mediate decreasing effects on neuronal number (Sapolsky et al., 1985). Morphological aging studies in rodents however show mixed results, with some studies showing a decrease of neuronal density, neuronal body size and synapses with age and others showing no differences in these morphological parameters (for details see appendix table 1). A decrease in hippocampal neurogenesis was long thought to contribute to age related cognitive impairment (Kuhn et al., 1996). However, recent studies show, that a decrease in proliferation of neuronal progenitor cells happens very early in life, staying constant throughout adulthood until late in life (Ben Abdallah et al., 2010; Knoth et al., 2010). Nevertheless, some studies have shown correlations between the extent of memory impairment in aged rodents and the magnitude of glucose metabolism deterioration as well as electrophysiological parameters in the hippocampus (Gage et al., 1984; Barnes and McNaughton, 1985; Tombaugh et al., 2002).

A decline in memory and other cognitive functions are the main criteria for diagnosis of dementia and Alzheimer's disease (American Psychiatric Association, 2000; Selkoe, 2001). More than 50 % of dementia cases are considered to be primarily degenerative type Alzheimer's (Lobo et al., 2000). It has been shown, that the hippocampus is especially

Introduction

affected by neurodegeneration in Alzheimer's disease and it has been suggested that hippocampal atrophy rates might be useful in diagnosing the disease and tracking its progression (Barnes et al., 2009). Alzheimer's disease leads to the occurrence of neurofibrillary tangles and plaque development. However, it is not clear whether the neurofibrillary tangles or the amyloid plaques lead to neuronal atrophy and the development of dementia and if so which principle molecular components of the tangles and plaques are involved. Two hypotheses are discussed in recent literature; the *tau*-based and the amyloid-based (Ashe, 2001; Chapman, 2001). Mutations in *tau* have been connected to neurofibrillary tangle development. Although no family studies have linked Alzheimer's disease to mutations in *tau*, some cases of dementia occur without plaque development, indicating a connection between abnormal *tau* metabolism and dementia (Hutton et al., 1998; Poorkaj et al., 1998). Transgenic mice overexpressing the amyloid precursor protein, due to mutations in Alzheimer's associated genes, show enhanced β -amyloid production leading to abnormal plaque development. Nevertheless, only few studies show a correlation between number of plaques and dementia (Chapman, 2001). Most of these mouse models show impairment in learning and memory and some even show loss of synapses and neurons, in the hippocampus and other brain areas (Games et al., 1995; Calhoun et al., 1998; Takeuchi et al., 2000; Ashe, 2001). In most models however, age-dependent and -independent changes in behavior and cognition are difficult to separate and none of the models show neurodegeneration to the degree that is seen in human patients with Alzheimer's. These studies imply interesting discrepancies indicating that the number of synapses and neurons in the hippocampus is not necessarily connected to learning and memory function.

Drug addiction, although technically among mental disorders leads to different

Introduction

neurological diseases connected to dementia and hippocampal functioning (Hulse et al., 2005). For example the Wernicke-Korsakoff syndrome, a condition brought on by excessive alcohol consumption, is accompanied by structural brain changes including volumetric changes of the hippocampus (Sullivan and Pfefferbaum, 2009). Visualization of the structural changes in animal models of chronic alcohol consumption and observations of its progression following different treatment regimes could lead to a deeper understanding and an effective therapy of this syndrome (Sullivan and Pfefferbaum, 2009).

Another prevalent neurological disorder, costing health care more than 1 billion Euros a year in Germany alone, is epilepsy (Lobo et al., 2000). It is the most common acquired chronic neurological disorder, occurring most frequently in children and the elderly (Picot et al., 2008). Half of the patients treated with antiepileptic drugs continue to experience seizures, which is particularly common in patients having epilepsy with a temporal-lobe origin (Picot et al., 2008; Yang et al., 2010). Learning and memory difficulties are the most frequent cognitive alterations in patients with temporal lobe epilepsy, and are related to hippocampal sclerosis (Glowinsky, 1973; Giovagnoli and Avanzini, 1999). This sclerosis is a reliable marker in the detection of epilepsy and can, if diagnosed early enough, lead to an effective treatment of patients (Woermann and Vollmar, 2009). The characteristic seizures occurring as a result of abnormal, excessive or synchronous neuronal activity are caused by various things, such as infections, lesions, trauma, Tumors, central nervous system abnormalities, drug use or degenerative diseases (Fisher et al., 2005).

Further neurological diseases leading to alterations of hippocampal volume are Cushing's disease and Autism (Patil et al., 2007). Other neurological diseases such as Parkinson's disease, Huntington's disease and progressive supranuclear palsy are related

Introduction

to impaired memory function without reported disturbance of the hippocampus (Caine et al., 1978; Levin et al., 1992; Litvan, 1994). Besides the association of hippocampal atrophy and subsequent cognitive deficits seen in Cushing's disease and Autism, the study of neurological diseases without direct impairment of the hippocampus can reveal more about other brain structures involved in learning and memory. For example, Parkinson's and Huntington's disease have revealed more about the connections between the basal ganglia and the frontal lobe and their involvement in working and spatial memory (Caine et al., 1978; Albert et al., 1981; Levin et al., 1992). Further studies on Huntington's disease could also shed more light on the pathology of the neocortex and its involvement in the progressive cognitive deficits associated with this disease (Panegyres, 2004). The study of progressive supranuclear palsy could also reveal more about the involvement of subcortical structures such as the pallidum and mesencephalic reticular activation system, and their connections to the frontal cortex in working memory (Litvan, 1994; Pillon et al., 1994).

Compromised hippocampal functioning has also been implicated in psychiatric disorders such as depression and anxiety. One of the most frequent findings associated with depression is memory impairment (Burt et al., 1995). In major depressive disorder a great variety of studies have reported hippocampal volume loss between 10 and 15 %, making it a characteristic symptom of this disorder (Campbell et al., 2004). The duration of the depressive episode correlates closely with hippocampal volume, meaning smaller hippocampal volume is related to longer depressive episodes (Sheline et al., 1999). Functional studies on major depressive disorder suggest that high hippocampal metabolism, as measured by positron emission tomography (PET), is a marker of successful therapy and recovery from major depression (Kennedy et al., 2001; Goldapple

Introduction

et al., 2004). It should be noted that hippocampal volume is not necessarily reduced as consequence of depression, but may also function as a predisposition marker for the subsequent development or remission of depressive symptoms (Neumeister et al., 2005). Shrinkage of hippocampal volume in depressed patients was long attributed to HPA-axis hyperactivity, as found in depressed patients, and therefore the outcome of prolonged hormonal stress (Sapolsky, 2000). Although many preclinical studies report neuronal loss after severe stress, human postmortem studies of depressed patients have not found any differences in neuronal number in the hippocampus (Sapolsky et al., 1985; Lucassen et al., 2001). Many different factors such as alteration of hippocampal neurogenesis, enhancement of apoptosis of newborn cells, alteration in synaptic and axonal composition, reduction of glial cells and rearrangement of fluid concentration between hippocampus and lateral ventricle are discussed, indicating that the mechanisms leading to hippocampal shrinkage in depression are still not understood (Czéh and Lucassen, 2007).

Memory impairment in some task has also been shown in bipolar disorder (Kieseppä et al., 2005). The findings on morphological changes of the hippocampus in bipolar disorder are mixed, however, more studies report preserved hippocampal volume (Savitz and Drevets, 2009). One study suggested hippocampal volume as a risk factor for the subsequent development of the illness in offspring of bipolar sufferers (Ladouceur et al., 2008).

One of the most commonly studied anxiety disorders in relation to hippocampal functioning is post-traumatic stress disorder (PTSD) and memory impairment in PTSD patients has been reported in a number of studies (Brandes et al., 2002). N-acetylaspartate (NAA) is closely related to neuronal integrity as it is exclusively present in neurons. In PTSD patients changes in NAA, as measured by magnetic resonance

Introduction

spectroscopy (MRS), and volumetric changes of the hippocampus, measured by MRI, have been widely detected (Karl and Werner, 2010; Woon et al., 2010). A twin-study in humans as well as a preclinical study in a mouse model of PTSD both revealed that differences in hippocampal integrity are not merely a consequence of PTSD but could also function as a susceptibility marker for the development of PTSD (Gilbertson et al., 2002; Siegmund, Kaltwasser et al., 2009). Nevertheless, the causal relationship between hippocampal integrity, trauma experience and the development of PTSD symptoms is not understood and, it should be noted, that some studies fail to detect hippocampal volume decrease in PTSD (Fennema-Notestine et al., 2002; Yehuda et al., 2007; Savitz and Drevets, 2009).

Differences in hippocampal integrity have also been reported in other psychiatric disorders, such as schizophrenia as well as in personality disorders such as borderline personality disorder and dissociative identity disorder (Heckers, 2001; Schmahl, 2003; Vermetten et al., 2006).

Overall, a method to detect and trace hippocampal function and volume in humans and animal models seems to be a key feature in diagnosing neurological diseases and psychiatric disorders; understanding the role of the hippocampus in the susceptibility, development and maintenance of these diseases; and monitoring treatment progress .

1.3. Methods to determine hippocampal morphology

Structural analysis of the hippocampus to assess neurodegeneration is often conducted *ex vivo* by microscopic methods, such as light microscopy, fluorescent microscopy, electron microscopy or ultramicroscopy (Gerdes and Kaether, 1996; Fairén, 2005; Dodt et al., 2007; Smith et al., 2010). To visualize neurons staining-methods are

Introduction

applied, such as standard Nissl-staining for neuronal cell bodies or Golgi- or Green Fluorescence Protein-staining for selective neurons (Gould et al., 1990; Gerdes and Kaether, 1996; Fairén, 2005; Ndode-Ekane et al., 2010). Staining procedures make resolution in the nanometer range possible and enable the examination of dendritic morphology. Microscopic methods in combination with tissue staining provide good to excellent resolution for visualizing neurons on the cellular level. A drawback of these methods is that the brain tissue has to be frozen or perfused with a fixative solution, which affects fundamental neuroanatomical characteristics of the tissue. Not only is the tissue affected by the fixation, but it is also differentially affected by varying fixation methods making it impossible to compare between staining methods that depend on different fixation procedures (Lavenex et al., 2009). Fixation and cutting also interfere with tissue fluid content leading to a significant effect on the ventricular system in particular. Furthermore, volumetric measurements of whole structures are difficult. The hippocampus for example ranges from Bregma -4.04 mm to Bregma -0.94 mm according to Paxinos mouse brain atlas, and at a typically used slice thickness of $30\ \mu\text{m}$, 103 slices would have to be analyzed to gain a total volume measurement of the hippocampus (Paxinos and Franklin, 2004). Additionally, many knockout animals differ from their wildtype littermates in total brain volume, making it necessary to normalize structures to total brain volumes in order to determine if volumetric differences can be ascribed to selective effects on certain brain structures or to a overall effect on brain volume in the knockout line. Additionally, *ex vivo* methods only allow depiction of neuroanatomical structures at one time point per animal.

In vivo methods, in contrast, open up the possibility to repeatedly assess structural characteristics in one animal. This increases statistical power and decreases the amount

Introduction

of animals required. Depicting hippocampal volume using magnetic resonance imaging (MRI) is a frequently used method in this context. A Medline search in February 2011 using the Medical subject heading (MeSH) search terms “hippocampus” combined with “MRI” and “shape” or “volume” extracted 1864 publications. Modern imaging techniques in humans enable reliable measurement of hippocampal volume using native MRI contrast by defining hippocampal borders using gray and white matter contrast differences (Konrad et al., 2009). Over the last decade high resolution 3D-images of mice, providing good structural insight, have been made possible by the development of adequate data acquisition protocols for small animal MRI (Natt et al., 2002). Despite these technical advances, few studies use native contrast for hippocampal volume delineation, which define hippocampal borders manually (Maheswaran et al., 2009; Radyushkin et al., 2010). Low grey-white matter contrast in native MR images of mice makes it difficult to differentiate regional borders. To enhance image contrast, brains are fixed and scanned using high field scanners and long MRI scans, a method called magnetic resonance microscopy (MRM) (Badea et al., 2007). However this method does not utilize the great advantage of MRI, namely the possibility to repeatedly assess brain morphology *in vivo*. To overcome low regional intensity differences *in vivo*, contrast agents can be applied (Mendonça-Dias et al., 1983). The manganese ion Mn^{2+} turns out to exhibit very promising features as a contrast agent, by selectively enhancing certain structures in an activity-dependent manner (Koretsky and Silva, 2004). This method is known as manganese enhanced MRI (MEMRI). Hippocampal contrast intensity increases especially dramatically (cf. Fig.1A), thus enabling reliable delineation of hippocampus volume.

Introduction

2. Manganese enhanced magnetic resonance imaging (MEMRI)

The following will introduce the method of MEMRI by first dealing with the contrast agent manganese. Then the basic principles of MRI are explained and last the possible application fields of MEMRI are displayed.

2.1. Manganese

The usage of manganese (Mn^{2+}) in magnetic resonance imaging (MRI) to enhance magnetic relaxation times and thereby enhancing image contrast goes back to the discovery of nuclear magnetic resonance (NMR) itself (Connick and Poulson, 1959). A drawback in its usage as a contrast agent in humans is its toxicity (Aschner et al., 2005). Manganese is considered to be an essential trace element in many animals since severe deficiency generally leads to severe illness and death (Kemmerer et al., 1931; Orent and McCollum, 1931; Rucker et al., 2010). Excess of essential elements does not usually cause illness; however, at concentrations beyond those necessary for their biological functions they can be toxic (Fraga, 2005; Rucker et al., 2010). To evaluate the full toxic risk of Mn^{2+} to humans investigations about its occurrence in the environment and the body, absorption into the body and effects on the body and brain must be made.

2.1.1. Occurrence in the environment and uses

The human body is confronted with manganese in different forms. Manganese is found ubiquitously in the environment, with highest concentrations in descending order found in soil and food and lower concentrations in water and air. With a mean concentration of 330 ppm in soil it occurs in more than 100 minerals (Barceloux, 1999). Manganese in higher oxidation forms is mainly used by the industry to enhance hardness,

Introduction

stiffness and strength of steel (Agency for Toxic Substances and Disease Registry, 2008). In this form it poses a toxicological threat to miners and people confronted with manganese as dust (e.g. welder). Nonmetallurgic uses for the biologically available form of manganese include production of dry cell batteries, plant fertilizers and animal feed, as well as use as brick colorant (Barceloux, 1999; Agency for Toxic Substances and Disease Registry, 2008).

In food highest concentrations of manganese are found in nuts (32 ppm), leguminous plants (4.5 ppm), vegetables and tea (2ppm) (Wenlock and Buss, 1979; Gillies and Birkbeck, 1983; Pennington et al., 1986). Median concentration of manganese were reported ten times higher in rivers (0.024 ppm) than in seawater (0.002 ppm) (Smith et al., 1987; Barceloux, 1999; Agency for Toxic Substances and Disease Registry, 2008). In modern urban areas, the estimated average background level of manganese in the air is relatively low (approximately 0.00003 ppm) compared to slightly higher levels in the early 50s (0.0001 ppm) (Agency for Toxic Substances and Disease Registry, 2008; U.S. EPA, 2009)

2.1.2. Occurrence in the body

The total manganese concentration in the human body is estimated to be 12-20 mg (Underwood 1977). Manganese forms complexes with many other substances which is why its free plasma and tissue concentrations tend to be extremely low (Cotzias et al., 1968). It is heterogeneously distributed throughout the bodily tissues with higher concentrations in mitochondria-rich tissues; as manganese has an important role in mitochondrial enzymatic functions (Reynolds et al., 1998). In humans, rats and monkeys the liver, pancreas and kidney were found to have the highest concentrations of

Introduction

manganese (Aschner et al., 2005). Concentrations also vary throughout the mammalian brain; where the highest concentrations, overall, occur in the olfactory bulb and pineal gland (Aschner et al., 2005). Additionally, in rats similarly high concentrations are also found in the hypothalamus (Prohaska, 1987). The Putamen and globus pallidus contain slightly elevated manganese levels in all mammals, with rats also showing similar levels in the cerebellum (Bird et al., 1984; Bush et al., 1995; St-Pierre et al., 2001)

2.1.3. Absorption of manganese into the body

Although ingestion is the principal route by which most people are exposed to manganese, animal studies suggest that excessive dietary intake of manganese is counterbalanced by decreased absorption efficiency (Nielsen, 2006). Despite gut absorption being a regulatory step in manganese homeostasis, studies show high manganese accumulation in the brain after subchronic oral exposure (Rodríguez et al., 1998). Estimated Safe and Adequate Daily Dietary Intake (ESADDI) for adults has been set at 2-5 mg of intake per day; however, there is no Recommended Dietary Allowance (Commission on Life Science (CLS), 1989). Dietary studies have found mean manganese intake to be in the lower range of this recommendation, with the highest intakes not exceeding it (Institute of Medicine (IOM), 2001). Direct stomach infusions of manganese bypass the homeostatic mechanism of the gut creating a potential risk for manganese toxicity (Malecki et al., 1995). Although, only a small portion of manganese is accumulated in the brain via the blood-brain barrier and manganese, as Mn^{2+} is reported to be cleared rapidly from the blood, these indications can be misleading, as only small, oxidized amounts of manganese in higher valency forms may play a key role in its toxicity, a factor that has received little attention in experimental toxicology (Gibbons et al., 1976; Aschner

and Gannon, 1994). Manganese inhaled as dust shows adverse effects on the central nervous system at much smaller doses. The olfactory neuronal pathway efficiently absorbs inhaled Manganese oxide as solid ultrafine particles directly to the central nervous system, leading to an accumulation of manganese in the olfactory bulb (Dorman et al., 2004; Elder et al., 2006). From there it has the ability to pass synaptic junctions and migrate through the olfactory tract to more distal brain regions, including the hypothalamus (Tjälve et al., 1995). Excessive manganese accumulation within the striatum, putamen, and globus pallidus was also reported following high-dose inhalation or oral exposure (Aschner et al., 2005; Dorman et al., 2006).

2.1.4. Manganese deficiency and toxicity

Explicit evidence of manganese deficiency in humans has not yet been reported. Several studies on animals fed a diet deficient in manganese demonstrate poor skeletal growth, bone mineralization, cartilage development, and wound healing (Gallup and Norris, 1938; Frost et al., 1959; Hurley, 1981; Strause et al., 1986; Tenaud et al., 1999). Manganese deficiency is also connected to impaired reproduction and inadequate fetal development (Apgar, 1968; Hansen et al., 2006). These effects are ascribed to the role of manganese as a cofactor for certain transferases necessary for glycoprotein synthesis occurring in connective tissue (Leach and Muenster, 1962; Leach et al., 1969; Leach, 1971; Institute of Medicine (IOM), 2001). The functional loss of the manganese-containing enzyme, superoxide dismutase, as a result of manganese deficiency, could lead to the development of some forms of cancer (Oberley and Buettner, 1979). This is mainly due to the involvement of superoxide dismutase in cellular protection from damaging free radical species. A metabolic association of manganese and choline is a factor in defective lipid

Introduction

metabolism leading to increased fat deposition and malfunctioning cell membrane integrity, which influences cell function and ultrastructure, particularly in mitochondria and immune function (Plumlee et al., 1956; Rabinovitch and DeStefano, 1973; Bell and Hurley, 1973; Klimis-Tavantzis et al., 1983; Hurley and Keen, 1987). Manganese deficient rats also show diabetes like symptoms, as the low Mn^{2+} levels compromise carbohydrate and insulin metabolism (Baly et al., 1990). The absence of manganese, as a critical cofactor of enzymes which are involved in the formation of glutamine, is additionally connected to disturbed protein and energy metabolism and malfunctioning metabolic regulation (Mertz, 1995; Institute of Medicine (IOM), 2001).

Most human studies reporting cases of manganese toxicity are primarily in miners that have inhaled manganese-charged dust (Lee, 2000). The inhalation of high doses of manganese, as described in miners, initially produced an acute psychiatric syndrome called "manganese madness," first described by Couper in 1837 (Couper, 1837). Characteristic symptoms of this syndrome include compulsive and aberrant behavior, emotional lability, and hallucinations. Chronic manganese exposure was shown to produce parkinsonism and dystonia (Cotzias et al., 1971; Barbeau et al., 1976). The parkinson-like symptoms could be a consequence of neuropathology in the basal ganglia, especially the globus pallidus, as histopathological analysis of manganese-exposed subjects has shown massive neuronal degeneration in the globus pallidus accompanied by high manganese accumulation and neurodegeneration in the substantia nigra and in the caudate nucleus and putamen of the striatum (Yamada et al., 1986; Eriksson et al., 1992). Together with a reduction of dopamine content in the striatum, these results show the direct impact of manganese exposure on the dopaminergic system (Bernheimer et al., 1973). It is hypothesized that the mechanism affecting the extrapyramidal motor system is

Introduction

manganese-induced destruction of neurons of the globus pallidus, which leads to a loss of tonic inhibition of the subthalamic nucleus, possibly resulting in death of dopaminergic neurons in the substantia nigra (Bird et al., 1984; Wright et al., 2004; Wright and Arbutnott, 2007). It is generally accepted, that this manganese-induced neural toxicity is caused by disruption of mitochondria function (Roth, 2009). Acute exposure to high levels of manganese causes oxidative stress by alteration of glutathione and superoxide dismutase enzyme activity, two important antioxidants in mitochondria comprising major cellular defense mechanisms against oxyradicals (Sloot et al., 1996; Normandin and Hazell, 2002; Morello et al., 2007). The local formation of oxyradicals is accompanied by disturbance of iron homeostasis and function in mitochondria (Zheng et al., 1998). It has been hypothesized that manganese-catalyzed production of free radicals enhances auto-oxidation of catecholamines, like dopamine, and/or enhances production of 6-hydroxydopamine, a selective neurotoxin of dopaminergic and noradrenergic neurons, which could eventually lead to cell death (Cohen and Heikkila, 1974; Archibald and Tyree, 1987; Garner and Nachtman, 1989). Nevertheless the exact biochemical and molecular mechanisms of manganese toxicity are not fully understood.

2.2. Magnetic resonance imaging (MRI)

MRI utilizes the principles of nuclear magnetic resonance (NMR) in liquids and solids, discovered by Felix Bloch and Edward Purcell in 1946, and translates these principles into images (Purcell et al., 1946; Bloch, 1946). Each elemental isotope has a certain nuclear rotation frequency, called the Larmor frequency. In a constant magnetic field, certain isotopes within a given element show paramagnetic polarization. This polarization occurs only along the longitudinal axis, which is the direction of the constant

Introduction

magnetic field. Bloch and Purcell observed that the direction of this polarization can be displaced by an angled radiofrequency field equal to the Larmor frequency of the given element. This displacement causes a rotation of the nuclear polarization axis around the longitudinal axis. Additionally, this displacement gives rise to a magnetic component in the transverse axis. Of the total polarization, there is a decay of the longitudinal component and a rise in the transverse component, which results in an observable electrical potential. When the radiofrequency field is turned off the transverse component decays and the longitudinal component rises back to its original magnitude – this is called relaxation. The time it takes for the longitudinal polarization to return to its original value is called the spin-lattice relaxation or T_1 -relaxation. This relaxation time is dependent on the density of molecular motion, meaning temperature and viscosity, at the Larmor frequency of a certain solution or tissue. As the temperature differences between different tissues in an organism are minimal, the T_1 -relaxation in organisms mainly depends on the viscosity of different tissues. Additionally, transverse polarization decays over time because nuclei rotate at their own Larmor frequency. The measure of the decay of the transverse polarization over time is called the spin-spin relaxation or T_2 -relaxation. This relaxation time is dependent on the number of molecular motions, which means on the chemical environment, at the Larmor frequency.

Generally both relaxations happen at the same time, but depending on the acquisition sequence of an image the contrast can mainly be attributed to T_1 - or T_2 -relaxation, called T_1 - or T_2 -weighted images. Paul Lauterbur and Peter Mansfield determined the spatial position of a particle, by switching on magnetic field gradients. These magnetic field gradients select particles or spins of particles of a specific slice and encode the position on the other two axes by slightly altering the particles' Larmor

Introduction

frequency and phase. The magnitude of the alteration depends linearly on the position. These slight differences in phase and frequency can then be translated by Fourier transformation into an image. Lauterbur and Mansfield were credited with the Nobel Prize for the development of these basic principles MRI, meaning spatial encoding through application of gradient fields and translation into an image (Lauterbur, 1973; Mansfield, 1977).

2.3. Manganese as a contrast agent in MRI

As discussed in the introduction to the methods to determine hippocampal volume (cf. 1.3), MRI of the naive rodent brain is limited by low contrast among different cerebral compartments, making it difficult to delineate cortical and subcortical regions. To enhance the regional contrast specificity, paramagnetic agents are frequently applied (Mendonça-Dias et al., 1983). Manganese was the first paramagnetic ion used to show that relaxation times of water could be altered (Lauterbur, 1973). Studying the effects of Mn^{2+} on relaxation times of blood and different tissues helped further understanding of the many issues associated with relaxation times in complex biological media (Mendonça-Dias et al., 1983; Kang and Gore, 1984). Besides its physical property of paramagnetism, manganese has interesting chemical and biological properties. Due to its chemical similarity to calcium (Ca^{2+}), Mn^{2+} may enter neuronal cells through voltage-gated Ca^{2+} channels during depolarization, enabling an activity dependent enhancement of neuronal tissues (Drapeau and Nachshen, 1984; Simpson et al., 1995; Pautler and Koretsky, 2002; Pautler et al., 2003). Inside the cell Mn^{2+} is taken up into the endoplasmic reticulum where it is accumulated in vesicles. From there it can be transported anterogradely in axonal tracts to the synaptic cleft, where it is released and taken up by the next neuron (Sloot and

Introduction

Gramsbergen, 1994; Pautler et al., 1998; Pautler and Koretsky, 2002). The MEMRI has gained increased interest over the last years since several reviews introduced its application range in 2004 (Koretsky and Silva, 2004; Silva et al., 2004; Pautler, 2004; Aoki et al., 2004a; Wendland, 2004). Appendix table 2 summarizes all *in-vivo* MEMRI studies conducted in non-primate animals. $MnCl_2$ can be applied systemically or locally. Routes of systemic application include intraperitoneal, subcutaneous or intravenous injections. Intravenous injections are applied via the tail vein or the jugular vein. Local administrations of $MnCl_2$ are conducted intranasally, intravitreally or intracranially. The physical, chemical and biological properties of Mn^{2+} have led to three major fields of Mn^{2+} application in MRI.

Firstly, the propensity of Mn^{2+} to move along neuronal tracts allows for the possibility to study neuronal networks and to trace neuronal connections *in vivo*. This method of neuronal tract tracing was first performed by Pautler and colleagues in 1998 (Pautler et al., 1998; review Pautler, 2004). It was used to map connections of peripheral nerves, as well as the amygdala, central tegmental area, entorhinal cortex, hippocampus, striatum, prefrontal cortex, olfactory bulb and other cortices (cf. appendix table 2). Even connections among the neuronal song centers of songbirds could be visualized which enabled monitoring and study of regional plasticity as a function of seasonal and hormonal influences (Van der Linden et al., 2004).

Secondly, the activity dependent accumulation of Mn^{2+} in cells enables its use as a functional MRI tool. Functional accumulation of manganese due to visual, olfactory, auditory, gustatory or somatosensory stimulation has been shown (cf. appendix table 2). Since the MEMRI signal shows not only region but also layer-specificity it has been used for retinotopic mapping of the visual cortex and superior colliculus, tonotopic mapping of the inferior colliculus and even mapping of individual glomeruli of the olfactory cortex (cf.

Introduction

appendix table2). Activity dependent differences in Mn^{2+} accumulation have been shown after wheel running, fasting and the consumption of diets, oxidative stress, pain and drug application (for details see appendix table 2).

Thirdly, Mn^{2+} is used as an agent to enhance tissue contrast. As already mentioned in the previous chapter, systemic application of Mn^{2+} leads to an accumulation predominantly in the basal ganglia (Aschner et al., 2005). Additionally, the hippocampus shows enhanced accumulation of Mn^{2+} . The tissue specific accumulation of Mn^{2+} seems to be dependent on CSF-brain transport mechanisms from the lateral ventricles leading to a facilitated uptake in adjacent areas (Bock et al., 2008a). On one hand the specificity of Mn^{2+} accumulation in different tissues has increased the knowledge about its selective neurotoxicity. On the other hand, the tissue specific enhancement of T1 weighted (T1w) signal also produces higher contrast images, enhancing the recognition of neuroarchitecture (Lucchini et al., 2000; Watanabe et al., 2002; Zheng et al., 2011). A number of studies have shown that images of detailed cytoarchitecture can be obtained from the rodent and bird brain, enabling even *in-vivo* visualization of brain development (Aoki et al., 2004b; Tindemans et al., 2006; Silva et al., 2008; Deans et al., 2008) . Manganese not only enables identification of specific brain regions, but also contrast within certain regions, which enables the detection of specific neuronal cell layers (Pautler and Koretsky, 2002; Soria et al., 2008). Besides contrast enhancement of brain tissue, Mn^{2+} is also used to produce higher contrast in non-CNS tissues such as the heart or eye, which enables volumetric studies of these structures and their substructures (Wendland, 2004; Berkowitz et al., 2006). Additionally, enhancement of ocular-, heart- and neuro-architecture has been used to study ocular injury, heart infarction, optic nerve injury and tumor development, stroke, hypoxic ischemia, brain and spinal chord injury and

Introduction

neurological diseases (for details see appendix table 2),

3. Mice and animal models examined for hippocampal differences

The method presented hereupon utilizes T1w signal enhancement of the hippocampus after systemic administration of $MnCl_2$ enabling a semi-automatic definition of hippocampal borders. This method is probed in animals with genetically determined smaller hippocampi (Cyclin D2 knockouts) and animals with a ibotenic acid lesioned hippocampi. Furthermore sensitivity of the method is examined in a mouse model of post traumatic stress disorder.

3.1. Cyclin D2

D-type cyclins are cell cycle regulatory proteins that control specific cyclin-dependent kinases. They are expressed in all proliferating cell types and mice lacking one of the three described D-type cyclins, D1, D2 and D3, show tissue specific abnormalities. D1-deficient mice show developmental and neurological disturbances, as well as abnormalities in the retina and mammary glands (Sicinski et al., 1995). Cyclin D2 knockout (KO) animals have disturbed gonadal cell proliferation and oncogenesis, showing abnormalities in testes and ovaries (Sicinski et al., 1996). Mice lacking D3-type cyclins also display deficiencies in the development of T lymphocytes (Sicinska et al., 2003). Most interesting with regard to hippocampal development is that, lack of functional cyclin D2 results in complete absence of proliferation of neuronal precursors in the adult brain, which was shown to affect neuronal number in the hippocampus and hippocampal volume (Kowalczyk et al., 2004). These animals still develop a brain with all structures present; however some are significantly reduced, including the hippocampus, occipital cortex,

cerebellum, and olfactory bulb (Kowalczyk et al., 2004).

3.2. Ibotenic acid

Ibotenic acid is a psychoactive substances in the mushroom fly agaric (*Amantia muscaria*) that are present in it in concentrations that can become harmful to the human body (Michelot, 2003). Ibotenic acid is a conformational derivatives of glutamic acid and has the ability to cross the blood-brain barrier (Olpe, 1978). Its primary action is at glutamate receptor sites, mainly agonizing glutamate receptors and direct application into the brain causes excitotoxic lesions with considerable loss of cells over a relatively large area (Walker et al., 1971; Cleland, 1996). However hippocampal application of ibotenic acid results in sharp boundaries separating damaged areas from non damaged areas (Jarrard, 1989). The advantage of ibotenic acid for lesion studies is the fact that it does not damage fibers of passage, and that afferents terminating in the lesioned area are minimally affected.

3.3. Posttraumatic stress disorder (PTSD)

Over 50% of the female and 60% of all male US citizens experience at least one traumatic event in their life (Kessler et al., 1995). Generally, the experience of a traumatic event does not lead to long-term psychological problems; however, one third of those who witness or experience a traumatic event develop PTSD, with some traumatic experiences, such as rape, associated with higher rates of over 50 % (Kessler et al., 1995). Disturbed memory of the trauma, in the form of re-experiencing certain details as well as problems with recollection of other details, are key features of PTSD. Malfunctioning of affective and cognitive processing are related to a number of characteristic symptoms of the disorder

Introduction

(Brewin, 2001; Brewin et al., 2007). These symptoms include impaired extinction of the fear responses, hypervigilance and hyperarousal (American Psychiatric Association, 2000). Cognitive impairment is commonly reported in PTSD patients, including memory and attentional deficits (Brandes et al., 2002). Memory impairments are predominantly shown explicit memory, such as difficulties to recall autobiographical details and difficulties in tasks of working memory (McNally et al., 1995; Golier et al., 2002; Vasterling et al., 2002; Brewin et al., 2007). A connection between explicit memory performance and hippocampal function has been widely shown and relates to numerous studies showing that PTSD patients have disturbed hippocampal integrity (Squire, 1992; Karl and Werner, 2010; Woon et al., 2010). PTSD patients show a decrease in hippocampal volume as well as in hippocampal N-acetylaspartate level (NAA), a metabolite exclusively present in neurons (Simmons et al., 1991). In line with this, long-term treatment with paroxetine, a selective serotonin reuptake inhibitor promoting neurogenesis and reversing the effects of stress on hippocampal atrophy, is associated with improvement of verbal declarative memory deficits and an increase in hippocampal volume leading to a significant improvement of PTSD-symptoms (Vermetten, 2003). Despite findings clearly indicating a relationship between PTSD and hippocampal integrity, a recent meta analysis showed that hippocampal shrinkage seems to be more generally related to trauma exposure than to the development of PTSD symptomatology (Woon et al., 2010). Additionally, the lower hippocampal integrity seen in PTSD patients has also been hypothesized to be a susceptibility factor for the development of PTSD (Gilbertson et al., 2002). This study observed a negative correlation between hippocampal volume and the development of PTSD in genetically identical twins, where one went into combat and the other stayed at home. The combat exposed twins, who developed PTSD had smaller hippocampal

Introduction

volumes than those combat exposed twins, who did not develop PTSD; however, hippocampal volume resembled that of the stay-at-home twin in both cases, indicating volumetric differences as a predisposition to the development of the disease. It should be noted, however that some studies also failed to see hippocampal differences in PTSD patients or hippocampal shrinkage after trauma exposure (De Bellis et al., 2001; Bonne et al., 2001). These controversies show, that the role of hippocampal integrity in PTSD is still not understood and needs further clarification. Clinical studies are limited by the number of patients available and the difficulty in performing longitudinal studies with participants being studied before and after trauma exposure, due to the inability to forecast a trauma. Additionally, confounding factors such as methodological and sample heterogeneity in terms of: type and severity of the trauma, incubation time, psychiatric comorbidities, medical treatment, age and drug abuse, make the interpretation of clinical data difficult. Such issues encourage the use of animal models to decipher the factors leading to the illness from the factors resulting from its development as well as clarify the involvement of the hippocampus in the development and maintenance of PTSD (Breslau et al., 2003; Golier et al., 2006). In the present thesis a study was conducted using the animal model of PTSD established in the group of Dr. Wotjak (Sigmund and Wotjak, 2007; Golub et al., 2010)

Introduction

4. Aims of the study

The major aims of the studies underlying this thesis are as follows:

- (1) Establishment of a manganese enhanced MRI (MEMRI) protocol in mice
- (2) Optimization of a Mn^{2+} application procedure to reduce toxic side effects
- (3) Development of an automatized method to determine hippocampal volume
- (4) Validation of volumetric MEMRI (vMEMRI) analysis
- (5) Application of volumetric analysis in mouse models of psychopathology

5. Structure of the thesis

The present doctoral thesis starts with a general description of the methods, followed by a specific description of the methods for each of the 3 studies and the experimental designs. The results and the discussion section is divided into studies dealing with Mn^{2+} toxicity, validation of volumetric MEMRI (vMEMRI) and the application of vMEMRI in a mouse model of post traumatic stress disorder. The thesis concludes with a general discussion of the results including an outlook. Study 1 deals with Mn^{2+} toxicity and introduces a method to considerably reduce toxic side effects. Study 2 deals with the validation of vMEMRI as a method to reliably determine hippocampal volume and its utilization it in animals with genetically and chemically modified hippocampi. Study 3 displays the application vMEMRI in a mouse model of psychiatric disorder. The underlying outlines and working hypothesis are outlined in the following.

6. Outlines and working hypothesis

6.1. Study 1: Manganese toxicity

As described in subsection 2.1 of this introduction, manganese is known to produce toxic side effects if the body is overexposed to it. This may lead to unwanted toxic side effects if Mn^{2+} is being used as contrast agent in MRI studies. Therefore, the underlying experiments of this chapter were aimed at determining the toxic side effects of Mn^{2+} in mice, when systemically applied in the form of manganese chloride ($MnCl_2$) at dosages routinely used in MRI studies. Furthermore it is explored, whether a fractionated application of $MnCl_2$ in small dosages is able to reduce these effects, allowing for an application which does not interfere with body temperature, locomotion or behavioral and endocrine function. The following working hypotheses were probed for study 1 :

- (1) Systemic application of Mn^{2+} , at dosages routinely used in MRI studies, leads to toxic side effects quantifiable with measures of locomotion and body temperature and behavioral and endocrine functioning.
- (2) Repeated application of manganese in small dosages minimizes toxic side effects and distress, while providing adequate MEMRI contrast.
- (3) Fractionated application of manganese has no long-term effects on learning and memory processes.

6.2. Study 2: Validation of volumetric MEMRI (vMEMRI)

As described, Mn^{2+} contrast enhancement in the brain is remarkably high within the hippocampus. A method to semi-automatically determine hippocampal volume with Mn^{2+} contrast enhancement named volumetric MEMRI (vMEMRI) is introduced, validated and tested in mice with genetically and chemically modified hippocampi. To validate whether

Introduction

hippocampal borders were properly detected by semi-automatic means, the obtained values were compared to manually obtained values. Cyclin D2 KO mice show no adult neurogenesis in the brain, which was shown to have an effect on hippocampal volume. It was tested whether the reported volumetric differences between cyclin D2 wildtype (WT) and KO animals could be detected with vMEMRI. Furthermore, mice were injected with ibotenic acid and detectability of hippocampal lesions of these animals was tested. Altogether, the following working hypothesis were addressed:

- (1) Semi-automatic detection of hippocampal volume correlates with manually obtained values
- (2) Cyclin D2 KO mice show smaller hippocampal volume compared to their WT littermates
- (3) Mice with lesioned hippocampi following ibotenic acid administration show smaller hippocampal volume

6.4. Study 3: Application of vMEMRI in a mouse model of PTSD

In the third study it was investigated whether trauma exposure leads to hippocampal volume decrease. Furthermore, it was tested whether this decrease could be prevented or whether hippocampal volume can be increased before trauma leading to a significant improvement of PTSD-symptoms as suggested by Vermetten and colleagues (Vermetten, 2003). Hippocampal neurogenesis was promoted housing the animals under an enriched environment rather than with the use of selective serotonin reuptake inhibitors (Kempermann et al., 1997). Volumetric changes were also investigated by means of ultramicroscopy along with vMEMRI (Dodt et al., 2007). The following working hypothesis were probed:

Introduction

- (1) Application of a trauma (shock) leads to a volume reduction of the hippocampus measurable with vMEMRI
- (2) Hippocampal volume changes and PTSD-like symptoms are modifiable by environmental conditions
- (3) vMEMRI can mirror volumetric alterations of the hippocampus measured with ultramicroscopy

Methods

B. Methods

The methods are divided into a general methods section and a section describing the specific methods and the experimental design for each study.

B.I. General Methods

1. Animals

A total of 348 animals were used. Study 1 experiment 1: n = 11, C57BL/6NCrI; study 1 experiment 2: n = 32, C57BL/6NCrI (therefrom also in study 2 experiment 1.1: n = 24); study 1 experiment 3.1: n = 70, C57BL/6NCrI; study 1 experiment 3.2: n = 72, C57BL/6NCrI; study 2 experiment 1.3 and experiment 2.1: n = 12, Cyclin D2; study 2 experiment 2.2: n = 23, C57BL/6NCrI; study 3 experiment 1 and study 2 experiment 1.1: n = 64, C57BL/6NCrI (therefrom also in study 2 experiment 1.4: n = 29); study 3 experiment 2: n = 64, C57BL/6NCrI. Male C57BL/6NCrI mice were purchased from Charles River (Sulzfeld, Germany) at the age of 6 – 9 weeks. Male cyclin D2 knockouts and wildtypes were provided by Dr. Anja Urbach¹. Animals were housed with an inverse 12:12 light/dark cycle (lights on at 21:00). They had free access to food and water. Animals were either housed singly or in groups where indicated.

The Committees on Animal Health and Care of the local government (Regierungspräsidium Oberbayern) approved all experimental procedures (AZ 55.2-1-54-2531-133-06 and 55.2-1-54-2531-41-09), which were carried out in accordance with the European Communities Council Directive of 24th November 1986 (86/609/EEC).

¹Friedrich-Schiller-University; Dept. of Neurology Experimental Neurology Erlanger Allee 101/FZL 07747 Jena

2. Manganese chloride application

A solution of 50 mM manganese chloride ($\text{MnCl}_2 \times 4\text{H}_2\text{O}$; Sigma, Germany) was prepared in 0.9 % NaCl. pH was adjusted to 7.0 with HCl and NaOH. MnCl_2 injections were administered intraperitoneally. The dosage of MnCl_2 administered was adjusted by injection volume.

3. Manganese Enhanced MRI (MEMRI)

3.1. MRI measurements

MRI experiments were performed on a 7 T Avance Biospec 70/30 scanner (Bruker BioSpin, Ettlingen, Germany). To enhance T1-weighted (T1w) MRI contrast, animals were injected with a manganese chloride (MnCl_2 ; cf. general methods 2). Mice were scanned 24 - 32 h after the last injection. Animals were anaesthetized with isoflurane (DeltaSelect, Germany) and fixed in a prone position on a saddle-shaped receive-only coil, where they were further kept under inhalation anaesthesia with an isoflurane-oxygen mixture (1.5–1.9 vol% with an oxygen flow of 1.2–1.4 l/min). Head movements were prevented by fixing the frontal teeth with a surgical fibre and by fixing the head with earbars (only for study 1 experiment 2 and 3, study 2 experiment 1 and 2.2). Body temperature was monitored with a rectal thermometer (Thermalert TH-5, Physitemp Instruments, USA) and kept between 34 °C and 36 °C using a heating pad. Pulse rate was continuously monitored by a plethysmographic pulse oxymeter (Nonin 8600V, Nonin Medical Inc., USA).

T1w brain images were acquired using a 3D gradient echo pulse sequence (TR = 50 ms, TE = 3.2 ms, matrix size = $128 \times 106 \times 106$ zero filled to $128 \times 128 \times 128$, field of view (FOV) = $16 \times 16 \times 18 \text{ mm}^3$, number of averages = 10, resulting in a spatial resolution of $125 \times 125 \times 140.6 \mu\text{m}^3$ with a total measurement duration of 90 min. Additionally, 3D T2-

Methods

weighted (T2w) images were obtained using a RARE (rapid acquisition relaxation enhanced) pulse sequence (TR = 1000 ms, TE = 10 ms, matrix size = $128 \times 112 \times 112$ zero filled to $128 \times 128 \times 128$, FOV = $16 \times 16 \times 18 \text{ mm}^3$, number of averages = 2, Rare factor = 16, $TE_{\text{eff}} = 78.6 \text{ ms}$, resulting in a resolution of $125 \times 125 \times 140.6 \mu\text{m}^3$, with a measuring time of around 30 min). T1w- and T2w-images were acquired using identical image orientation and geometry. Total measurement time was around 2 h.

3.2. MRI data processing

Images were reconstructed using Paravision software (Bruker BioSpin, Ettlingen, Germany) and transferred to standard ANALYZE format. Further post-processing was performed using SPM2 (www.fil.ion.ucl.ac.uk/spm). T1w- and T2w-images were first co-registered using affine transformations. Bias correction step is described in detail in the experimental design of study 2 (cf. experimental design 2.1.2). In short, images were bias-corrected to remove intensity gradients introduced by the geometry of the surface coil. A representative T1w- and T2w-image, respectively, of one animal was selected that served as a first template for the generation of a customized second generator template.

Normalization steps are described in detail in the experimental design of study 2 (cf. experimental design 2.1.4). Briefly, images of all mice were normalized to the single animal template chosen randomly from the group of images to be normalized. A group template was then produced based on an average of all images. Bias corrected images of all individual animals were then normalized a second time to the group template. For improved normalization of T1w-images, independent of extra-brain tissue as well as signal hyperintensity of large vessels in the T1w-images, normalization steps of T2w-images were carried out first. Due to the better contrast between parenchyma and other tissue

types and no signal hyperintensity of large vessels compared to T1w-images, a brain extraction step could be performed as follows: a binary mask defining the intracranial vault excluding large vessels (whole brain) was defined (MRicro, www.sph.sc.edu/comd/rorden/mricro.html) on the T2w-group template, and transformed to native (co-registered) space of each individual animal (by inverted spatial normalization). Brain extracted images of the co-registered and bias-corrected T1w-images were then used for the normalization steps of T1w-images. Regions of interest were depicted as described in the following. Binary masks were back-transformed into native space as described for the whole brain.

3.3. Regions of interest

Regions of interest (ROIs) were defined on the T1w-group template for selected structures (except for the whole brain ROI and when indicated), based on the anatomical atlas of the C57BL/6 mouse by Franklin and Paxinos (Paxinos and Franklin, 2004). The ROIs for the respective experiment were defined as follows:

Study 2 experiment 1.1: the bilateral inferior colliculi (colliculi), CA1+2 and CA3+dentate gyrus (DG) regions of the total hippocampus, the caudate putamen, the thalamus and hypothalamus, and part of the cortex (cf. figure 18). In addition, an area of the muscle surrounding the skull was defined to serve as a measure of global signal intensity.

Study 2 experiment 1.2: T1w- and T2w-images: two rectangular ROIs at the dorsal and at the ventral part of the brain respectively, one rectangular ROI the left side and the right side of the brain respectively (cf. figure 19 and 20).

T1w-images: the hippocampus and a region surrounding the hippocampus (cf. figure 19).

T2w-images: the whole brain and a ROI surrounding the whole brain (cf. figure 20).

Methods

Study 2 experiment 1.3: the total hippocampus

Study 2 experiment 1.4.1: the whole brain (cf. figure 21)

Study 2 experiment 1.4.2: the total hippocampus (cf. figure 21)

Study 2 experiment 2.1: the whole brain and the total hippocampus

Study 2 experiment 2.2: the total hippocampus

Study 3 experiment 1: the hippocampus and the central amygdala on both sides separately and the lateral ventricles and the olfactory bulb.

Volume measurements of each ROI were performed on the bias-corrected raw T1w-images of each animal using an in-house written software in IDL (www.creaso.com). Volume measurements are presented as volumes (mm³) or relative volumes, where volumes of extracted ROIs are divided by volumes of extracted whole brains. For study 2 experiment 1.1 also intensity measurements were performed. Mean intensities (summarized intensity divided by the number of voxels) of the ROIs within the brain are divided by the mean intensity of a muscle ROI.

3.4. Image presentation

All images are presented in their original image matrix size of 128 x 128 x 128 except for figure 17. To visualize the capacity of the fractionated application schemes and resolve cerebral fine structure, e.g. cortical layers, the original image matrix size provides insufficient resolution. Therefore, we reprocessed representative MEMRI images of each group to an image matrix size of 256 x 256 x 256 points with subsequent bias correction. On coronal sections, truncation artifacts ('Gibbs ringing') are visible which hamper precise evaluation of cortical layer structures, especially parallel to the skull surface. To avoid contamination by such artifacts, we only evaluated cortical structures running

perpendicular to the skull surface, e.g. the retrosplenial granular cortex (figure 17).

4. Ultramicroscopy

Brains were fixed in 4% and then 0.4% PFA (paraformaldehyde; Sigma-Aldrich, Munich, Germany) at 4°C for 10 and 4 days, respectively, followed by hippocampal dissection, blind to the history of the animals. Left and right hippocampi were pooled for each animal. The protocols described by Dodt and colleagues to obtain a transparent hippocampus for ultramicroscopic imaging were followed (Dodt et al., 2007). Briefly, hippocampi were dehydrated using a series of graded ethanol (EtOH, 50%, 80% and 96%, for 1 h each). After 100% EtOH overnight and a final step of 100% EtOH for 1 h, hippocampi were transferred to a mixture of benzylalcohol and benzylbenzoat (BABB, Sigma-Aldrich) at a ratio of 1:2.

Ultramicroscopic imaging was performed essentially as described before (Dodt et al., 2007). Briefly, specimens were placed on a black platform in a small chamber filled with BABB. The Argon-Ion laser beam (Innova 90, Coherent, Dieburg, Germany) with a wavelength of 488 nm was channeled to the specimens via two mirrors. A cylinder lens (80 mm focal distance) and a slit aperture (4 mm) were used to form the light sheet. Images were recorded by a charge-coupled device (CCD) camera (CoolSnap Cf, 1392 1040 pixels, Roper Scientific, Ottobrunn, Germany) using a 2.5 objective (numerical aperture (NA) = 0.12, Zeiss Fluar, Zeiss, Munich, Germany). Above the objective a band pass filter was positioned (Brightline HC536/40, AHF Analysetechnik, Tübingen, Germany). In this configuration 1 pixel accounted for 13.32 μm^2 . The camera was mounted on a modified microscope (Zeiss) which was oriented perpendicular to the light beam. About 700 images were then taken by moving the specimen chamber in increments of 3.65 μm vertically

Methods

through the light sheet.

For analyzing hippocampal volume (cf. figure 24), images were loaded into a custom-made IGOR routine. The area containing the hippocampal image on each recorded image was calculated and multiplied with the number of recorded images times 3.65 mm, reporting the hippocampal volume in mm³.

5. Mouse model of posttraumatic stress disorder (PTSD)

All experiments were performed during the active phase of the animals (lights off). The experimental setup and procedure was used as previously described (Kamprath and Wotjak, 2004). Freezing was analyzed to three different contexts: (1) the shock context, a cubic-shaped box made of transparent Plexiglas with a metal grid for shock application, (2) the grid context, a hexagonal shaped prism made of non-transparent Plexiglas with a metal grid floor as a dominant reminder of the shock context, and (3) the neutral context, a cylinder made of transparent Plexiglas with wood shavings as bedding. All contexts were cleaned thoroughly after each trial with different detergents: 70 % EtOH (shock context), 0.05% isoamylacetate (grid context) and 1% acetic acid (neutral context) and bedding was changed. Any changes to this procedure are indicated

For foot shock application, animals were placed into the shock chamber. After 198 s a single, inescapable, scrambled electric foot shock (2 s, 1.5 mA) was administered via the metal grid. Animals remained in the shock chamber for another 60 s before they were returned to their home cages. Control animals were also placed into the same context for 260 s without shock application.

Nonassociative, sensitized fear, context specificity and contextual fear tests were performed 4 weeks after shock application, and videotaped by small CCD cameras

Methods

(Conrad Electronics, Hirschau, Germany). Nonassociative, sensitized fear was measured by scoring freezing response to a 3 min tone presentation (80 dB, 9kHz) in the neutral context after a 3 min pre-exposure to the context. Animals were returned to their homecage 1 min after termination of the tone and a total of 7 min after being placed into the neutral context. Context specificity was tested the next day in the morning by a 3 min exposure to the grid context. To test for contextual fear, mice were re-exposed to the shock chamber for 3 min in the afternoon on the same day. Any changes to this procedure are indicated. Animals' behavior was rated off-line by a trained observer who was blind to the experimental condition of the animals (Kamprath and Wotjak, 2004). Freezing behavior was defined as immobility except for respiration movements.

6. Acoustic startle response (ASR)

Acoustic startle responses were measured as follows. Mice were placed into one out of 6 identical startle set-ups, consisting of a non-restrictive Plexiglas cylinder (inner diameter 4 cm, length 8 cm) mounted onto a plastic platform, each housed in a sound attenuated chamber (SR-LAB, San Diego Instruments SDI, San Diego, CA, USA). The cylinder movement was detected by a piezoelectric element mounted under each platform and the voltage output of the piezo was amplified and then digitized (sampling rate 1 kHz) by a computer interface (I/O-board provided by SDI). The startle amplitude was defined as the peak voltage output within the first 50 ms after stimulus onset and quantified by means of SR-LAB software. Before startle measurements, response sensitivities for each chamber were calibrated in order to assure identical output levels. Startle stimuli and background noise were delivered through a high-frequency speaker placed 20 cm above each cage. The 3 different startle stimuli consisted of white noise bursts of 20 ms duration

Methods

of 75, 105 and 115 dB(A) intensity (INT). Startle stimuli were presented in a constant background noise of 50 dB(A). Sound intensities were measured using an audiometer (Radio Shack, 33-2055, RadioShack, Fort Worth, TX, USA). On control trials only background noise was present. After an acclimatization period of 5 min duration, 10 control trials and 20 startle stimuli of each intensity were presented in pseudorandom order in each test session. The interstimulus interval was on average 15 s (13–17 s, pseudo-randomized).

The startle set-ups were located in a different room from the conditioning chambers and startle measurements were performed by a scientist unfamiliar to the animals' condition in order to avoid context reminders, thus minimizing confounding influences of context generalization. The plexiglas cylinders were cleaned thoroughly with soap water after each trial.

7. Conditioned odor avoidance (CODA) task

The conditioned odor avoidance (CODA) task was performed as described before (Pamplona et al., 2010). CODA was conducted in a rectangular box made of white polyvinyl chloride (PVC) walls and a dark gray PVC floor. The box was divided into three compartments (30 x 30 x 30 cm³ each) that were interconnected by small opening (6 x 5 cm²) with guillotine doors. A filter paper-lined Petri dish (10 cm diameter), containing own home-cage bedding (nest compartment, center), EtOH 70% or acetate 1% (left or right compartment, counterbalanced) was placed in each compartment. Ethanol and acetate compartments were also cleaned with the respective solution, whereas the center (nest) compartment was cleaned with a damp cloth and soapy water and dried with paper towels. For CODA testing, mice were enclosed in the nest compartment for 5 min (habituation

Methods

phase) followed by 5 min of free apparatus exploration (test phase). During testing, the latency to the first exit from the nest compartment, the number of entries into the ethanol and acetate compartments and the time spent in each of the compartments were recorded. The animals' behavior was observed and rated online by means of a CCD camera positioned above the CODA apparatus and a stop-watch.

8. Behavioral scoring in viewing arena

Behavior and general health status of the animals was assessed after each injection and prior to each blood collection (figure 5). All measures were assessed according to the European Mouse Phenotyping Resource of Standardized Screens guidelines (EMPRESS) (<http://empress.har.mrc.ac.uk>). Instructions given, for behavioural scoring in viewing arena: Use a clean arena (Makrolon type IV cage: L60.0 W38.0 H20.0 cm³). Remove a mouse from its home cage, gripping the tail between the thumb and the forefinger and place into the viewing arena. Record the following highlighted behaviours without disturbing the mouse. Record any incidents of bizarre behaviour, stereotypy and convulsions separately.

Body Position: Observe the mouse and identify whether it appears to be inactive, active or excessively active.

0 = Inactive; 1 = Active; 2 = Excessive Activity

Tremor: Make a note of whether or not the mouse appears to tremble.

0 = Absent; 1 = Present

Palpebral Closure: Study the mouse for palpebral closure.

0 = Eyes open; 1 = Eyes closed

Coat Appearance: Look carefully at the mouse coat and determine how tidy and well groomed it is, making a note of any deviances.

Methods

0 = Tidy and well groomed coat; 1 = Irregularities

Whiskers: Make a note of whether the mouse has intact or trimmed whiskers.

0 = Present; 1 = Absent (include any further comments)

Lacrimation: Make a note of the presence or absence of lacrimation.

0 = Absent; 1 = Present

Defecation: Make a note of whether or not the mouse defecates.

0 = Present; 1 = Absent

9. Endocrine measurements

To investigate activation of the hypothalamic-pituitary-adrenal axis (HPA-axis) in response to the different $\text{MnCl}_2 \times 4\text{H}_2\text{O}$ application schemes in study 1 experiment 2.2, corticosterone levels were measured in all animals on the first day, at time points 4 h (d1_4h) and 12 h (d1_12h) after Mn^{2+} -injection, and on the fifth day after 12 h (d5_12h) (figure 4). Blood samples were collected in capillary tubes containing ethylenediamine-tetraacetic acid (EDTA, Kabe Labortechnik, Germany) to prevent clotting. Samples were kept on ice until centrifuged (8000 RPM, 15 min, 48°C), after which plasma was collected and stored at -20°C. Plasma corticosterone measurements were performed using an ImmuChem Double Antibody Corticosterone ^{125}I -Radioimmunoassay kit (MP Biomedicals, Eschwege, Germany) with a minimal detectable corticosterone concentration of 7.7 ng/ml. The coefficients for intra-assay and inter-assay variation were 7.3% and 6.9%, respectively.

10. Telemetric measurements

For study 1 experiments 1 and 2.3 telemetric devices (TA10TA-F20, PhysioTel

Methods

Implant, Data Sciences international, St.Paul, USA) were implanted at least 14 days before starting of recordings for locomotion and body temperature.

For the implantation procedure, mice were anesthetized using a combination of ketamine/xylazine (50 mg/kg ketamine (Essex Pharma GmbH, Germany) + 5 mg/kg xylazinhydrochloride (Rompun, Bayer Health Care, Germany)). Transponders were purified and sterilized with benzalchonium chloride (Sigma, Germany), repeatedly flushed with sterile 0.9% NaCl and inserted into the abdominal cavity. The wound was disinfected by Braunol (Braun AG, Melsungen; Germany). For analgesia, 0.5 mg/kg Metacam (Vetmedica GmbH, Boehringer Ingelheim, Germany) was injected subcutaneously directly after surgery. Animals had a recovery period of at least 14 days within which body weight and health appearance were controlled.

The monitoring of body temperature and locomotion was carried out using the Dataquest LabPRO (Data Sciences International, Version 3.11, USA, Minnesota) acquisition system. Locomotion is displayed as activity counts for the detected period. Activity counts depended strictly on the distance the animal moved horizontally with a velocity of above 1 cm/sec. Following the recovery period, telemetric devices were turned on for a three-day baseline recording. As temperature and locomotion of the animals follow a circadian rhythm, deviations of these measures from a mean of the three day baseline was calculated. For study 1 experiments 1 and 2.3 animals first received a NaCl injection (0.1 ml/10 g) three days before the Mn²⁺ injection protocols to investigate the influence of a single vehicle application on temperature and locomotion. These data also served as control for subsequent Mn²⁺ injections. Temperature and locomotion measurements were averaged for bins of 30 min for each animal. Additionally means of the adjacent 7.5 h are calculated. Grand means are calculated by adding means of the adjacent 7.5 h of all

Methods

injections and dividing them by the number of injections.

11. Ibotenic acid

11.1. Solution

Five mg of ibotenic acid (Sigma Aldrich, Germany) were dissolved in 0,5 ml of phosphate buffered saline (PBS) 0,1 M, (pH = 7.4) resulting in a solution with a concentration of 10 µg ibotenic acid per 1 µl PBS (Etchamendy et al., 2003; Célérier et al., 2004; Chauveau et al., 2005). To facilitate the dissolving of the Ibotenic acid, small drops of sodium hydroxide were added to make the solution slightly basic (Suzuki et al., 2011).

11.2 Surgery

Animals were briefly anaesthetized in a glass cylinder filled with isoflurane vapour (Forene, Abott, Wiesbaden, Germany). For preoperative analgesia the unconscious animals were then injected with a solution of Ketamin 10%, 0,5 ml (100 mg per 1 ml injection solution, Belapharm GmbH, Germany) and Xylazin 2%, 2 ml (Rompun, 20 mg per 1 ml injection solution, Bayer Vital GmbH, Germany) plus 7,5 ml NaCl. Of this solution, animals received 0,1 ml per 10 g body weight. During surgery animals were kept deeply anesthetized with Isoflurane (1,5-1,9 vol%).

Anesthetized animals were mounted to a stereotactic frame (TSE-Systems, Heidelberg, Germany). Hippocampal lesions were made by bilateral injection of ibotenic acid at three sites per hemisphere by use of a microinjector pump (UltraMicroPump III + Micro4 Controller, World Precision Instruments Inc., USA) that was mounted to the stereotactic frame

Injection coordinates were: (i) anterior/posterior (AP): 1,2 mm caudal to bregma;

lateral (L): $\pm 1,2$ mm lateral to the midline; ventral (V): 2,0 mm below the exposed dura mater; (ii) AP, 2,5 mm; L, $\pm 2,5$ mm; V, 2,2 mm; (iii) AP, 3,3 mm; L, 3,1 mm; V, 4,1 mm.

Injection volume was in all cases 190 nl of the ibotenic acid solution. Injection was performed over the time course of two minutes. Afterward, the cannula was left in place for an additional three minutes to allow for diffusion. Then, the cannula was removed slowly to prevent ibotenic acid solution from spreading up the injection canal.

The wound was disinfected with Braunoderm (B.Braun, Melsungen, Germany) and closed with sutures. The recovery process was monitored by daily visual inspection.

12. Water cross-maze

The water cross-maze (WCM) is used to assess cognitive ability for spatial and habitual learning in mice by measuring their ability for spatial orientation (spatial learning) or, depending on the training protocol, their ability to learn an induced habit behavior (response learning). In a third learning protocol mice could either use spatial cues or learn an induced habit behavior (free choice learning).

12.1. Apparatus

The WCM (custom made, MPI of Psychiatry, Germany) is made from 1 cm thick transparent Plexiglass to allow for visual orientation in the experimental room (e.g. sink, small grey cabinet, etc.). It has four arms, giving it the shape of a cross, with each arm being 10 cm wide, 50 cm long and 30 cm high. The arms are labeled North (N), East (E), South (S) and West (W) in clockwise order. A removable clear acrylic glass shield of fitting dimensions blocks entrance into one arm completely, rendering the WCM a functional T-maze during the single runs. The maze rests on a white circular table (diameter: 180 cm;

Methods

height: 27; figure 2A). An escape platform (8x8 cm; height: 10 cm) made of transparent Plexiglas is positioned at one of the outer ends of the arms.

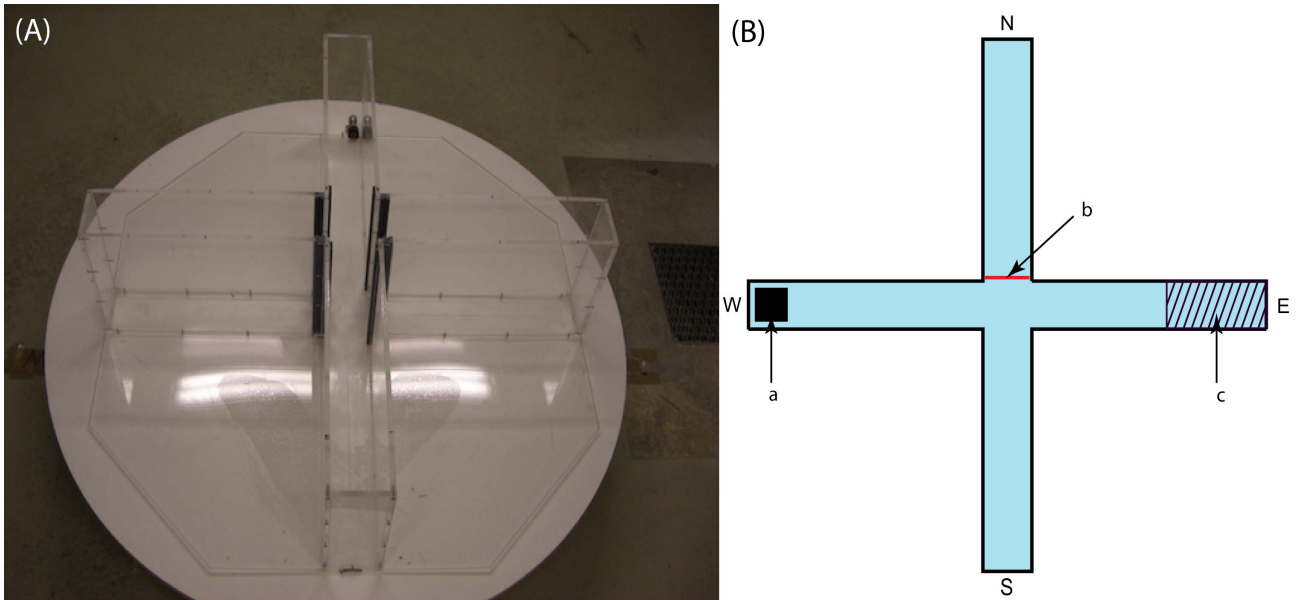


Figure 2: Water cross-maze (WCM): **A)** picture of the WCM apparatus. **B)** Diagram of the WCM. N: north, E: east, S: south, W: west, a: escape platform, b: separator, c: zone platform zone.

12.2. General procedure for training

The maze is filled up to 11.5 cm water level with fresh tap water at 23°C every day before testing. The escape platform is submerged by the water and has to be found by the animals to successfully complete a trial. Animals are brought into the room from an adjacent room, put into the water facing the wall and trained in one of three training protocols: the spatial training protocol, the response training protocol and the free choice training protocol. After completion of a trial, the animal is taken out of the water using a mesh scoop attached to a stick (without the experimenter touching the animal) and placed back into its home cage near an infrared light (150 Watt, GE, Germany) to dry and warm up. Half of the cage is placed outside the infrared beam to avoid overheating, to dry and warm up. Animals are tested in groups of six for each training protocol, resulting in an inter

trial interval of 10 minutes for the individual animal. The maze walls are dried and the water is stirred every three runs to avoid cuing of swimming paths by urine or pheromones as well as to remove potentially anxiogenic odors present despite dilution by the water. Swimming time is recorded with a standard laboratory stop watch (Digital Timer, VWR, Germany). The testing room is dimly illuminated, with 20 lx at the upper edge of the maze and 14 lx at the height of the platform at the animal's swimming level. The alignment of the WCM, in combination with the level of illumination, was chosen the way that cues were of similar visual salience.

12.3. Learning protocols

Learning protocols take place over a period of five training days. Each training day consists of six trials, for which starting positions are varied in a pseudo-random manner (NSSNNS on uneven days, SNNSSN on even days) to ensure correct balance of starting positions, while creating enough variability to avoid procedural learning. An exception is the free choice learning protocol for which animals are always started from south (figure 3).

12.3.1. Spatial learning protocol

The escape platform is always at the end of the W arm, while the animals starting position alternates between N and S in a pseudo-random manner (figure 3A). This learning protocol enforces spatial learning via allocentric navigation and requires acquisition of the spatially constant platform position to solve the WCM. This ensures that only the use of a spatial learning strategy is successful to escape the aversive situation (swimming, cold water) and spatial learning is thereby enforced.

Methods

12.3.2. Response learning protocol

The escape platform is always on the left side of the animal facing the middle of the maze (i.e. the animal has to perform a body turn to the left to find the platform). This means the position of the escape platform is spatially altered according to the starting position (i.e. start from S, escape platform is located W; starting from N, escape platform is located E; figure 3B). This learning protocol enforces response learning via egocentric navigation and requires acquisition of a constant body turn to solve the WCM. This ensures, that only a response learning strategy is successful in escaping the water maze and habitual learning thereby enforced.

12.3.3. Free choice learning protocol

In this protocol the spatial position of the escape platform and starting point are kept constant (figure 3C). This protocol allows for the use of either of the before mentioned navigation strategies (spatial-allothetic; response-egocentric) to solve the WCM.

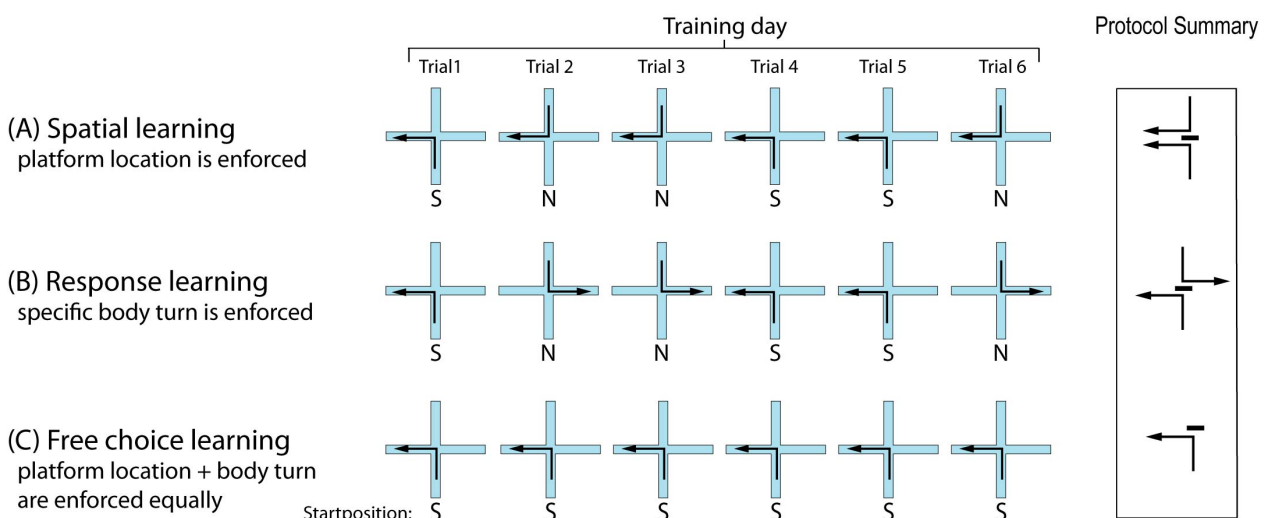


Figure 3: Training protocols for water cross-maze: Every training day consists of 6 trials. **A)** Spatial learning: For spatial learning animals started south (S) and north (N) in a pseudo-randomized manner with the escape platform always positioned west. **B)** Response learning: Animals started S and N in a pseudo-randomized manner with the escape platform always positioned to their left side when facing the middle of the maze. **C)** Free choice learning: animals always started S with the platform always positioned west.

12.4. Data presentation

Data is presented as accuracy. Accuracy measures success or failure of the animal to swim the correct path to the platform. An animal swims accurate if it enters no other arms other than the goal arm (the arm that contains the platform). It enters the goal arm only once and finds the platform and climbs onto it. In this case the run is given the value 1, if a run is not correct it is given the value 0. The sum of correct runs is divided by the total number of runs, and the percentage calculated [(number of correct runs/total number of runs)*100]. When a mouse swims minimum 5 out of 6 runs correctly, equal to an accuracy of 83,3%, it is considered a learner.

13. Data presentation and statistics

Generally all data are presented as mean \pm standard error mean (SEM), unless otherwise indicated, using GraphPad Prism 4.0 (GraphPad Software Inc., San Diego, CA, USA). The unit of all data is indicated. Relative calculations of data are described in the following.

MEMRI data is presented as volume or intensity (cf. general methods 3.2 + 3.3). Volume measurements are presented as volumes (mm³) or relative volumes, where volumes of extracted ROIs are divided by volumes of extracted whole brains. Volumes are calculated by multiplying the number of voxels (3 dimensional pixel) with the spatial resolution of $125 \times 125 \times 140.6 \mu\text{m}^3$. For study 2 experiment 1.1 also intensity measurements were performed. Mean intensities (summarized intensity divided by the number of voxels) of the ROIs within the brain are divided by the mean intensity of a muscle ROI.

Freezing responses to the different contexts were measured over the entire 3 min exposures and expressed as a percentage of the observation interval [(freezing time/total

Methods

interval time) x 100; cf. general methods 5]

Telemetric measurements are presented as locomotion or activity (cf. general methods 10). Locomotion is displayed as activity counts for the detected period. Activity counts depend strictly on the distance the animal moves horizontally with a velocity of above 1 cm/sec. Following the recovery period, telemetric devices were turned on for a three-day baseline recording. As temperature and locomotion of the animals follow a circadian rhythm, deviations of these measures from a mean of the three day baseline was calculated.

Learning in the water cross maze is presented as accuracy (cf. general methods 12.4). The sum of correct runs is divided by the total number of runs, and the percentage calculated $[(\text{number of correct runs}/\text{total number of runs}) \times 100]$.

Data were analyzed by t-test, one-way, two-way and repeated measurement analysis of variance (ANOVA) by means of SPSS 16.0 (Chicago, IL, USA). Statistica 5.0 (Statsoft, 1995). was used to conduct pair wise post-hoc comparisons. Applied statistical test and post-hoc test, if appropriate, are indicated in the respective result section. Correlations were conducted by spearman rank correlation test or pearson correlation where indicated. Statistical significance was accepted for $p < 0.05$.

B.II. Experimental design

1. Study 1: Manganese toxicity

All Mn²⁺ or vehicle injections were administered intraperitoneally (i.p.). To account for the circadian rhythm of body temperature and locomotion, a three day baseline of these values was calculated. Experimental values were compared to this calculated baseline (cf. general methods 10). Circadian fluctuations in corticosterone secretion were counterbalanced by always injecting the animals at the beginning of the dark phase. Animals were returned to their home cages after each injection.

1.1. Single application of manganese

In a pilot experiment the impact of a dosage of 99 mg/kg MnCl₂ on locomotion and body temperature compared to a control injection of similar volume of 0.9% NaCl in 11 C57BL/6N mice was determined. This dose of MnCl₂ is below the LD₅₀ of 121 mg/kg and below maximal nontoxic dosages used via i.p. injection in previous MEMRI studies (Silva et al., 2004). This was a within subject design with control injections performed one week before MnCl₂ injection. For measurement of locomotion and core temperature animals were surgically implanted with telemetric devices at least 2 weeks before baseline measurement (cf. general methods 10).

1.2. Comparison of different fractionated application protocols of manganese

To determine whether repeated application of smaller dosages produce lower toxic side effects, the impact of different application protocols on body temperature and locomotion, and behavioral and endocrine functioning was tested. Thirty two C57BL/6N mice were randomly assigned to one of two groups. The first group consisted of 24

Methods

animals, that were used to investigate behavioral markers and activation of the hypothalamic-pituitary-adrenal axis (HPA-axis) in response to the different MnCl_2 application schemes. The second group consisted of 18 animals, that were used to investigate locomotion and body temperature with telemetric recording in response to the different MnCl_2 application schemes.

For measurement of behavioral markers and activation of the hypothalamic-pituitary-adrenal axis, animals were randomly assigned to one of four subgroups containing six animals per group: The first group received three injections of 60 mg/kg MnCl_2 with an inter-injection interval of 48 h (hereafter referred to as 3x60/48). The second group received 8 injections of 30 mg/kg of the solution with an inter-injection interval of 24 h (hereafter referred to as 8x30/24). The third group received a single injection of 99 mg/kg (1x99). Since two animals of the third group showed severe side effects of Mn^{2+} toxicity shortly after injection and had to be sacrificed, the injection protocol was changed for the remaining four animals to 6 injections of 30 mg/kg with an inter-injection interval of 48 h (hereafter referred to as 6x30/48). The fourth group served as a control group, receiving three injections of similar volumes of 0.9% NaCl every 48 h (figure 4). Behaviour and general health status of the animals was assessed according to EMPRESS guidelines (<http://empress.har.mrc.ac.uk>; cf. general methods 8) after each injection and prior to each blood collection. Corticosterone levels were measured in blood taken from the tail vein (cf. general methods 9). Blood samples were taken from all animals on the first day, at 4 h (d1_4h) and 12 h (d1_12h) after MnCl_2 injection, and on the fifth day 12 h after injection (d5_12h; figure 4).

For telemetry, animals were randomly assigned to one out of three subgroups containing six animals per group. One group received the 3x60/48 protocol, one group the

Methods

8x30/24 protocol and one group the 6x30/48 protocol. All animals received a vehicle injection of similar volumes of 0.9% NaCl, 3 days before MnCl₂ injections started. Telemetric devices were implanted at least 14 days before starting of the recordings (figure 5)

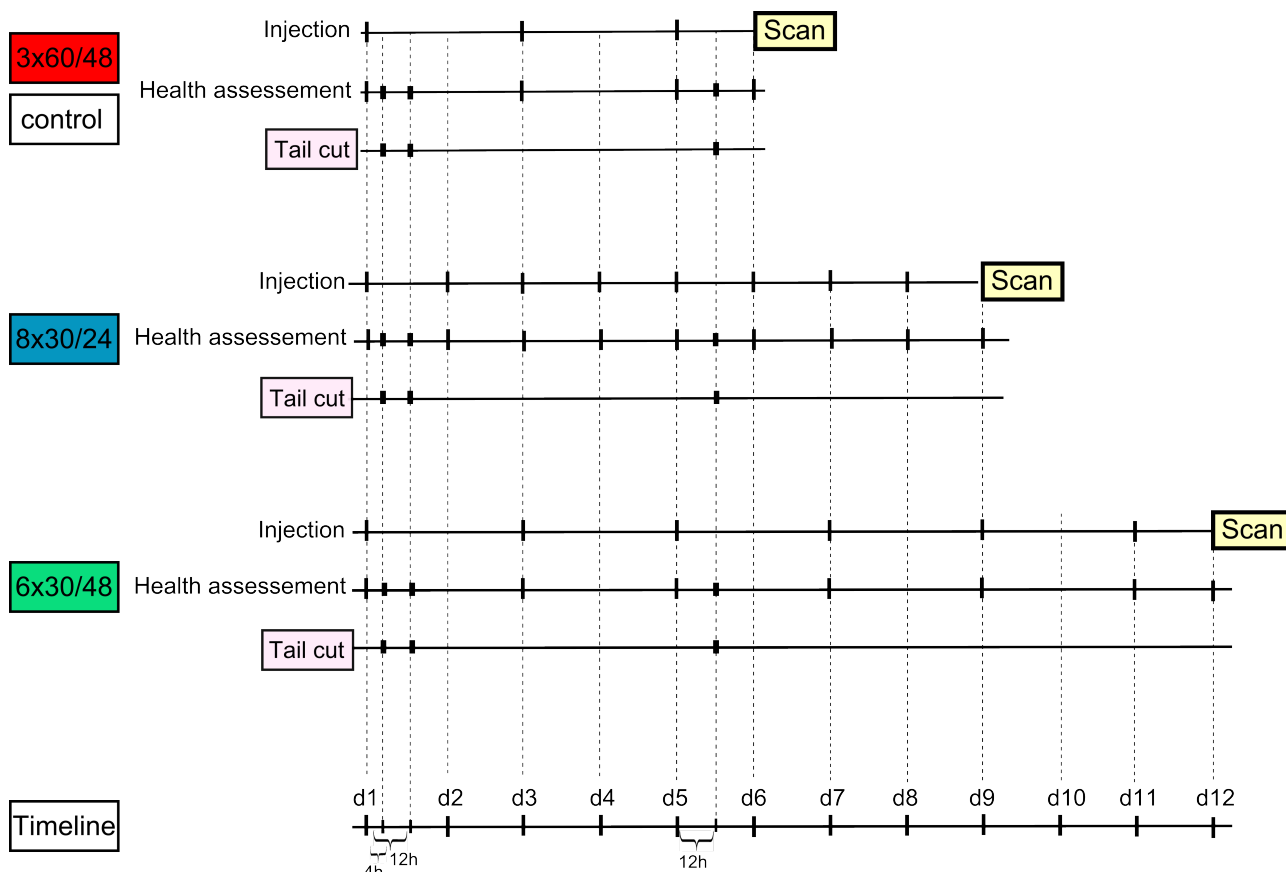


Figure 4: Experimental schedule of health assessment and corticosterone measurements (tail cut), after fractionated application of MnCl₂. Time points of injections (application schemes), health assessment, corticosterone measurements, and the MR scanning (scan) are indicated. Control animals were injected according to the 3x60/48 scheme. 3X60/48: 3 injections of 60 mg/kg MnCl₂, inter-injection interval 48 h; 8x30/24: eight injections of 30 mg/kg MnCl₂, inter-injection interval 24 h; 6x30/48: six injections of 30 mg/kg MnCl₂, inter-injection interval 48 h;

Methods

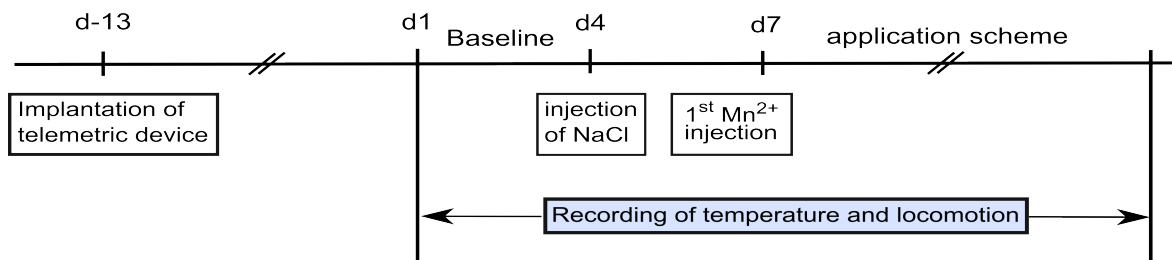


Figure 5: Experimental schedule of telemetric measurements. After implantation of the telemetric device, animals had two weeks of recovery after which a three day baseline recording was started. A NaCl injection was applied three days prior to starting point of the MnCl₂ application scheme (cf. figure 4).

1.3. Acute and long-term effects of manganese application on associative and specific hippocampus-dependent learning

1.3.1. Effects of manganese application on on associative learning

To determine whether manganese application has an effect on associative learning (i.e. contextual fear and fear conditioning), mice were injected prior to the procedure of the PTSD model (cf. general methods 5). After three weeks of single housing 70 C57BL/6N mice were randomly assigned to one out two groups. The first group (n = 42) received MnCl₂ injections according to the 8x30 protocol. The second group (n = 28) received eight vehicle injections of similar volume of 0.9% NaCl. Twenty-four hours after the last injection every animal was scanned. Within every group animals were assigned to receive either a shock or to serve as non-shock controls, with at least 10 days between scanning and shock exposure. This results in four groups: (i) 14 non-shocked (NS) vehicle (Veh) treated animals (ii) 14 shocked (S) Veh treated animals (iii) 14 NS MnCl₂ treated animals (iv) 28 S MnCl₂ treated animals. All animals were tested for freezing to the shock context, a neutral context and a context reminder (cf. general methods 5), hyperarousal (i.e. startle response; cf. general methods 6) and other PTSD-like symptoms (i.e. conditioned odor avoidance (CODA); cf. General methods 7) four weeks after shock application or exposure

to the shock context (Figure 6).

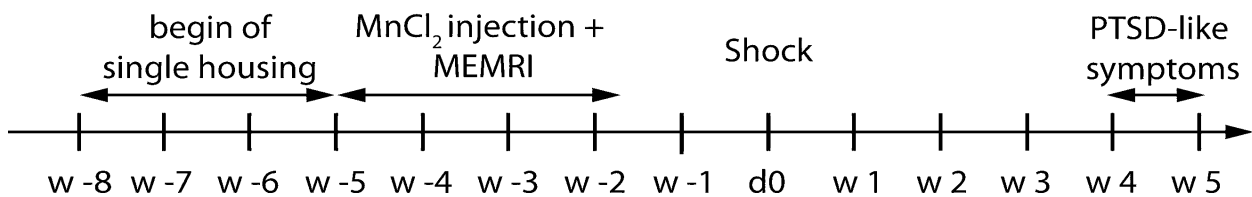


Figure 6: Experimental schedule of testing for long term effects of manganese application on hyperarousal and contextual learning. All animals were housed singly beginning eight weeks before shock application (w-8). Beginning five weeks (w -5) before shock animals were either treated with MnCl₂ or NaCl according to the 8x30 protocol and scanned 24 h after last injection. Shock application was done at least 10 days after scanning. All animals were tested for contextual fear and hyperarousal four weeks after shock (PTSD-like symptoms).

1.3.2. Effects of manganese application on learning in the water cross-maze

Short-term effects of MnCl₂ application on spatial, response and free choice learning were tested in the water cross-maze (cf. general methods 12). Mice were injected with MnCl₂ according to the 8x30 protocol (cf. general methods 2 and study 1 experiment 1), with injections in the evening at approximately 9:30 pm (i.e. at the end of their activity phase) to allow manganese accumulation in the pituitary and the brain during the night and to account for circadian rhythm of corticosterone secretion. Three groups, each group consisted of 12 mice, were trained on 5 consecutive with either the spatial, place or free choice protocol (cf. general methods 12.3) beginning at least 12 h after MnCl₂ application. Mice were not trained after the first injection to avoid increased stress levels (cf. study 1 results experiment 2.2). An equal number of control animals (n = 36) were tested with each protocol without injection.

2. Study 2: Validation of vMEMRI

2.1. Methodological validation of vMEMRI

Methodological validation of vMEMRI was conducted by testing several different

Methods

parameters of the analysis process. First, it was determined which of the different fractionated application protocols of MnCl_2 delivered the best contrast enhancement. Signal enhancement within the brain after the different fractionated application protocols was examined on images of the same 24 animals that were used to investigate behavioral markers and activation of the HPA-axis (cf. study 1 experiments 2.2 and 2.3). The animals were scanned 24 h after the last MnCl_2 application (cf. figure 4).

Second, signal gradients¹, introduced by the geometry (saddle shape, slightly higher on one side) and placement (directly above skull of the mouse) of the surface coil, from dorsal to ventral and from left to right, were determined and adjusted by bias correction. To test parameters for bias correction images from the animals of the first PTSD-study of study 3 (cf. study 3 experiment 1) were reanalyzed.

Third, general accuracy of manual ROI definition was verified with three task-trained raters that analyzed the same image data set of 12 animals independently.

Fourth, manual detection of the brain and hippocampal volume were conducted. With manual detection ROIs are defined on every individual image, whereas with semi-automatic detection, which uses the normalization option of the analysis program SPM2², ROIs are defined once on a group template. The comparison of manual and semi-automatic determination of brain and hippocampal volume was done with images from 29 randomly chosen animals of the first PTSD study of study 3 (cf. study 3 experiment 1).

All definitions of ROIs were performed by a task-trained scientists blind to the experimental condition of the animals. Methodological proceedings of the different steps are described hereafter.

1 Uncorrected images show higher signal in the dorsal vs. ventral and the left vs. right brain regions

2 Statistical parametric mapping (analysis program; www.fil.ion.ucl.ac.uk/spm)

2.1.1. Image contrast of the different fractionated application protocols of manganese

In order to determine which fractionated application protocol produced the best contrast (cf. figure 4 and study 1 experiment 2), ROI analyses were conducted on whole brain intensity and several cortical and subcortical structures (cf. figure 18). These structures included the caudate putamen, part of the cortex, CA1 and CA2 subregions of the hippocampus, the hypothalamus and the thalamus. Note that figure 18 only depicts one slice, however, ROIs were outlined on all slices including the defined region. All ROIs were defined according to the Paxinos mouse brain atlas (Paxinos and Franklin, 2004). To account for unspecific differences in signal intensity, which are not related to manganese enhancement, values were normalized to the intensity of surrounding muscle tissue.

2.1.2. Bias correction

T1w- and T2w-images were first aligned using affine¹ transformations. Before images were bias corrected, all raw images were cut out with a the same cuboid shaped ROI to separate them from the main part of the tissue surrounding the brain, which could interfere with the bias correction (figure 7). Different bias correction parameters were tested ranging from no bias correction to strong bias correction: no bias, light, medium, strong and very strong. Note that SPM¹ uses misleading denomination namely hard for light bias correction and light for strong bias correction. ROI analysis was conducted to determine the bias correction parameter which adjusts the signal gradient without disturbing the contrast between tissues (cf. figure 7). The adjustment of the dorsal-ventral

¹ Consists of a linear transformation followed by a translation

¹ Statistical parametric mapping (analysis program; www.fil.ion.ucl.ac.uk/spm)

Methods

field gradient was determined by comparison of dorsal and ventral ROIs. Adjustment of lateral differences in signal intensity were determined by comparing a ROI from the left side of the brain with a ROI from the right side of the brain. Additionally, a brain and a non-brain ROI for T2w-images and a hippocampus and a hippocampus surrounding ROI for T1w-images were defined to determine whether the contrast between the tissues was preserved by the different bias corrections.

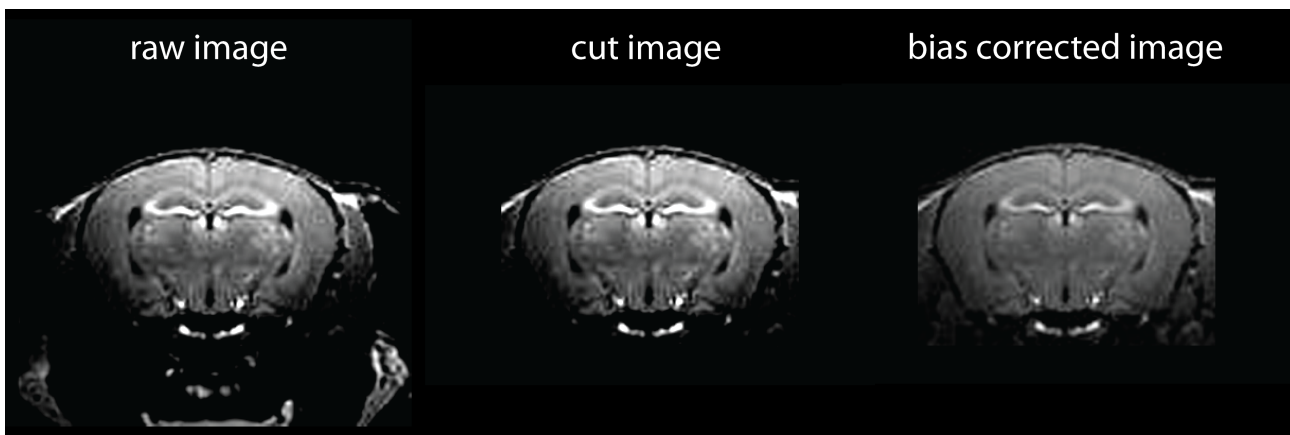


Figure 7: Scheme of proceedings for bias correction of the images. Raw images (left) were cut with a cuboid ROI to separate them from the main part of the non-brain tissue. Bias correction was conducted on cut images (middle). An individual manganese enhanced T1-weighted (T1w) image of a C57BL/6N mouse is shown. Note that both, T1w- and T2w-images underwent same procedure.

2.1.3. Accuracy of manual determination of hippocampal volume

To test for accuracy of manual ROI definition, three individuals were trained to rate images manually. The raters had prior no experience in evaluating MR images. The training included program handling and introduction into basal anatomy of the mouse brain. Each rater was given the T1w-images of the 12 Cyclin D2 animals (to ensure high variability of hippocampal volume), with no indication of the genotype of the animal. Each rater was instructed to independently delineate the hippocampus manually with MRIcro (www.sph.sc.edu/comd/rorden/micro.html) on each slide where it is visible.

2.1.4. Comparison of semi-automatic and manual determination of volume

For improved normalization of T1w-images, independent of extra-brain tissue as well as signal hyperintensity of large vessels in the T1w-images, normalization steps of T2w-images were carried out first. As both, T1w- and T2w-images were aligned and acquired with the same geometry, ROIs acquired for T2w-images could also be applied on T1w-images. Since manual ROI determination is a very reliable method (cf. study 2 results experiment 1.3), the semi-automatic results were proofed against the manually determined results for brain and hippocampal volume.

2.1.4.1. Brain volume

Ultimately, T1w-images will be used in whole brain analysis because it is these images that show the Mn^{2+} enhanced contrast. However, due to the relatively intense imaging of blood vessels on the ventral side of the brain in T1w-images, they cannot be used for whole brain normalization procedures. Direct normalization of whole brain T1w-images would result in a normalization highly biased to the blood vessels themselves. Due to the better contrast between brain tissue and other tissue types and no signal hyperintensity of blood vessels in T2w-images compared to T1w-images, a brain extraction step was performed on T2w-images as shown in figure 8. From all bias corrected raw images (original images) one is randomly chosen to serve as a template (individual template) to which all the other images are normalized. Normalization is achieved by morphing each image in three dimensions to match the size and layout of the individual template. A group template (1st group template) was generated by averaging the normalized images and served as a template for the second normalization. The generation of a group template was conducted to avoid biases of the normalization images due to

Methods

Whole brain extraction

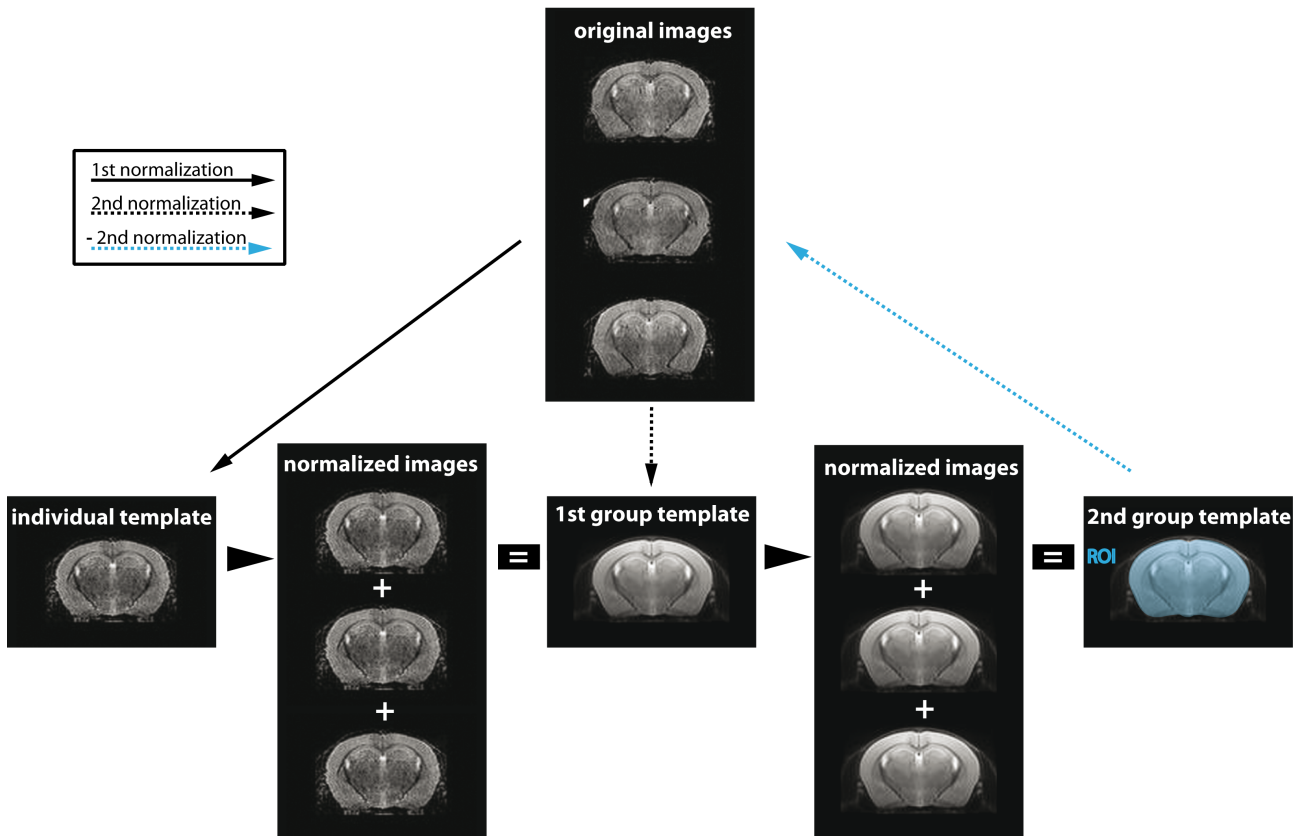


Figure 8: Brain extraction. Original T2w-images (Bias corrected) were normalized (solid arrow) to an individual template (representative image of one animal). A 1st group template was generated by averaging the normalized images. The original images were normalized (dotted arrow) to the 1st group template and a 2nd group template was generated by averaging the resulting images from this normalization step. On the 2nd group template a whole brain ROI was defined. This ROI was transformed to the original images of each individual animal by applying the inverted 2nd normalization step (blue dotted arrow). T2w-images of C57Bl/6N mice are shown. T2w-images do not show signal enhancement due to manganese. Note that whole brain extraction of only 3 images is shown here. The procedure can be done with various number of images.

specific characteristics of the individual template. The original images were normalized again to the 1st group template and a 2nd group template was generated by averaging these normalized images. On the 2nd group template a whole brain ROI was defined, which excluded areas where large ventral blood vessels would be seen in the T1w images. The resulting binary mask (ROI) of the whole brain was transformed to fit the original images of each individual animal by applying the 2nd normalization step in reverse. The transformed binary masks could then be used for brain extraction of the T1w-images that excluded the

large vessels. Brain extracted images of the aligned and bias corrected T1w-images were then used for the normalization steps of T1w-images. To determine the normalization parameters resulting in an adequate transformation of the images, the images from 29 C57Bl/6N mice were randomly chosen from an experiment and reanalyzed. Transformed ROIs were compared to ROIs that were manually determined for each individual.

2.1.4.2. Hippocampal volume

The extraction of the hippocampus was conducted similar to the brain extraction procedure using the T1w-images obtained from the whole brain analysis procedure (figure 9). Brain extracted images from the bias corrected raw images (original images) were normalized to an individual template, an image selected randomly from the original images. A mean group image was generated from the normalized images (1st group template). This served as template for a second normalization. The original images were normalized to the 1st group template and a 2nd group template was generated by averaging the normalized images. On the 2nd group template a hippocampal ROI was defined. The resulting ROI of the hippocampus was transformed to fit original images of each individual animal by applying the 2nd normalization step in reverse. The transformed binary masks (ROIs) could then be used for hippocampal extraction on the original T1w-images. To determine normalization parameters resulting in an adequate transformation of the images, transformed ROIs were compared to ROIs that were manually determined for each individual.

Methods

Hippocampus Extraction

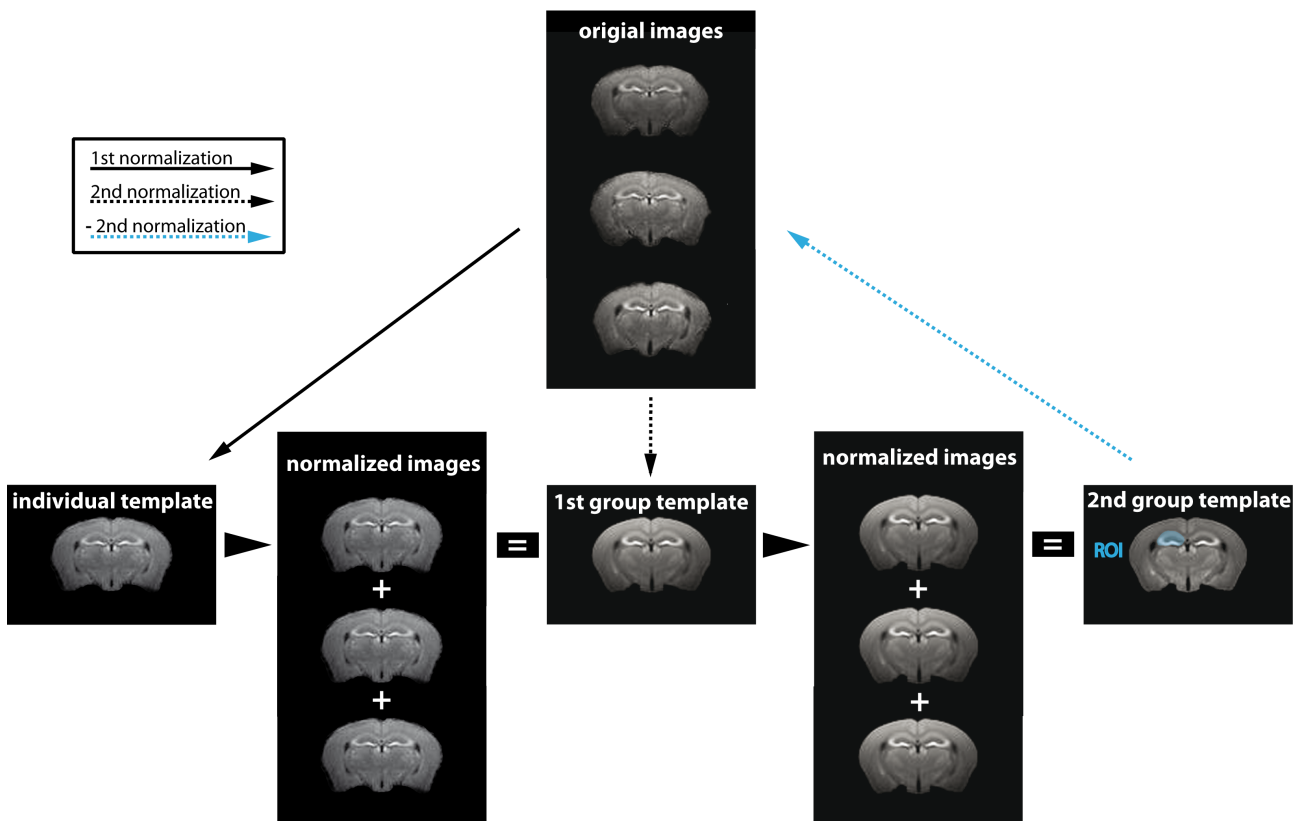


Figure 9: Hippocampal extraction. Original manganese enhanced T1w-images (Bias corrected, brain extracted) were normalized (solid arrow) to an individual template (representative image of one animal). A 1st group template was generated by averaging the normalized images. The original images were normalized (dotted arrow) to the 1st group template and a 2nd group template was generated by averaging the resulting images from this normalization step. On the 2nd group template a hippocampal ROI was defined. This ROI was transformed to the original images of each individual animal by applying the inverted 2nd normalization step (blue dotted arrow). Manganese enhanced T1w-images of C57Bl/6N mice are shown. Note that hippocampal extraction of only 3 images is shown here. The procedure can be done with various number of images.

2.2. Experimental validation of vMEMRI

To validate whether the vMEMRI method works, the method was tested in animals with presumably big differences in hippocampal volume. These included mice with genetically altered adult neurogenesis in the hippocampus (Cyclin D2 KO) and C57Bl/6N mice with ibotenic acid lesioned hippocampi.

2.2.1. vMEMRI in cyclin D2 animals

For vMEMRI in Cyclin D2 animals, n = 6 KO animals and n = 6 WT littermates were scanned. Animals were injected with the 3x60/48 protocol and scanned 24 h after last injection (cf. figure 4 and study 1 experiment 2).

2.2.2. vMEMRI in ibotenic acid lesioned animals

Surgery and intracerebral infusion (cf. general methods 11) of ibotenic acid or vehicle were done between 50 and 64 days before application of the 8x30/24 protocol. Animals were scanned 24 h after the last injection. Eleven vehicle treated and 12 ibotenic acid injected C57Bl/6N mice were scanned. As ibotenic acid animals showed high variability of hippocampal structure, images were reanalyzed manually.

3. Study 3: Application of vMEMRI in a mouse model of PTSD

In the first set of experiments of this study, trauma-related changes in behavioral performance (PTSD-like symptoms) and hippocampal volume were tested. Behavioral and volumetric consequences were compared between animals housed under normal and enriched conditions. In the second second set of experiments, behavioral and volumetric consequences following trauma exposure were assessed in groups of animals which differed in the time point of enriched housing exposure with respect to the trauma.

3.1. Experiment 1: volumetric and behavioral changes after trauma and environmental enrichment

Animals were housed in groups of four in either standard cages (Makrolon type II cages: length: 26.5 cm, width: 20.5 cm, height: 14.5 cm) with regular bedding and wood

Methods

shavings as nest material or in an enriched environment, provided by larger cages (Makrolon type IV cages: length: 60.0 cm, width: 38.0 cm, height: 20.0 cm) and running wheels and toys that were changed every week. Six weeks later, half of the animals of each housing condition received an inescapable foot shock, while the other half was placed in the shock chamber without any shock delivery (exposure controls; cf. general methods 5). Animals were returned to their home cages and kept under their respective housing conditions. One month after the shock exposure all animals were tested for hyperarousal (i.e. acoustic startle responses), fear generalization (i.e. freezing in the grid context) and contextual fear (i.e. freezing in the shock chamber context; cf. general methods 5). Behavioral tests were followed by vMEMRI with an application of the 3x60/48 protocol (cf. figure 4 and study 1 experiment 2.). Mice were scanned 24h after the last Mn²⁺ injection (cf. figure 4). Mice brains were fixed directly after scanning followed by hippocampal dissection for ultramicroscopy (cf. general methods 4). The experimental data is presented first for the standard housed group alone, to determine behavioral changes and volumetric changes of the hippocampus in reference to trauma exposure (results study 3 experiment 1.1.). The subsection 1.2. includes animals housed in enriched conditions, investigating behavioral effects and volumetric effects on the hippocampus of an enriched environment in shocked and non-shocked animals. In subsection 3.1.3. morphological changes in other brain structures are assessed.

3.2. Experiment 2: effects of pre- and post-shock environmental enrichment on PTSD-like symptoms and hippocampal volume loss

Animals were randomly assigned to one out of four groups, which differed in the time point of enriched housing exposure with respect to the trauma. Except for time point

Methods

and duration of environmental enrichment exposure, the housing conditions remained as described for Experiment 1. Group 1 was housed under standard conditions throughout the experiment. Group 2 was housed under enriched conditions throughout the experiment. Group 3 was housed under enriched conditions before trauma and under standard conditions after trauma, whereas group 4 was housed under standard conditions before trauma and enriched conditions after trauma. All animals received an electric foot shock and PTSD-like symptoms were assessed as described for the first set of experiments for this study.

Results

C. Results

1. Study 1: Manganese toxicity

1.1. Single application of manganese

As shown in figure 10A, animals injected with 99 mg/kg MnCl_2 show a maximal mean body temperature deviation from a three day baseline of $-7.3\text{ }^\circ\text{C}$, whereas the vehicle injection, with similar volume of 0.9 % NaCl, shows a mean temperature drop of maximal $0.2\text{ }^\circ\text{C}$. Low body temperature after MnCl_2 application returned to baseline levels over 12.5 h after injection. The mean over the 12.5 h following the injection shows highly significant differences in temperature between vehicle (0.04 ± 0.04) and MnCl_2 (-4.31 ± 0.68) injection ($p < 0.001$, paired t-test; figure 10B). Locomotion is measured as locomotion counts, which are strictly dependent on the distance the animal moves with a velocity of above 1 cm/s. Locomotion counts 12.5 h after MnCl_2 injection are exclusively negative, meaning locomotion is reduced, with a minimum of -3.1 locomotion counts. On the other hand, after i.p. injection of NaCl, locomotion deviation from a three day baseline is both, negative and positive, ranging from -0.3 to 0.4 (cf. figure 10C). The grand mean over the 12.5 h following the injection shows significant differences in locomotion between vehicle (-0.06 ± 0.15) and MnCl_2 (-1.6 ± 0.16) injection ($p < 0.001$, paired t-test, figure 10D). Both locomotion and temperature measurements show an exclusively high negative deviation (i.e. reduction) in their values from a three day baseline after MnCl_2 injection. Measurements after NaCl injection show small deviations around the mean (cf. figure 10A+C). Grand means of the adjacent 12.5 h after MnCl_2 and NaCl injection reveal highly significant differences in temperature and locomotion deviation (cf. figure 10B+D).

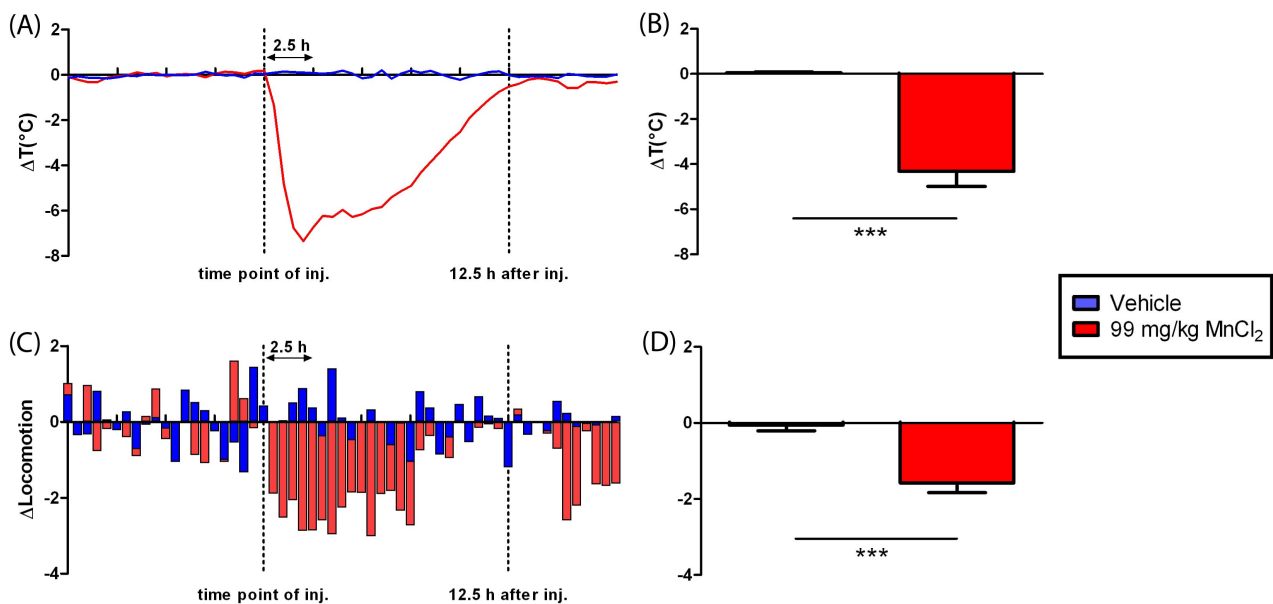


Figure 10: Effect of a single i.p. injection of 99 mg/kg manganese chloride (MnCl_2) or 0.9% NaCl (Vehicle) on locomotion and body temperature: A) Body temperature deviation shown as a mean curve of 0.5 h intervals before and after the injection (inj.) from the corresponding 0.5 h intervals of the three day baseline mean. The 99mg/kg MnCl_2 injection shows a mean temperature drop of 7.3 °C whereas the vehicle injection shows temperature drop of maximal 0.2 °C. **B)** Grand mean of body temperature over adjacent 12.5 h after injection. **C)** Locomotion deviation shown as mean column bars of 0.5 h intervals after the injection (inj.) from the corresponding 0.5 h intervals of the three day baseline mean. The 99mg/kg MnCl_2 injection shows a mean locomotion count drop of 3.0 whereas the vehicle injection shows locomotion count drop of maximal 1.4. Locomotion counts are strictly dependent on the distance the animal moves with a velocity of above 1 cm/s. **D)** Grand mean of locomotion counts over adjacent 12.5 h after injection. *** $p < 0.001$ (paired t-test)

1.2. Comparison of different fractionated application protocols of manganese

The following data has already been published (Grünecker, Kaltwasser et al., 2010)

1.2.1. Visual image contrast of different fractionated application protocols of MnCl_2

Visual inspection of T1 weighted images (figure 11) after application of different application protocols of MnCl_2 shows that all images of animals injected with Mn^{2+} show higher signal intensities than images of NaCl injected (control) animals. The 8x30/24 group shows highest intensity and best contrast enhancement, followed by the 3x60/48 and 6x30/48 group. The hippocampus is outlined best in the 8x30/24 group. Chapter II experiment 1.1 will take a closer look on image contrast of the different fractionated

Results

application protocols of MnCl_2 .

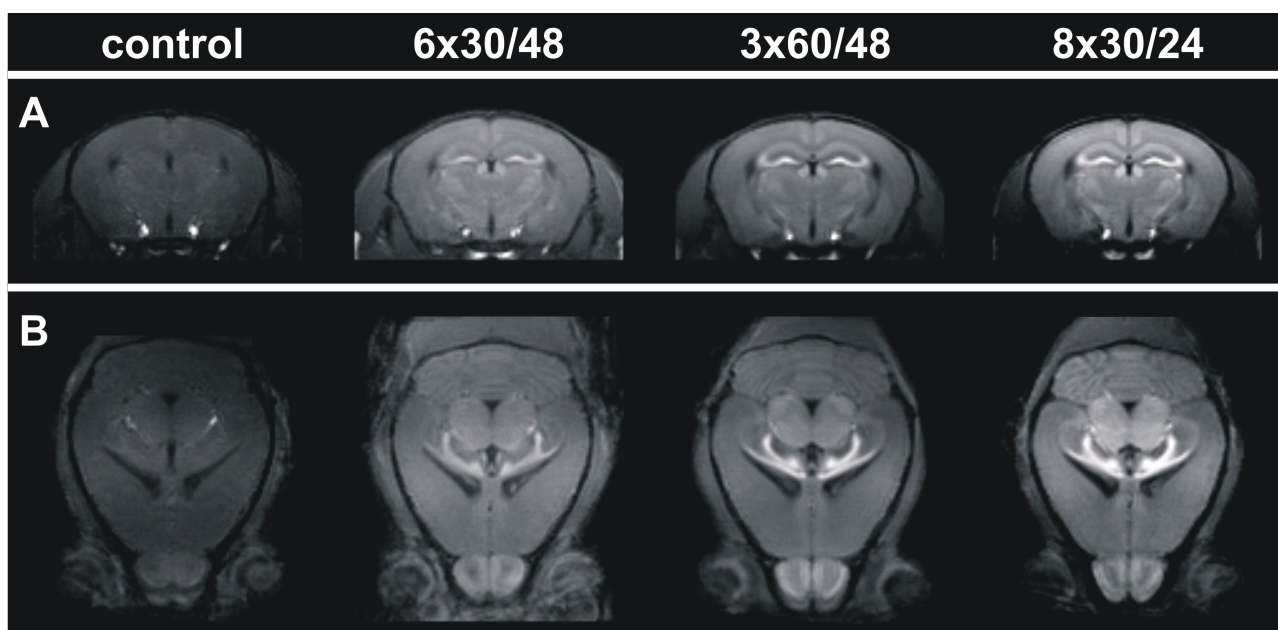


Figure 11: Image contrast of different fractionated application protocols of MnCl_2 . A) Coronal and B) horizontal slices of T1 weighted images for control, 6x30/48, 3x60/48 and 8x30/24 application schemes. Mean images of the different groups are shown.

1.2.2. Health assessment

The general health status (general methods 8) of the animals was assessed after every injection and blood collection (figure 5). In contrast to the 1x99 application no effect of MnCl_2 application on observable health parameters was noted (table 1). Statistical analysis of body weight showed group and time effect ($F_{3,18} = 5.73$, $p = 0.006$ and $F_{2,36} = 10.52$, $p = 0.005$ respectively; two-way ANOVA). Also the group x time interaction showed significant differences ($F_{6,36} = 3.77$, $p = 0.005$), indicating different development of body weight over time. All Mn^{2+} groups showed weight loss after the first injection, but those losses reached significance only for the 8x30/24 and the 3x60/48 groups. For all groups body weights recovered after two days (figure 12).

Results

Table 1: Health assessment of animals in each group. Measures were assessed according to the EMPRESS guidelines. The two animals used for the 1x99 protocol showed severe side effects shortly after injection and had to be sacrificed. No detectable changes in health conditions were observed in animals which were not used for telemetry.

	Control	3x60/48	8x30/24	6x30/48	1x99
Number of animals	6	6	6	4	2
Observation period in days	5	5	8	11	1
Deaths	0	0	0	0	2
Body position	Normal	Normal	Normal	Normal	inactive
Tremor	Normal	Normal	Normal	Normal	n/a
Palpebral closure	Normal	Normal	Normal	Normal	Eyes closed
Coat appearance	Normal	Normal	Normal	Normal	n/a
Whiskers	Normal	Normal	Normal	Normal	n/a
Lacrimation	Normal	Normal	Normal	Normal	n/a
Defecation	Normal	Normal	Normal	Normal	n/a
Gait	Normal	Normal	Normal	Normal	n/a
Tail elevation	Normal	Normal	Normal	Normal	n/a

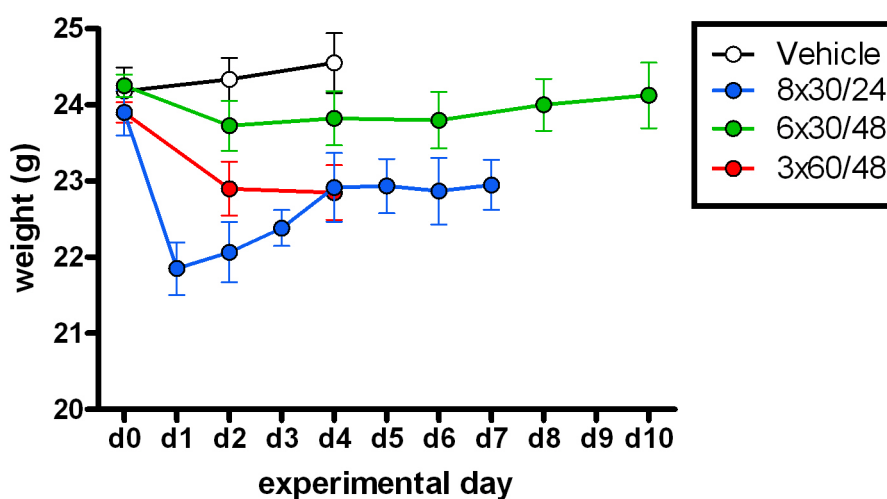


Figure 12: Effect of $MnCl_2$ and vehicle treatment on weight. After weight loss in $MnCl_2$ groups adjacent to first injection all groups show body weight recovery.

Results

1.2.3. Telemetry

Grand means (mean of all 7.5 h means after injection) of body temperature deviation from the three day baseline measurement (cf. general methods 10) showed significant differences between groups ($F_{2,12} = 57.25$, $p < 0.0001$; one-way ANOVA). Post hoc comparison revealed significant differences between the 3x60/48 and the 6x30/48 group ($p < 0.0001$) as well as between the 3x60/48 and the 8x30/24 group ($p < 0.0001$; Fisher LSD). There was no significant difference between the 6x30/48 and the 8x30/24 group (Fig. 13A). All groups differed significantly from the temperature response to the NaCl injection ($p < 0.002$; Fisher LSD). Temperature changes returned to baseline levels 7.5 h after $MnCl_2$ injection (Fig. 13 C). As for repeated injections, neither the 6x30/48 nor the 8x30/24 injection protocol showed a significant influence of time ($F_{5,10} = 0.80$, $p = 0.58$, and $F_{7,28} = 1.12$, $p = 0.38$, respectively; repeated measurement ANOVA), when temperature deviations from baseline were investigated over the time course of each application protocol separately per group. In contrast, the 3x60/48 group became sensitized to $MnCl_2$ induced hypothermia ($F_{2,10} = 6.01$, $p = 0.019$; Fig. 13B; repeated measurement ANOVA). The locomotion deviation from baseline showed a similar pattern but with weaker effects.

Grand means of locomotion also showed significant differences between groups ($F_{3,29} = 6.09$, $p = 0.003$; one-way ANOVA) with the 3x60/48 group being significantly different from the 6x30/48 ($p = 0.023$) and the 8x30/24 group ($p = 0.010$) as well as to the single NaCl injection applied three days before application of the injection scheme ($p < 0.0001$, Fisher LSD; figure 13D). Repeated measurements ANOVA for locomotion deviation from baseline failed to reveal significant differences between different time points in any of the application schemes (figure 13E).

1.2.4. Endocrine measurements

Figure 13F shows the stress response as measured by corticosterone levels to injection of vehicle or MnCl_2 at the different time points. On the first day (time point d1_4h and d1_12h) corticosterone measurements for the 6x30/48 and the 8x30/24 group were pooled (pooled 30), as both groups received first injection of 30 mg/kg of MnCl_2 . All groups showed the highest corticosterone levels on d1_4h, with mean levels of 64 ± 49 ng/ml for the vehicle, 160 ± 59 ng/ml for the pooled 30 and 192 ± 187 ng/ml for the 3x60/48 group. On d1_12h these levels have declined to 27 ± 19 , 80 ± 63 and 122 ± 84 ng/ml for vehicle, pooled 30 and 3x60/48 group, respectively. All MnCl_2 treated groups showed increased corticosterone levels on d1_4h and d1_12h compared to the vehicle group, but not on d5_12h. Statistical analysis failed to reveal a significant effect of group ($F_{2,19} = 2.37$, $p = 0.12$, one-way ANOVA) at the first time point (d1_4h). Post hoc tests showed a trend between vehicle and pooled 30 and 3x60/48 ($p = 0.1$ and $p = 0.05$, respectively; Fisher LSD). At the second time point (d1_12h) a significant effect of group could be detected ($F_{2,19} = 3.51$, $p = 0.05$; one-way ANOVA) with post hoc tests showing a trend between vehicle and pooled 30 group ($p = 0.1$) and significant differences between vehicle and 3x60/48 ($p = 0.02$). At day 5 (d5_12h) statistical analysis failed to reveal significant differences ($F_{3,18} = 2.37$, $p > 0.5$). In summary, these results indicate that the first injection with MnCl_2 causes a considerable amount of stress, but the animals rapidly tend to habituate to it upon repeated MnCl_2 injection.

Results

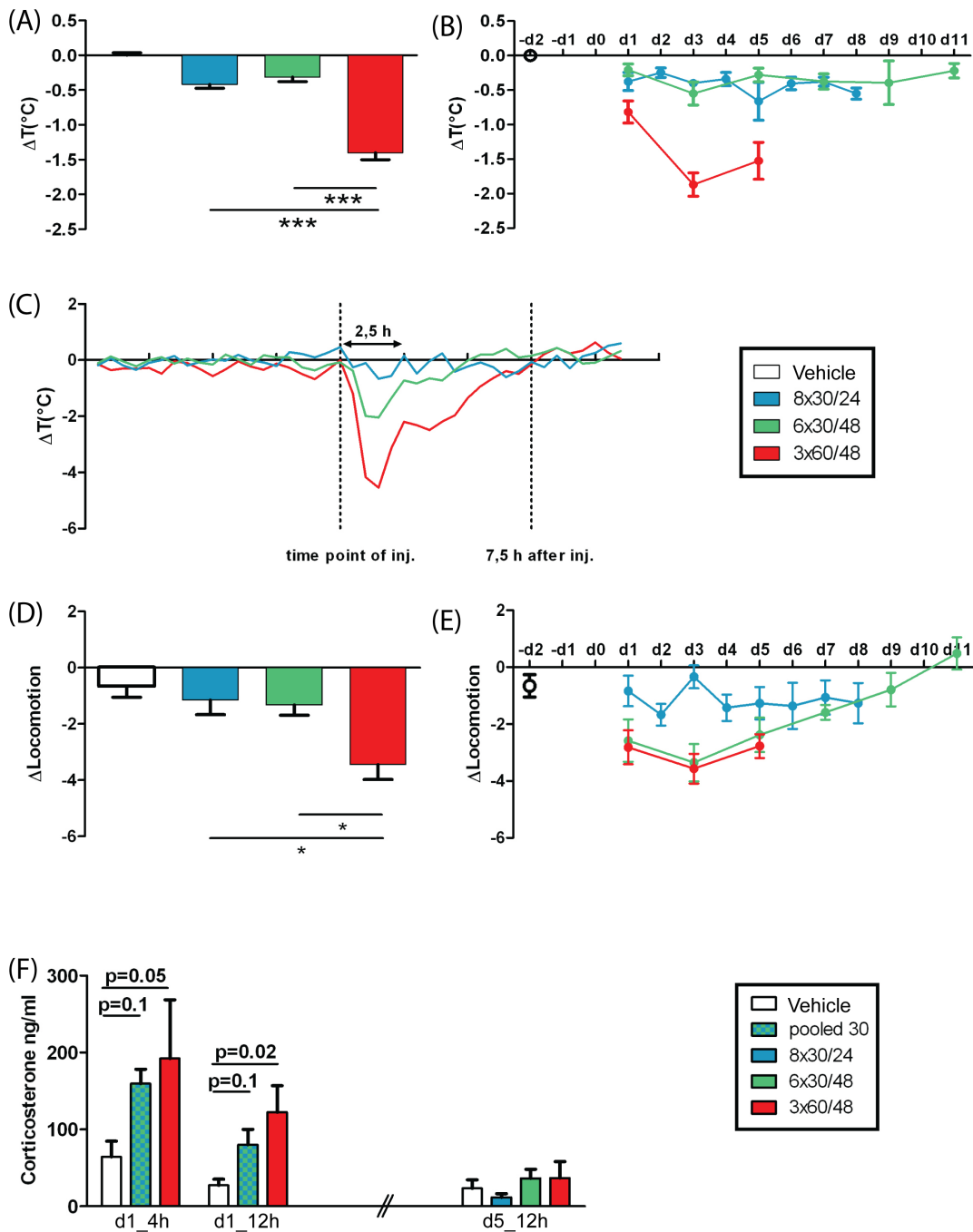


Figure 13: Effects of MnCl₂ treatment on temperature and locomotion and endocrine measures: A-C) Body temperature changes: **A)** Grand mean over all days of injection and **B)** time course mean of temperature deviation of the adjacent 7.5 h after injection from the corresponding 0.5 h intervals of the three day baseline mean. **C)** Temperature drop shown as a mean curve of 0.5 h intervals after the 2nd injection (d2 for 8x30/24, d3 for 3x60/48 and 6x30/48). The 3x60/48 application scheme shows a maximal mean temperature drop of around 5°C whereas the 8x30/24 group shows temperature drop of maximal 1.5°C. The 6x30/48 group caused a maximal temperature drop of around 2°C. **D-E)** Locomotion changes: **D)** Grand mean and **E)** time course mean of locomotion deviation of the adjacent 7.5 h after injection from the corresponding 0.5 h intervals of the three day baseline mean. Locomotion counts are strictly dependent on the distance the animal moves with a velocity of above 1 cm/s. **F)** Corticosterone levels at different time points for the different application schemes. 8x30/24 and 6x30/48 were pooled at d1 as both groups received first injection of 30 mg/kg MnCl₂. MnCl₂ groups started out with higher corticosterone levels than the vehicle group but reached levels of vehicle treated animals after repeated injection. *p<0.05, ***p<0.001

1.3. Acute and long-term effects of manganese application on associative and specific hippocampus-dependent learning

1.3.1. Effects of manganese application on associative learning

As expected from previous studies (Siegmund and Wotjak, 2007; Golub et al., 2009), a highly significant effect of shock application on freezing to the shock context (chamber; $F_{1,66} = 105.2$, $p < 0.001$; figure 14A), freezing to a shock context reminder (hexagon; $F_{1,66} = 65.0$, $p < 0.001$; figure 14B) and freezing to an unconditioned tone in a neutral context (tone; $F_{1,66} = 56.3$, $p < 0.001$; figure 14C; two-way ANOVA) was observed. Two-way ANOVA indicated that $MnCl_2$ application had no significant overall effect on freezing in the shocked and non shocked group. Neither in the chamber ($F_{1,66} = 1.4$, $p = 0.24$), nor the hexagon ($F_{1,66} = 2.1$, $p = 0.15$) nor to the tone ($F_{1,66} = 0.9$, $p = 0.35$). Nevertheless, a close to significance shock x $MnCl_2$ application interaction effect on freezing in the chamber ($F_{1,66} = 3.6$, $p = 0.06$) and a trend on freezing in the hexagon ($F_{1,66} = 2.6$, $p = 0.11$) was observed. No interaction on freezing to the tone could be found ($F_{1,66} = 1.5$, $p = 0.22$, two-way ANOVA). Post-hoc analysis revealed a significant difference between the $MnCl_2$ - and vehicle-treated animals of the shocked groups in freezing to the shock context ($p < 0.05$) and the context reminder ($p < 0.05$) but not to the unconditioned tone ($p > 0.05$; Newman Keuls).

Hyperarousal, as measured by acoustic startle response, was significantly different between shocked and non-shocked animals 4 weeks after shock application (interval (INT): $F_{4,276} = 115.4$, $p < 0.001$; shock application: $F_{1,276} = 3.7$, $p = 0.001$; shock application x INT: $F_{4,276} = 9.7$, $p < 0.001$; repeated measures ANOVA). In the non-shocked group $MnCl_2$ treatment had no effect on hyperarousal (INT: $F_{4,100} = 65.4$, $p < 0.001$; $MnCl_2$ treatment: $F_{1,100} = 0.1$, $p = 0.7$; $MnCl_2$ treatment x INT: $F_{4,100} = 0.5$, $p > 0.7$; repeated

Results

measures ANOVA; figure 14D). In the shock group MnCl₂ treatment had a nearly significant effect overall and significantly affected startle response depending on the tone intensity (INT: $F_{4,176} = 78.4$, $p < 0.001$; MnCl₂ treatment: $F_{1,176} = 3.7$, $p = 0.06$; MnCl₂ treatment x INT: $F_{4,176} = 3.7$, $p < 0.005$; repeated measures ANOVA; Figure 14E), with post-hoc tests revealing significant differences between MnCl₂ and vehicle treated animals at 105 ($p < 0.05$) and 115 db SPL ($p < 0.01$; Newman Keuls). These results show a specific effect of MnCl₂ application in shocked animals.

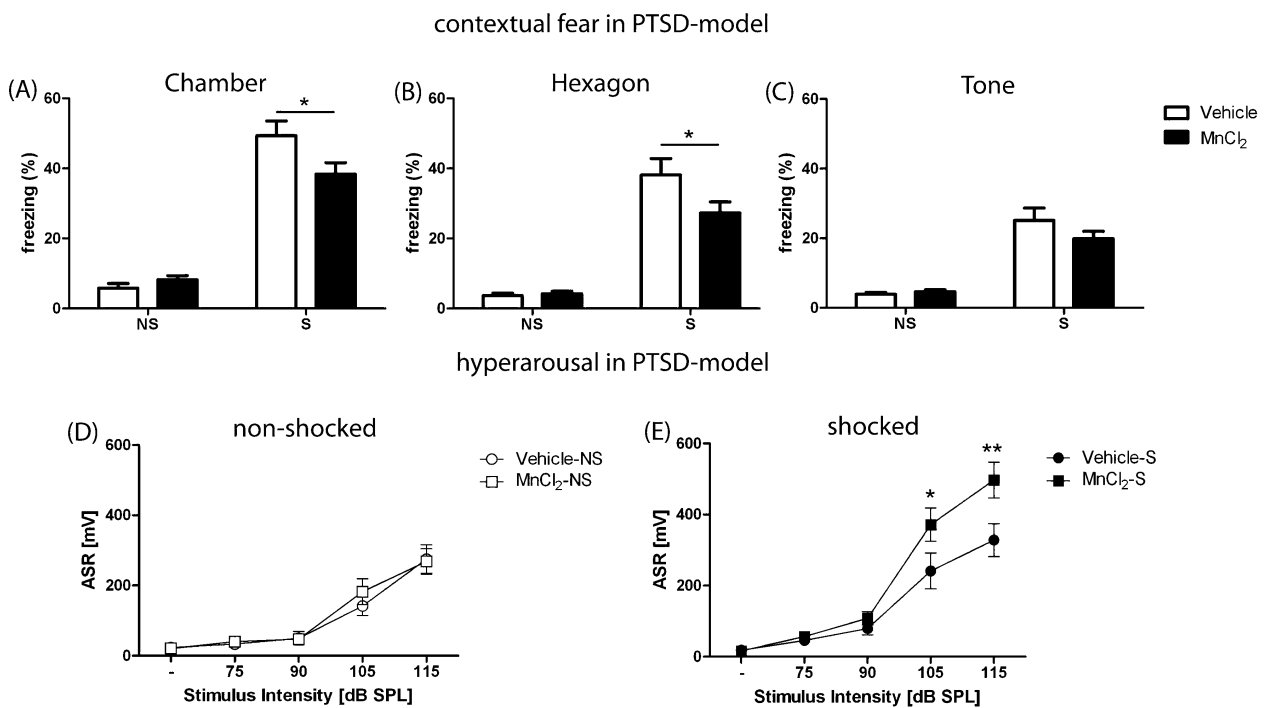


Figure 14: long-term effects of MnCl₂ application on contextual fear and hyperarousal in the mouse model of PTSD: (A-C) Freezing responses (A) to the shock-context, (B) to the context reminder and (C) to an unconditioned tone in a neutral context. Freezing duration was normalized to the 3-min observation intervals. (D-E) Acoustic startle response (ASR) to noise pulses of different intensities (D) of non shocked animals (E) of shocked animals. For the ASR the data represent mean peak startle amplitude in mV \pm SEM in response to 20 startle stimuli of each intensity. All data was acquired 4 weeks after shock application. * $p < 0.05$, ** $p < 0.01$ (Newman Keuls), NS: non-shocked, S: shocked.

Results

Additionally, avoidance of a compartment was measured in which a filter paper-lined Petri dish with a shock context specific odor (ethanol, cf. General methods 7) was placed (figure 15). Shock application had a significant effect on time spend in the nest ($F_{1,67} = 24.9$, $p < 0.001$; figure 15B) and in the ethanol compartment ($F_{1,67} = 6.7$, $p = 0.01$; figure 12 C) and no effect on time spend in the acetate compartment ($F_{1,67} = 3.9$, $p > 0.05$; two-way ANOVA; figure 15A). As one-way ANOVA indicated a significant different between groups in time spend in the nest ($F_{3,70} = 5.6$, $p < 0.001$) and in the ethanol compartment ($F_{3,70} = 3.0$, $p < 0.03$) post hoc analysis were conducted. Whereas shocked vehicle treated animals spend significantly more time in the nest compartment ($p < 0.01$) compared to non-shocked vehicle treated animals, no such effect was found for shocked $MnCl_2$ treated animals ($p > 0.05$; Newman Keuls). Additionally shocked vehicle treated animals spend

CODA

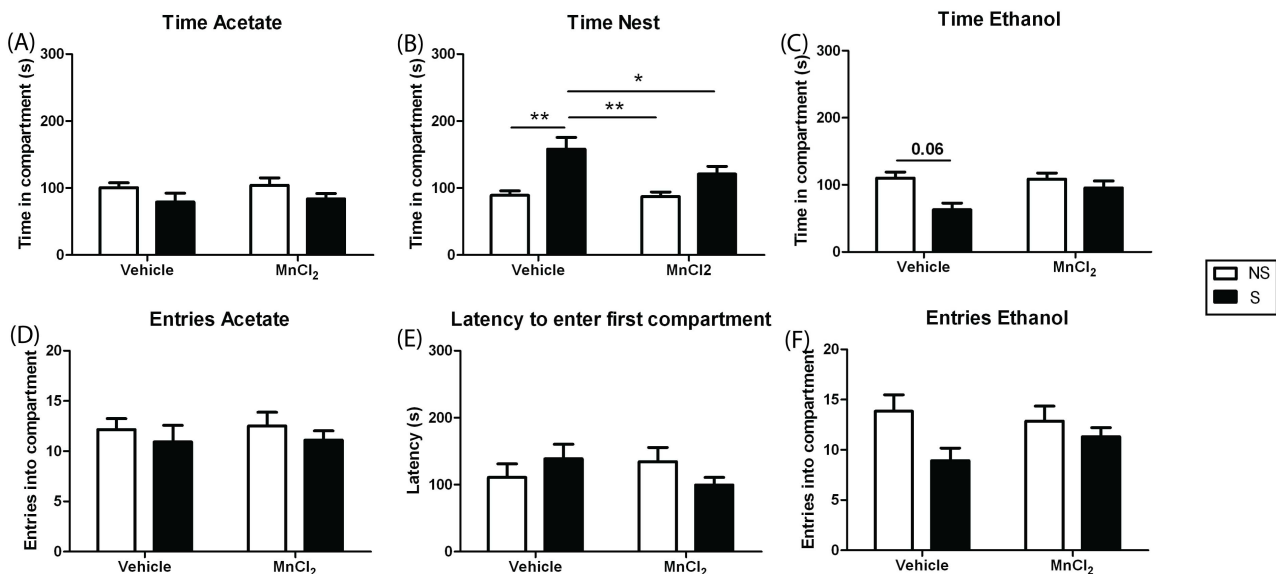


Figure 15: Avoidance of the ethanol compartment in shocked vehicle treated or shocked $MnCl_2$ treated mice. Mice were shocked (1.5 mA, 2 s) in an ethanol-scented conditioning chamber and tested in the conditioned odor avoidance (CODA) task 31 - 36 days after shock. CODA apparatus consisted of 3 compartments. After a habituation phase of 300 s in the center (nest) compartment where a Petri dish containing home-cage material was presented, the 2 other compartments, where ethanol (conditioned) and acetate (neutral) odors were presented in filter paper-lined Petri dishes, were accessible for 300s (cf. general methods 7 and Pamplona et al., 2010). **A)** Time spent in the acetate **B)** nest and **C)** ethanol compartment, as well as **D)** entries in the acetate and **F)** ethanol compartment and **E)** the latency to enter the first compartment were used as behavioral parameters. * $p < 0.05$ ** $p < 0.01$ (Newman Keuls). NS: non-shocked, S: shocked.

Results

nearly significantly less time in the ethanol compartment ($p < 0.06$) compared to non-shocked vehicle treated animals. With post hoc tests showing no difference between shocked mice and non-shocked mice of the MnCl_2 injected group ($p > 0.05$). Taken together, this suggests a failure of specific avoidance of conditioned odor cues in shocked MnCl_2 treated mice.

In summary this data indicates a specific effect of MnCl_2 application in the shocked group lowering contextual fear but not generalized fear, enhancing hyperarousal and impairing avoidance of conditioned odor cues.

1.3.2. Effects of manganese application on learning in the water cross-maze

Only accuracy data (cf. general methods 12) was examined as it was shown in previous experiments to be the best measure of hippocampus dependent learning (Kleinknecht et al., in prep.). MnCl_2 treated and vehicle treated animals both started at chance level upon training with the spatial learning protocol (figure 16A). The vehicle group reached the learning criterion of $\geq 83\%$ on day 4 and 5, whereas the learning score of the MnCl_2 group failed to do so. Statistical analysis revealed a significant effect of the training ($F_{4,88} = 19.6$, $p < 0.001$), and a significant interaction effect between MnCl_2 treatment and training ($F_{4,88} = 4.1$, $p = 0.004$; repeated measurement ANOVA). On day 5, all animals of the vehicle group trained with a spatial learning protocol reached the learning criterion of 5 correct trials out of 6 (83.3 %). Within the MnCl_2 treated animals only 50 % of the animals (6 out of 12) reached this criterion (figure 16 B). Interestingly, when MnCl_2 treated mice were divided into animals with higher signal intensity and lower signal intensity within the hippocampus, relating to a high and low Mn^{2+} accumulation respectively, it can be seen that 4 out of the 6 non-learners are mice with high Mn^{2+}

Results

accumulation in the brain. This indicates a specific impairment of hippocampus dependent learning in mice showing strong Mn^{2+} accumulation. This is supported by subsequent analysis of the success of training over all days with the spatial learning protocol in these subgroups. When mice with a high Mn^{2+} accumulation within the hippocampus are compared to the control animals, a significant effect of the $MnCl_2$ treatment ($F_{1,64} = 6.6$, $p = 0.02$) and a significant interaction effect of the treatment with the training ($F_{4,64} = 5.1$, $p = 0.001$; repeated measurement ANOVA; figure 16C) could be observed. Mice with a low Mn^{2+} accumulation within the hippocampus showed no effect of the $MnCl_2$ treatment ($F_{1,64} = 0.001$, $p = 0.9$) and no interaction effect of the treatment with ($F_{4,64} = 1.6$, $p = 0.18$; repeated measurement ANOVA; figure 16C)

If animals were trained with a response learning protocol that mainly relies on egocentric learning, no effect of $MnCl_2$ treatment ($F_{1,88} = 0.07$, $p = 0.78$) and no interaction effect between treatment and training ($F_{4,88} = 0.06$, $p = 0.99$) could be observed (figure 13D). Also the number of accurate learners on day 5 was similar with even one additional $MnCl_2$ treated animal reaching the learning criterion (10 out of 12) compared to the control group (9 out of 12; figure 16E).

The similarity in learning accuracy became even more pronounced when animals were trained with the free choice protocol, where animals had the choice to pick a spatial or response learning strategy or both. Again there was no indication of an effect of $MnCl_2$ treatment ($F_{1,88} = 0.06$, $p = 0.80$) and no interaction effect between $MnCl_2$ treatment and training ($F_{4,88} = 0.88$, $p = 0.48$; repeated measurement ANOVA; Figure 16F).

These results clearly indicate short term effects of $MnCl_2$ accumulation on spatial learning but not on response or free choice learning where response learning is also possible.

Results

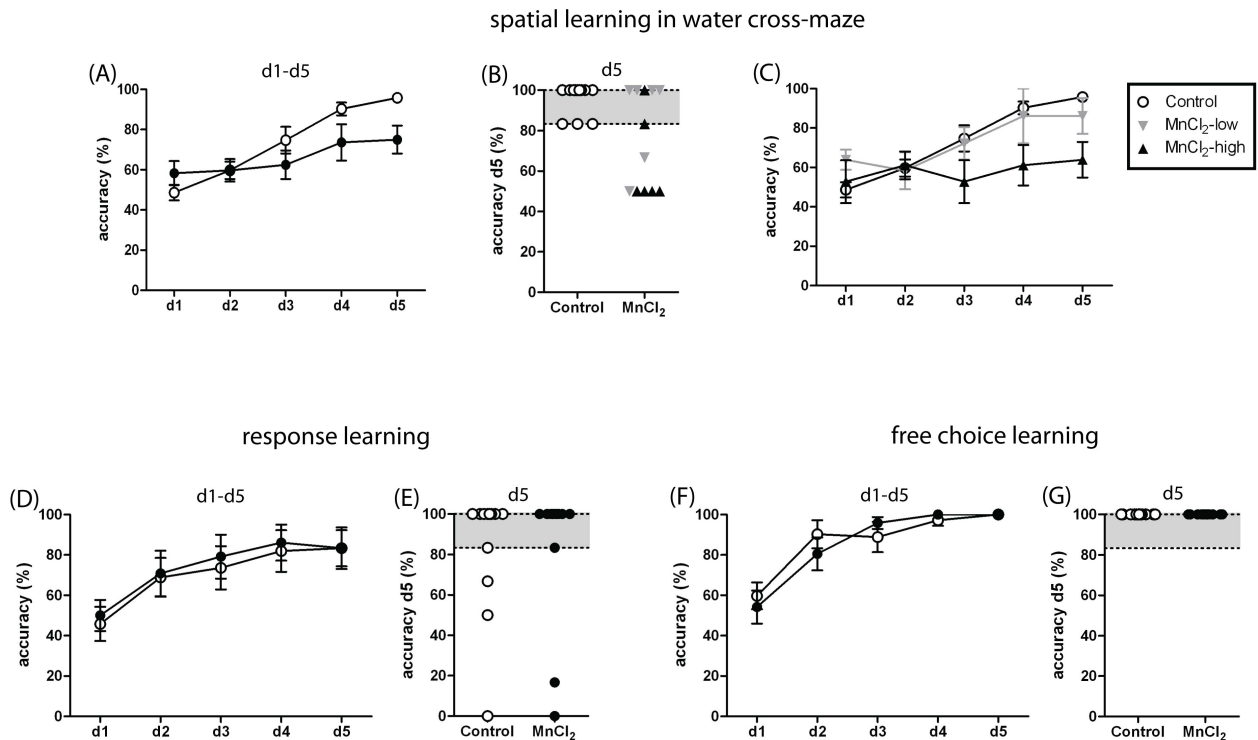


Figure 16: Acute effects of MnCl₂ application on spatial and habitual learning in the water cross-maze: mice were injected every day, 12 h before training. **A-C)** spatial learning: **A)** Mean accuracy to find the escape platform d1-d5. After starting at chance level, the MnCl₂ group did not reach mean accuracy levels over 80% in contrast to the control group. **C)** Learning score day 5: Only 6 out of 12 animals within MnCl₂ group reached learning criterion (5 correct trails out of 6 = 83.3%), in contrast to control group (12 out of 12). Mice with high and low Mn²⁺ accumulation in the hippocampus are marked black and gray respectively **D+E)** response learning **E+F)** free choice learning **D+F)** MnCl₂-injected and control mice showed no difference in mean learning accuracy across at all training days for the **D)** response learning or **F)** free choice learning protocol. **E+G)** Learning score at day 5: Also the number of accurate learners on day 5 did not differ between groups trained with the **E)** response learning or **G)** free choice learning protocol.

2. Study 2: Validation of vMEMRI

2.1. Methodological validation of vMEMRI

2.1.1. Image contrast of the different fractionated application protocols of manganese

The following data was already published (Grünecker et al., 2010). After application of MnCl₂, the layers of various neuronal structures were distinguishable (figure 17). The 8x30/24 protocol showed best signal enhancement and contrast of laminar structure in the olfactory bulb and cerebellum (figure 17A+B). Even cortical layers of the retrosplenial granular cortex can be distinguished in the group injected with the 8x30/24 protocol (figure

17C).

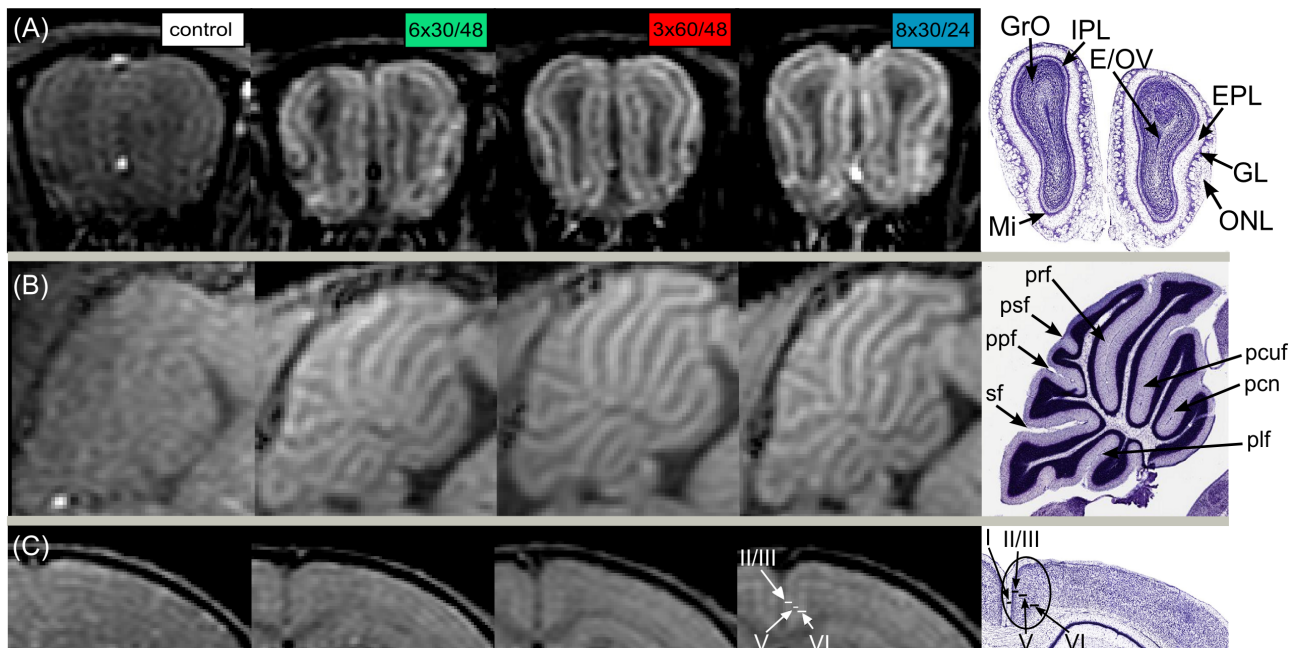


Figure 17: Visualization of fine structures in the olfactory bulb, cerebellum and cortex by different fractionated application protocols. Representative images for each group are shown. **A)** Coronal sections of the olfactory bulb. Layers are well distinguishable in every protocol involving Mn^{2+} . Different layers are indicated on the Nissl stain (right). **B)** Sagittal sections of the cerebellum. Delineation of laminar structure is not present in the control group, while Mn^{2+} application led to improved tissue contrast. A Nissl stain (right) at approximately the same location is inserted. **C)** Coronal sections of the cortex. The location of the retrosplenial granular cortex is indicated by the ellipse in the Nissl stain (right). Layers indicated on the Nissl stain are best discriminated on the image of a mouse treated with the 8x30/24 protocol. Note that on coronal sections, truncation artifacts ('Gibbs ringing') are visible which hamper precise evaluation of cortical layer structures, especially parallel to the skull surface. To avoid contamination by such artifacts, only cortical structures running perpendicular to the skull surface, e.g. the retrosplenial granular cortex, were evaluated. All layers were identified according to the Allen mouse brain atlas (<http://mouse.brain-map.org>). Olfactory bulb layers: E/OV: ependymal and subependymal layer/ olfactory ventricle, EPL: external plexiform layer, GL: glomerular layer, GrO: granular layer, IPL: internal plexiform layer, Mi: mitral cell layer, ONL: Olfactory bulb layer; Cerebellar layers: plf: posterolateral fissure; pcn: precentral fissure; pcuf: preculminate fissure; prf: primary fissure; psf: posterior superior fissure; ppf: prepyramidal fissure; sf: secondary fissure

Statistical analysis with 2-way ANOVA showed strong effects of both group ($F_{3,126} = 106.3$, $p < 0.0001$, 2-way ANOVA) and region ($F_{6,126} = 8.5$, $p < 0.0001$) on relative signal intensities in the areas depicted in figure 18A, yet the group x region interaction was not significant ($F_{18,126} = 1.4$, $p = 0.154$), indicating that the sorting of regional relative intensities was similar for all application protocols. Figure 18B shows that after administration of different $MnCl_2$ fractions all brain regions depicted in figure 18A differed significantly from vehicle injected animals in signal intensity relative to surrounding muscle ($p < 0.05$,

Results

Newman-Keuls). Relative intensity within the cortex, CA1, CA3, inferior colliculi, and thalamus of the 8x30/24 group was significantly higher compared to relative intensity within this regions of the 6x30/48 group. Additionally, relative intensity within the cortex also differed significantly between the 3x60/48 and 6x30/48 group. Within the CA1, CA3 and inferior colliculi a significantly higher relative signal intensity of the 8x30/24 compared to the 3x60/48 group could be detected. Analysis of the relative signal intensity within the whole brain showed significantly enhanced values of the 8x30/24 and 3x60/48 group compared to vehicle injected animals. Certain regions show a heightened number of significant differences among the relative intensities of the different fractionated application protocols, witch indicates inter-regional differences of Mn²⁺ accumulation; the CA3 region shows highest values for all protocols. Pair wise post-hoc comparisons (paired t-test) among regions were significant for 12 pairs for the 8x30/24 protocol, as compared with 5 and 2 pairs for the 3x60/48 and 6x30/48 protocol, respectively (cf. table 2)

For relative intensity in the whole brain and relative intensity over all cortical and subcortical regions, a significant effect of the application scheme was detected ($F > 15$, $p < 0.0001$; 1-way ANOVA). Post-hoc tests revealed the order of lowest to highest intensity to be vehicle, 6x30/48, 3x60/48, 8x30/24 (Newman-Keuls; figure 18C).

A moderate correlation was detected between the coefficient of variation (calculated across the 7 ROIs for each animal) and the total dose of Mn²⁺ (Spearman rank test, $\rho = 0.66$, $p = 0.001$; figure 18 D)

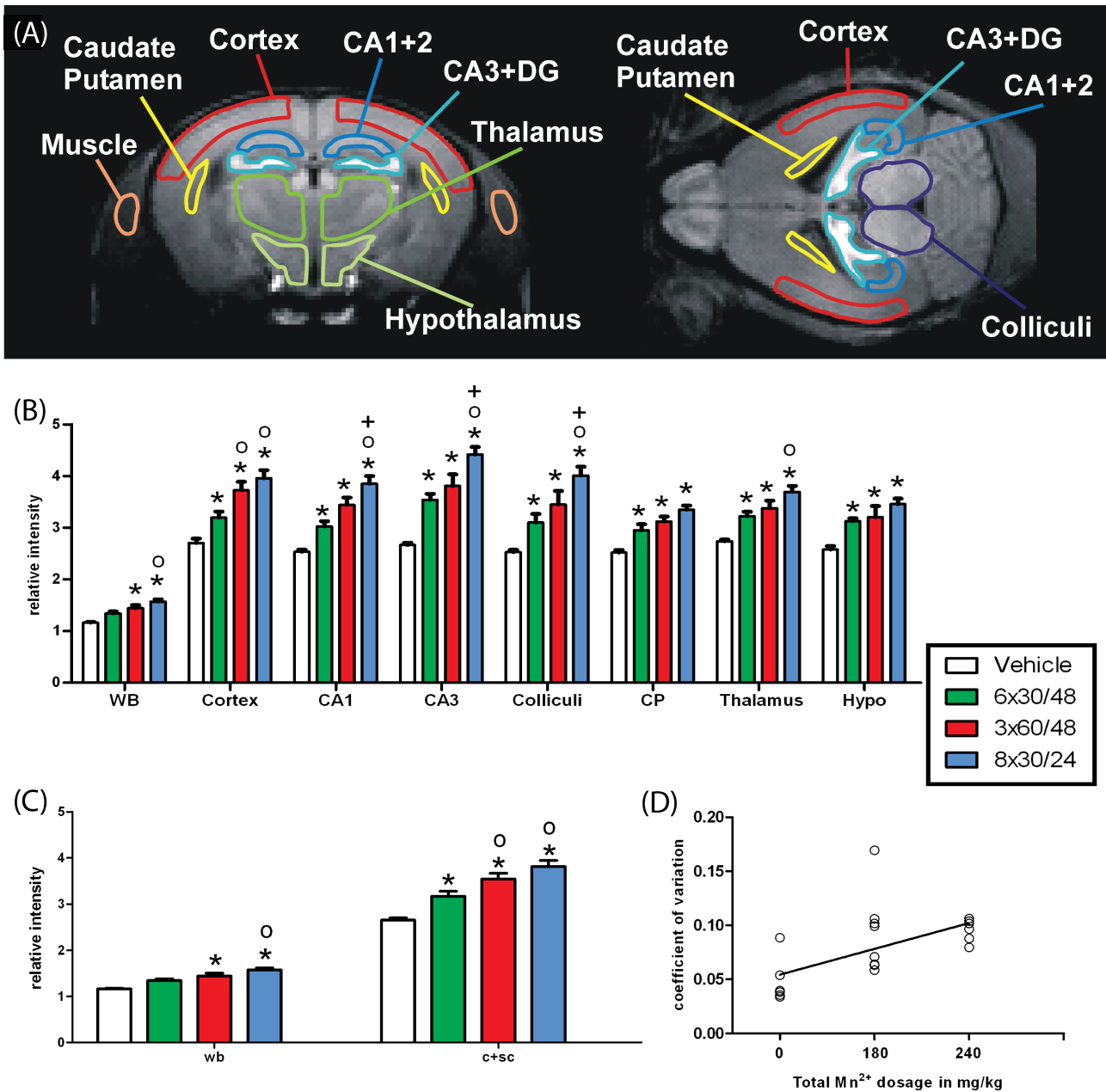


Figure 18: Relative intensities of distinct brain regions after administration of different MnCl₂ fractions. A) Regions of interest (ROIs) depicted for analysis. **B)** Relative signal intensities (normalized to surrounding muscle) in depicted ROIs. * significantly different from vehicle, o significantly different from 6x30/48, + significantly different from 3x60/48 (Newman Keuls post-hoc test) **C)** MRI signal enhancement in the whole brain (wb) and the average relative intensities over all cortical and subcortical (c+sc) ROIs. An increase in signal intensities was detectable from vehicle to 8x30/24 in both wb as well as in c+sc. * significantly different from vehicle, o significantly different from 6x30/48 (Newman Keuls) **D)** Coefficients of variation across regional relative intensities calculated for each animal. A Spearman rank test was applied to the coefficients of variation for the total Mn²⁺ dose delivered to the animals. The correlation coefficient was found to be rho = 0.66, with a p-value of p = 0.001, indicating that a higher total amount of Mn²⁺ applied provides a better contrast. Colliculi: inferior colliculi, CP: caudate putamen, Hypo: hypothalamus, WB: whole brain.

Results

Table 2: Significant differences ($p < 0.05$, paired t-test) in signal intensities between ROIs (cf. figure 18A) after application of different fractionated Mn^{2+} application protocols. $x = 6x30/48$, $o = 3x60/48$, $* = 8x30/24$

	Cortex			CA1			CA3			Colliculi			Striatum			Thalamus			Hypo- thalamus		
Cortex									*					o	*					o	*
CA1							x		*						*						*
CA3			*	x		*						*	x	o	*		o	*		o	*
Colliculi									*						*						*
Striatum		o	*			*	x	o	*			*									
Thalamus								o	*												
Hypo- thalamus		o	*			*		o	*			*									

2.1.2. Bias correction

Figure 19A shows differences in signal intensity between the left and right ROIs in T2w-images. Stronger bias correction successively lowered mean differences in signal intensity and SD between the left and right ROIs from 4.6 ± 10.7 (no bias) to 1.8 ± 3.2 (very strong), with mean differences from very strong bias correction still being significantly different from 0 ($p < 0.001$; t-test). Repeated measures ANOVA indicated a significant effect of bias correction on lateral differences in signal intensity ($F_{4,274} = 4.7$, $p < 0.001$), with post-hoc tests indicating significant differences between very strong and no bias correction, very strong and light bias correction and strong and no bias correction groups ($p < 0.05$; Newman-Keuls). Vertical difference in signal intensity was even heightened by stronger bias correction from 42.3 ± 16.4 (no bias) to 55.4 ± 23.8 (strong), with very strong bias correction again lowering mean difference and SD of signal intensity (30.0 ± 13.6 ; figure 19B). Stronger bias correction had a significant impact on vertical difference in signal intensity ($F_{4,274} = 112.2$, $p < 0.001$). Analysis of signal intensity contrast between the whole brain ROI and a ROI surrounding the whole brain ROI revealed, the bias correction

Results

had a significant impact on brain-nonbrain contrast ($F_{4,274} = 417.0$, $p < 0.001$), with post-hoc analysis showing significant differences between very strong bias correction and all other bias corrections and strong bias correction and all other bias corrections ($p < 0.001$; Newman Keuls; figure 19 C). This indicates, that a very strong bias correction significantly disturbs signal contrast between tissues, which is also shown when variance of signal intensities within the whole brain ROI is analyzed. Bias correction had a significant impact on variance of signal intensities within brain ROI ($F = 153.1$; $p < 0.001$), with the variance after very strong and strong bias correction being significantly lowered in comparison to all other bias corrections ($p < 0.01$; Newman Keuls; figure 19 D).

For normalization of T2w-images the image should have as less signal differences between left and right and ventral and dorsal side of the brain as possible as this indicates a signal gradient introduced by the surface coil and could compromise normalization. On the other hand signal differences between brain and non brain tissue should be preserved as a higher contrast between structures facilitates morphing (i.e. normalization) of the structure's outlines to one another. However a higher bias correction than a medium bias correction is not advisable as it significantly disturbs signal contrast between brain and non brain tissue and variance of signal intensities within the brain tissue. Furthermore a light and medium bias correction does not decrease signal gradient introduced by the surface coil. This leads to the conclusion that no bias correction of T2w-images should be conducted.

Results

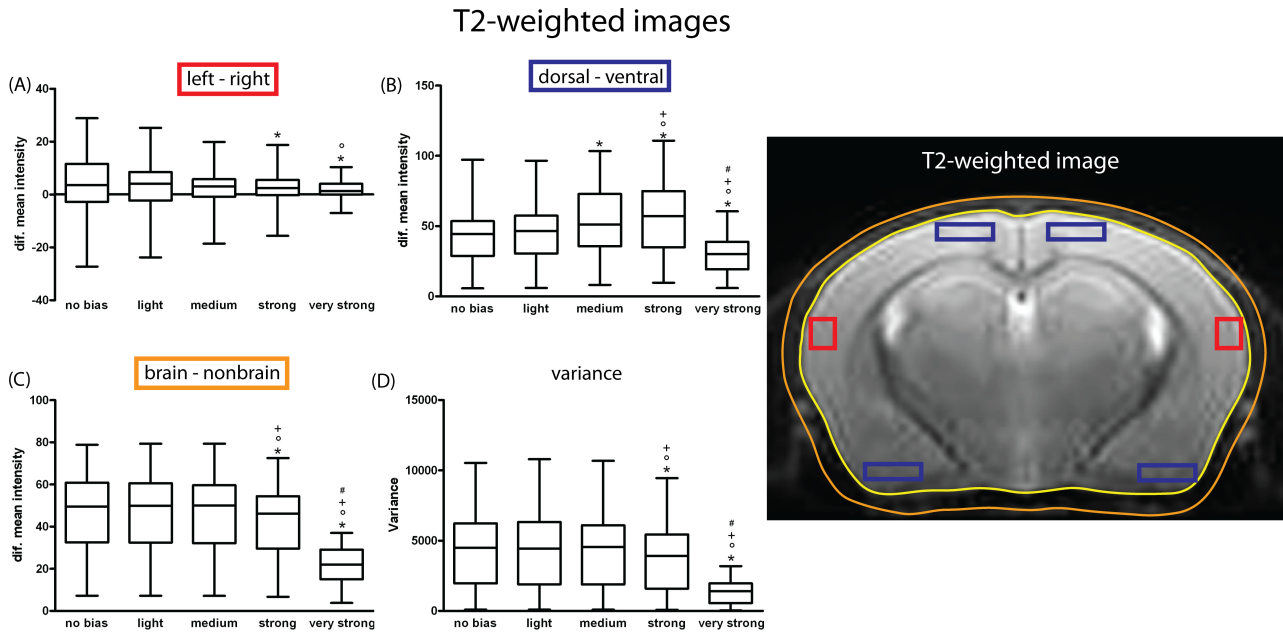


Figure 19: Impact of bias correction on lateral and vertical signal gradient and tissue contrast on T2w-images: ROIs are indicated on image (right). All graphs are ordered from no bias correction on the left to successively stronger bias correction to the right. **(A)** Difference in signal intensity between left and right ROI. **(B)** Difference in signal intensity between dorsal and ventral ROI. **(C)** Difference in signal intensity between brain and nonbrain ROI **(D)** Variance of signal intensity values within brain ROI. purple: dorsal-ventral ROIs; red: left-right ROIs, yellow: brain ROI, orange: non-brain ROI (inner boarder of non-brain ROI is brain ROI). Note, that ROIs were drawn on all slices of the midbrain. Analysis were conducted with 55 C57Bl/6N mice. * significantly different from no bias, ° significantly different from light, + significantly different from medium, # significantly different from strong ($p < 0.05$; Newman Keuls post-hoc)

Differences in signal intensity between left and right ROI in T1w-images were also steadily decreased by a stronger bias correction, with mean differences and SD between the left and right ROIs starting from -4.0 ± 7.4 (no bias) and reaching 0.0 ± 1.0 (very strong; figure 20A). Mean lateral differences in signal intensity after strong and very strong bias correction did not differ from 0 ($p > 0.5$; t-test). Repeated measures ANOVA indicated a significant effect of bias correction on differences in mean intensity ($F_{4,274} = 15.3$, $p < 0.001$), with post-hoc tests showing that every bias correction significantly lowered lateral differences in comparison to no bias correction. Additionally strong and very strong bias correction significantly lowered lateral differences in signal intensity in T1w-images compared to medium and light bias correction ($p < 0.01$; Newman-Keuls). Vertical difference in signal intensity of T1w-images was also significantly lowered by bias

Results

correction ($F_{4,274} = 528.2$, $p < 0.001$) from 44.9 ± 10.3 (no bias) to 4.4 ± 2.9 (very strong), but they were still significantly different from 0 ($p < 0.001$, t-test; figure 20B). Post-hoc test showed that all bias corrections significantly differed from one another ($p < 0.001$; except for difference between light and no bias correction $p < 0.05$, Newman Keuls). The difference in signal intensity between the hippocampal ROI and a ROI surrounding the hippocampus was preserved with light, medium and strong bias correction. Very strong bias correction reduced it (figure 20C). Bias correction had a significant effect on contrast between the hippocampus and surrounding tissue ($F_{4,274} = 54.3$, $p < 0.001$), with post-hoc analysis showing significant differences between very strong bias correction and all other bias corrections ($p < 0.01$; Newman-Keuls). This analysis indicates that a very strong bias correction significantly disturbs signal contrast whereas the other bias corrections preserve contrast between the regions while successively lowering the lateral and vertical signal gradient introduced by the surface coil. This is also shown by analysis of the variance of signal intensities within the whole brain ROI (figure 20 D). Bias correction had a significant impact on variance of signal intensities within whole brain ROI ($F_{4,274} = 163.2$, $p < 0.001$), with the variance after strong and very strong bias correction being significantly lowered in comparison to all other bias corrections ($p < 0.001$; Newman-Keuls).

Also on T1w-images vertical and lateral differences in signal intensity indicate a signal gradient introduced by the surface coil and could compromise normalization, whereas signal differences between the hippocampus and the hippocampus surrounding tissue should be preserved as a higher contrast between structures facilitates morphing (i.e. normalization) of the structure's outlines to one another. Very strong bias correction is not advisable as it significantly disturbs signal contrast between the hippocampus and its surrounding tissue and variance of signal intensities within the brain tissue. A strong bias

Results

correction decreases the signal gradient introduced by the surface coil and preserves contrast between the hippocampus and its surrounding tissue. This leads to the conclusion that a strong bias correction of T1w-images should be conducted.

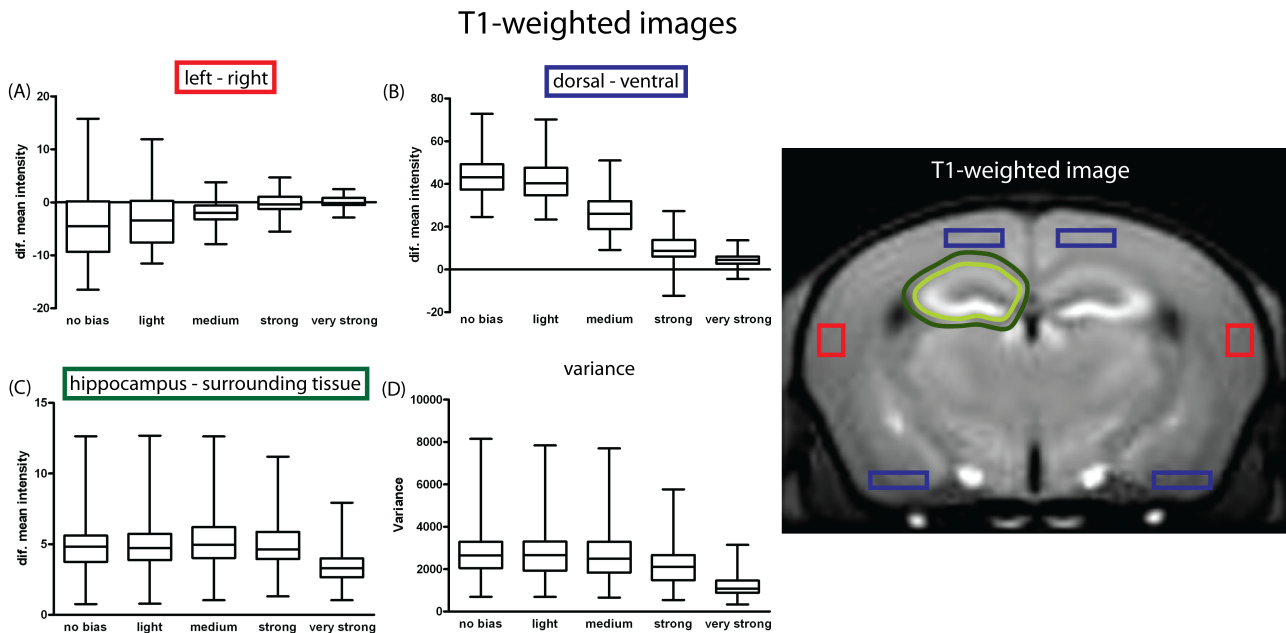


Figure 20: Impact of bias correction on lateral and vertical signal gradient and tissue contrast on T1w-images: ROIs are indicated on image (right). All graphs are ordered from no bias correction on the left to successively stronger bias correction to the right. **(A)** Difference in signal intensity between left and right ROI. **(B)** Difference in signal intensity between dorsal and ventral ROI. **(C)** Difference in signal intensity between brain and nonbrain ROI **(D)** Variance of signal intensity values within brain ROI. purple: dorsal-ventral ROIs; red: left-right ROIs, light green: hippocampus ROI, dark green: hippocampus surrounding ROI (inner boarder of hippocampus surrounding ROI is hippocampus ROI). Note, that ROIs were drawn on all slices of the midbrain. Analysis were conducted with 55 C57Bl/6N mice. * significantly different from no bias, ° significantly different from light, + significantly different from medium, # significantly different from strong ($p < 0.05$; Newman Keuls post-hoc)

2.1.3 Accuracy of manual determination of hippocampal volume

The correlation between the manually determined hippocampal volumes of Cyclin D2 mice of the three raters resulted in extremely high values ($r > 0.99$ and $p\text{-value} < 0.0001$; Pearson correlation). It should be noted however, that WT and KO animals showed variability of hippocampal volume within a distinct range for each genotype accounting for these extremely high correlations. When interrater correlations were calculated for each genotype ($n = 6$ for each genotype), values stayed very high ($r > 0.95$,

$p < 0.006$). This indicates that manual detection of hippocampal volume is reliable across different raters.

2.1.4. Comparison of semi-automatic and manual determination of volume

2.1.4.1. Brain volume

Figure 21A shows the correlation between semi-automatic acquired brain volumes with manually detected volumes of 29 C57Bl/6N mice. The correlation has an r-value of 0.91 a p-value smaller than 0.0001 (Pearson correlation), indicating a very good detection of the brain borders with the semi-automatic method.

2.1.4.2. Hippocampal volume

Figure 21B displays the correlation between manually and semi-automatically acquired hippocampal volumes of 29 C57Bl/6N mice . The correlation has an r-value of 0.77 and a p-value smaller than 0.0001 (Pearson correlation). Although weaker than the correlation for the brain volume, it is still quite high. These results indicate satisfactory detection of hippocampal volume with the semi-automatic volume detection method vMEMRI.

Results

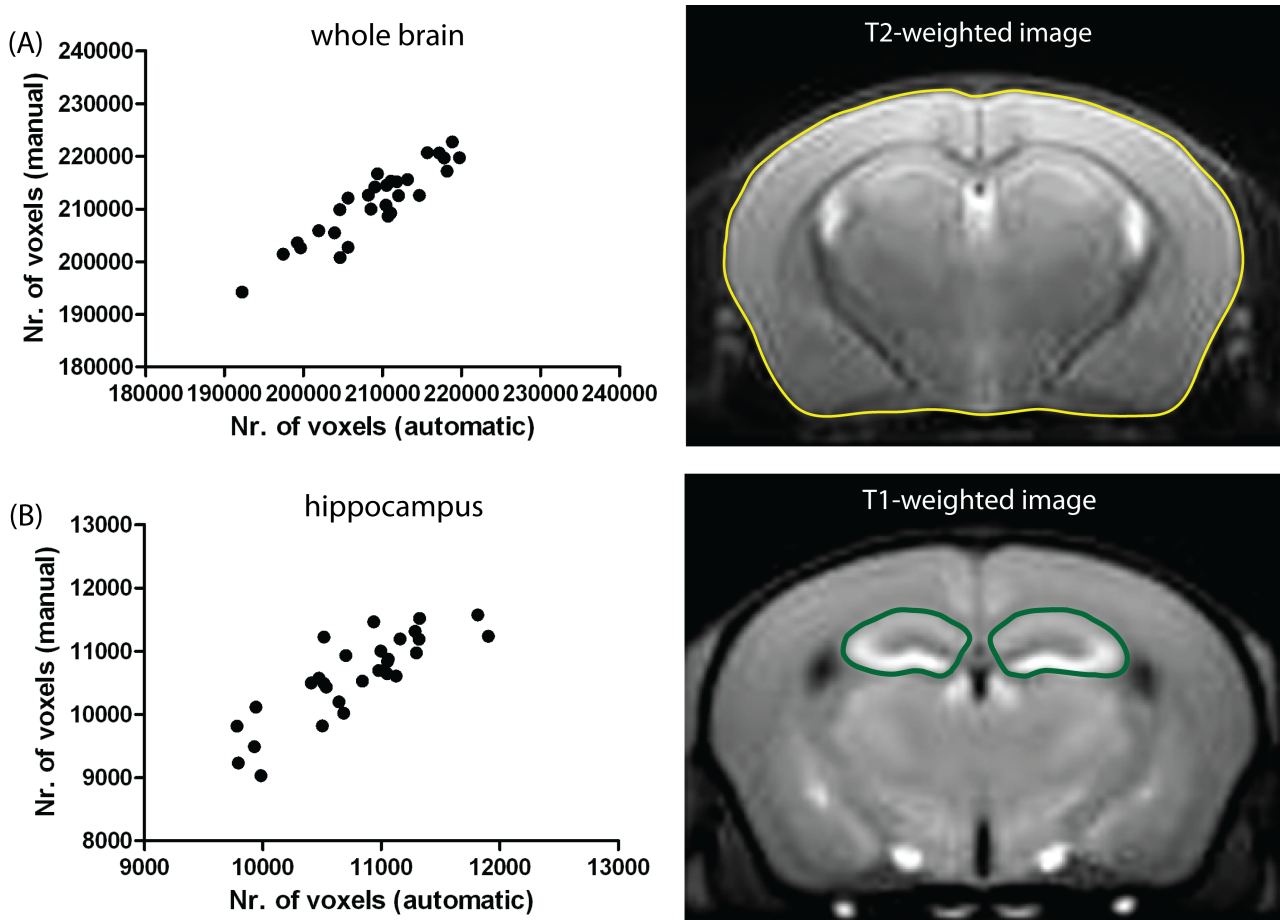


Figure 21: Correlations between manual and semi-automatic detected volumes. (A) Manually and semi-automatic detected brain volumes (ROI indicated right) correlated with : $r = 0.91$ $p < 0.0001$. (B) Manually and semi-automatic detected hippocampal volumes (ROI indicated on the right) correlated with: $r = 0.77$, $p < 0.0001$ (Pearson correlation). $N = 29$; C57Bl/6N mice

2.2. Experimental validation of vMEMRI

2.2.1. vMEMRI in Cyclin D2 animals

Figure 22A depicts selected coronal slices of representative T1w-images of a WT (right) and a KO (left) animal. Analysis of brain volume showed a significant reduction in whole brain volume of KO animals compared to WT animals of about 25 % ($p < 0.001$; unpaired t-test; figure 22B). Due to the significant differences in brain volume between KO and WT animals, hippocampal volumes of each animal were normalized to the individual whole brain volume. After normalization, difference of relative hippocampal volume of about 15 % could be detected between WT and KO animals ($p < 0.001$, unpaired t-test;

Results

figure 22C). This indicates, that the mutation of the KO mice in the cell cycle regulatory gene *Ccnd2*, encoding for Cyclin D2, not only completely ablates adult neurogenesis (Kowalczyk et al., 2004) but that this also leads to a specific reduction of hippocampal volume in these mice.

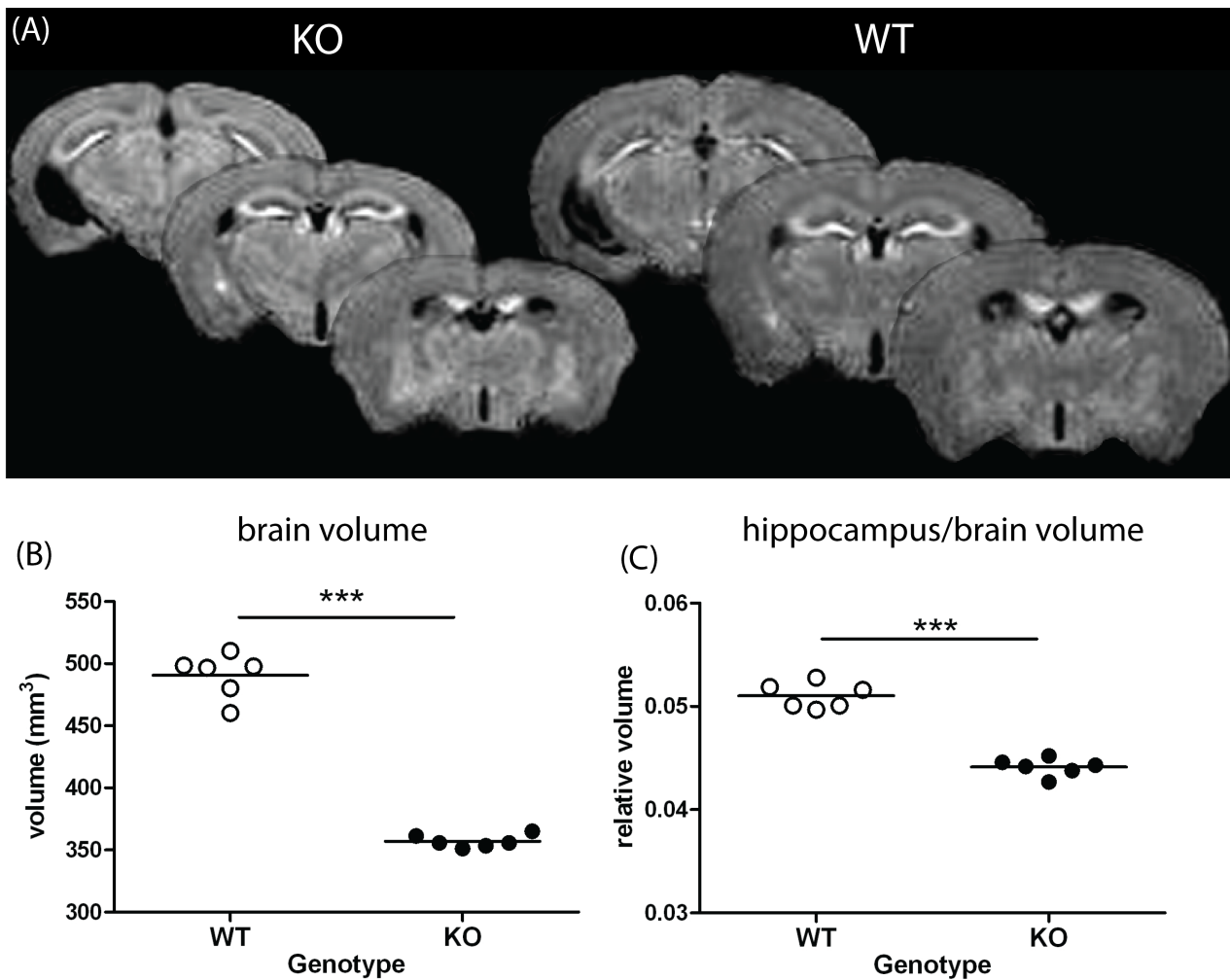


Figure 22: Brain and relative hippocampal volume of WT and Cyclin D2 KO animals: (A) selected coronal slices of a knockout (KO, left) and a wildtype (WT, right) Cyclin D2 mice. (B) Whole brain volume of WT and KO animals. A significantly lower brain volume of KO animals (approx. 25%) was detected. (C) Relative hippocampal volumes (normalized to individual brain volume) of WT and KO animals. A significantly lower relative hippocampal volume of KO animals (approx. 15%) was detected. *** p < 0.001 (unpaired t-test)

Results

2.2.2. vMEMRI in ibotenic acid lesioned animals

Figure 23A shows selected coronal slices of mean normalized group-images of vehicle and ibotenic acid injected animals. Hippocampal volume of a representative vehicle and ibotenic acid treated animal was reconstructed to show the 3-D surface image (figure 23B). Mean hippocampal volume of ibotenic acid injected animals was found to be significantly decreased by approximately 37% ($p < 0.05$, unpaired t-test; figure 23C). Despite high variability between hippocampi, correlation with manually detected hippocampal volume was very high ($r = 0.96$, $p < 0.001$, Pearson correlation; figure 23D). This shows that hippocampal volume can be reliably detected by the semi-automatic vMEMRI method even when volumes show a high variability.

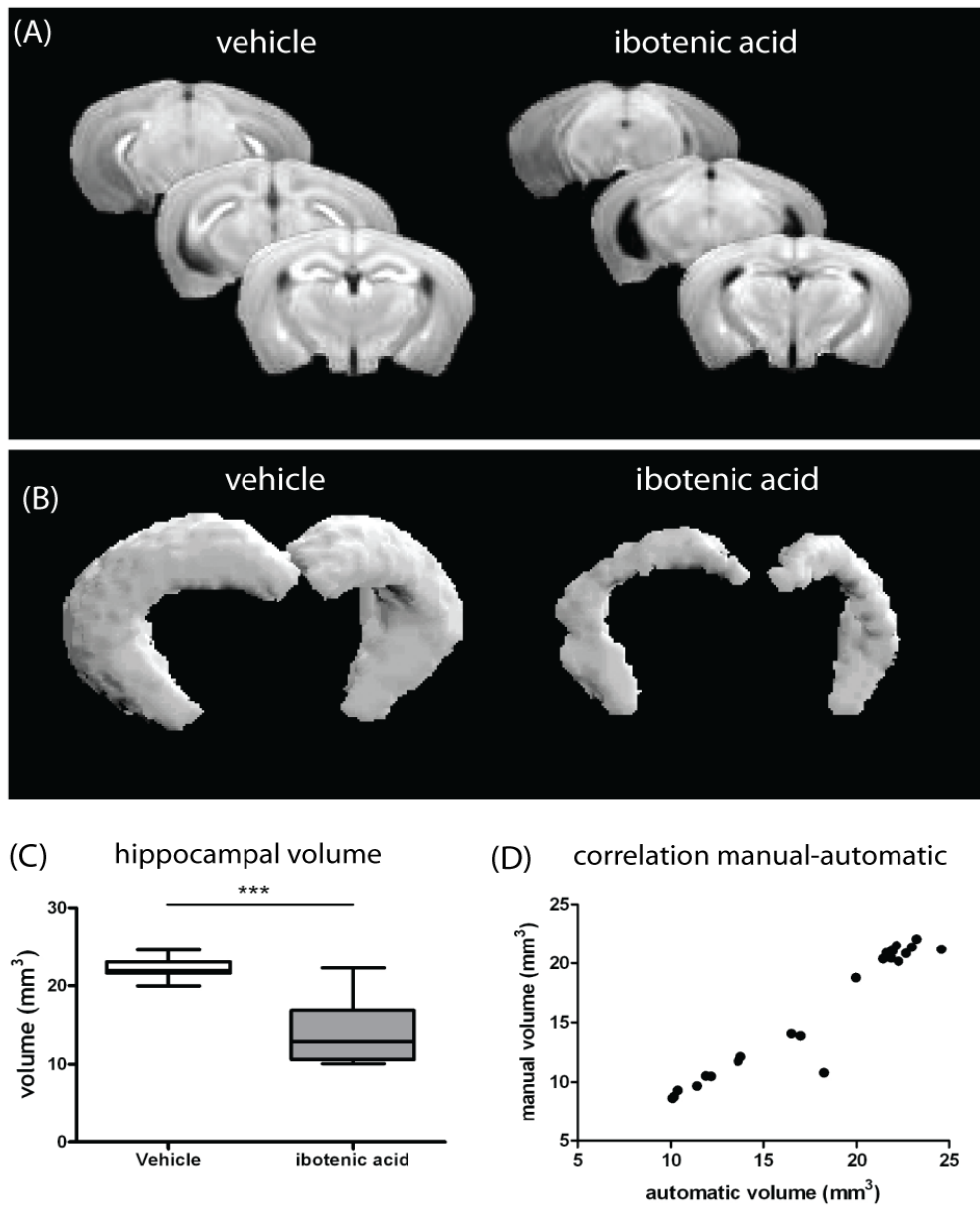


Figure 23: Hippocampal volume of ibotenic acid injected animals: (A) Selected coronal T1w-image slices of mean images of normalized vehicle (left) and ibotenic acid injected (right) animals. (B) 3D-reconstructed hippocampal volumes of representative vehicle (left) and ibotenic acid (right) injected animals. (C) Semi-automatic detected volumes with vMEMRI of vehicle and ibotenic acid injected animals show significant differences. (D) Correlation between manually and semi-automatic detected hippocampal volumes ($r = 0.96$, $p < 0.001$; Pearson correlation). *** $p < 0.001$ (unpaired t-test)

Results

3. Study 3: Application of vMEMRI in a mouse model of PTSD

3.1. Experiment 1: Volumetric and behavioral changes after trauma and EE

3.1.1. Trauma-related changes of PTSD-like symptoms and hippocampal volume

Experience of the inescapable foot shock led to the development of PTSD-like symptoms one month after trauma in mice housed under standard conditions. More precisely, shocked mice showed increased contextual fear ($p < 0.001$, unpaired t-test; figure 24A left) and increased fear to a single context reminder ($p < 0.001$, unpaired t-test; figure 24A middle). Repeated measurements ANOVA analysis of the acoustic startle responses (ASR) showed a significant effect of the shock ($F_{1,28} = 11.6$, $p = 0.002$) and an interaction between shock application and intensity of the applied startle pulse ($F_{1,130, 31.643} = 7.2$, $p = 0.009$; figure 24A right). This indicates a difference in hyperarousal between shocked and non-shocked mice, with post-hoc tests showing a significantly enhanced startle response of the shocked mice to the 115 dB startle pulse ($p < 0.001$; Fisher LSD).

Behavioral changes indicative of PTSD symptomatology coincided with a reduction in left hippocampal volume ($p = 0.049$, unpaired t-test; figure 24C left), as assessed by vMEMRI. No significant reduction of the right or total hippocampal volume could be found ($p > 0.07$; figure 24C middle + right). Ultramicroscopical measurements also showed reduced hippocampal volume after trauma ($p = 0.041$; figure 24B). Together, both vMEMRI data and ultramicroscopic measurements indicate post-traumatic volume loss of the hippocampus, with vMEMRI data pointing to slightly more pronounced changes in left hippocampus. Volumetric measurement, of total brain volume excluding ventricles, using vMEMRI, showed no effect of the trauma ($p = 0.239$). Furthermore, volumetric differences found for the left hippocampus did not reach statistical significance after normalization to total brain volume ($p > 0.14$, figure 24D left), indicating that either the changes in

Results

hippocampal volume are so subtle that they are not apparent following normalization procedures or that other brain regions also undergo shock-induced changes. Also, right and total hippocampal volume showed no significant differences between shocked and non-shocked animals after normalization to total brain volume (figure 24D)

Experiment 1

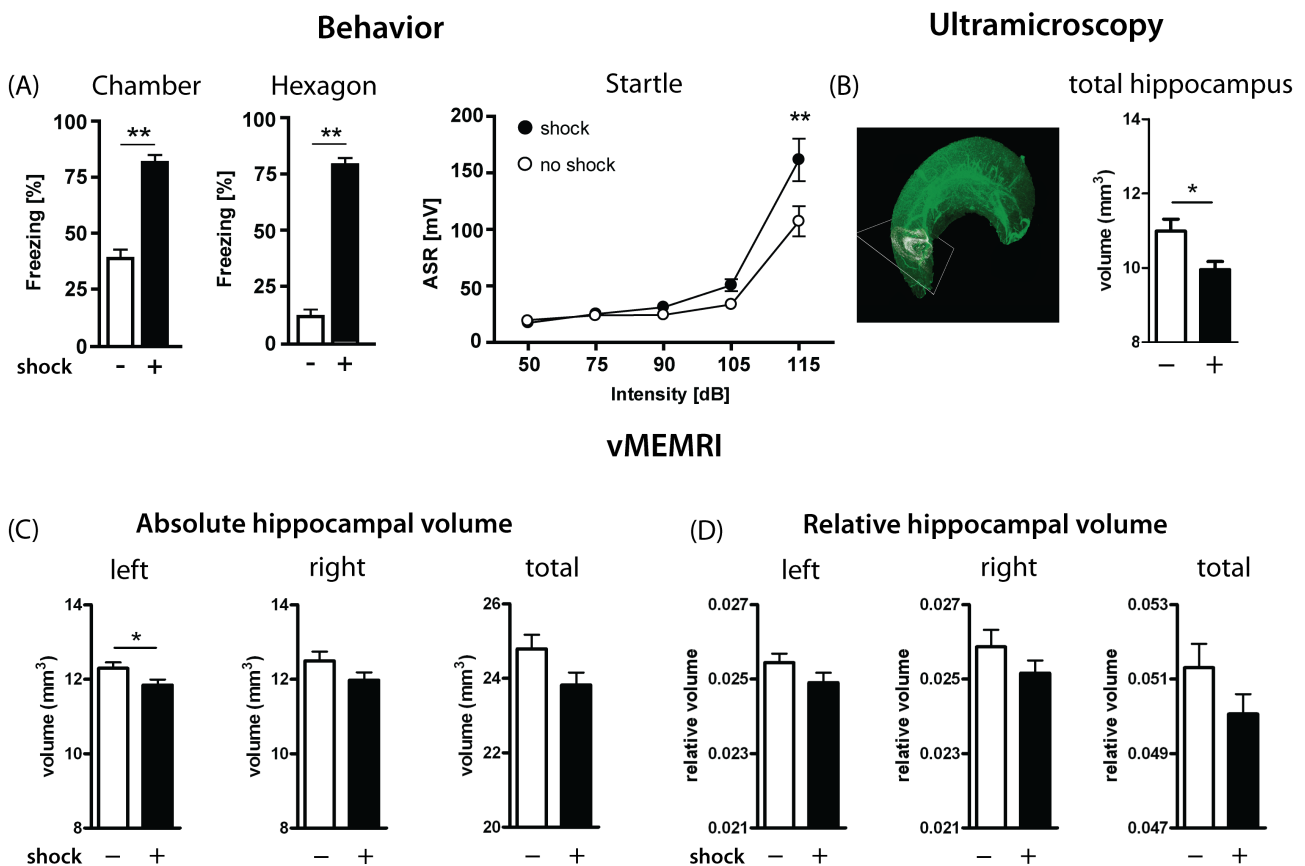


Figure 24. Associative and non-associative fear in standard-housed mice after shock and hippocampal volume measured with vMEMRI and ultramicroscopy. (A) Contextual fear measured as freezing response to the shock context (Chamber, left), fear generalization, measured as freezing response to the grid context (Hexagon, middle) and acoustic startle responses (Startle) to noise pulses of different intensities -all measures 4 weeks after shock. **(B)** Ultramicroscopic image of dissected hippocampus after clearing and digital reconstruction (left). A virtual slice in the ventral hippocampus (white frame) shows inner anatomy of the sample (left). Due to autofluorescence parts of the blood vessel system have been imaged. Total hippocampal volume measured by ultramicroscopy (right). **(C)** Volume of left hippocampus (left), right hippocampus and total hippocampus (right) measured by vMEMRI. **(D)** Left (left), right (middle) and total (right) hippocampal volume normalized to the total brain volume measured by vMEMRI. Statistical analysis were performed by unpaired t-test except for startle response, which was measured by a two-way repeated measures ANOVA, followed by Fisher's LSD post-hoc test. * $p < 0.05$, ** $p < 0.01$

Results

3.1.2. Impact of EE on PTSD-like symptoms and hippocampal volume

Housing ($F_{1,60} = 4.1$, $p = 0.048$; Two-way ANOVA) and shock application ($F_{1,60} = 61.0$, $p < 0.001$) both had a significant effect on contextual fear and there was no indication of an interaction between housing and shock application ($F_{1,60} = 3.0$, $p = 0.16$). Post-hoc analysis revealed a significant decrease in freezing response to the shock context of the shocked animals housed in an enriched environment compared to the shocked animals kept under normal conditions ($p < 0.01$, Fisher LSD; figure 25A). There was no significant difference between freezing responses of the non-shocked animals housed under either an enriched environment or under normal conditions ($p > 0.05$), indicating a specific effect of environmental enrichment on the freezing response (i.e. contextual fear) of the shocked animals. Generalized fear responses to the single feature of the shock context (i.e. shock grid) were also highly significantly affected by shock application, ($F_{1,60} = 185.4$, $p < 0.001$; Two-way ANOVA) but not by housing ($F_{1,60} = 0.19$, $p = 0.66$). The significant interaction between shock application and housing indicated a different effect of housing on the shocked and non-shocked animals ($F_{1,60} = 9.3$, $p = 0.003$; figure 25B). Post-hoc analysis revealed a significant decrease in freezing response to the shock context reminder of the shocked animals housed under an enriched environment compared to the shocked animals kept under normal conditions ($p < 0.01$, Fisher LSD), but showed no differences between non-shocked animals housed in either an enriched environment or in normal conditions ($p > 0.05$, Fisher LSD; figure 25B). In contrast to the findings of a lower contextual fear of the shocked animals housed under an enriched environment, enriched housing conditions appeared to increase hyperarousal as measured by acoustic startle responses. A repeated measurement ANOVA showed a significant effect of housing on the acoustic startle responses ($F_{1,58} = 4.1$, $p = 0.050$), and a trend was found in the

Results

interaction between housing and the applied acoustic startle pulse ($F_{1,371, 79.5} = 3.0$, $p = 0.073$). There was no interaction between shock application and housing conditions ($F_{1,58} = 0.02$, $p = 0.888$) or between the applied acoustic startle pulse, shock application and housing conditions ($F_{1,371, 79.5} = 0.77$, $p = 0.420$), which indicates a similar effect of housing on both, shocked and non-shocked animals (figure 25C).

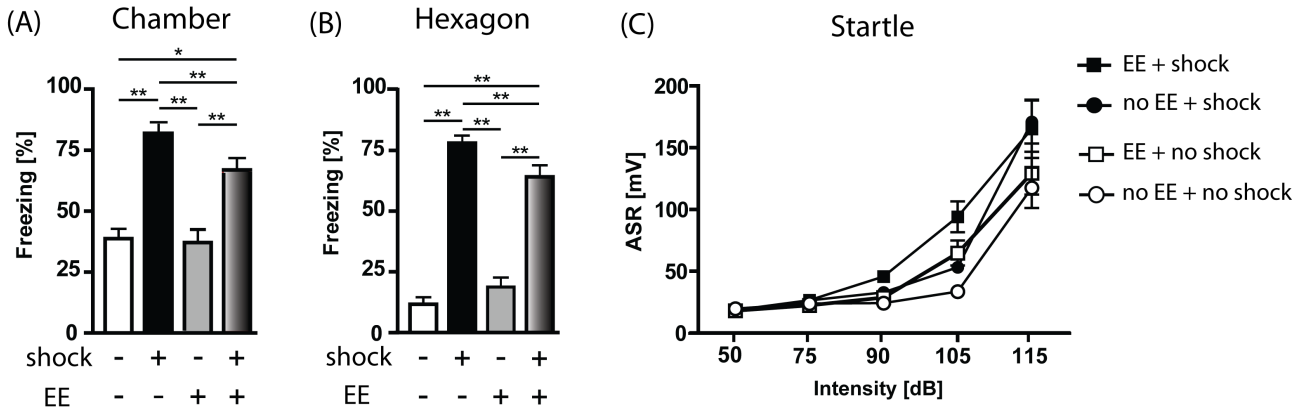
For volumetric analysis by means of vMEMRI and ultramicroscopy, measurements of all experimental groups were compared to the mean hippocampal volume of the non-shock standard-housed group. Two-way ANOVA of data from ultramicroscopic measurements revealed a significant shock x housing interaction ($F_{1,30} = 5.9$, $p = 0.021$; figure 25D), with post-hoc analysis showing a selective volume loss in shocked standard-housed mice that was abolished under enriched conditions ($p < 0.05$; Fisher LSD). In contrast to findings in vMEMRI (see following) ultramicroscopy failed to reveal a general effect of enriched housing on hippocampal volume.

Statistical analysis, by means of two-way ANOVA, showed a marginally significant effect of shock on left hippocampal volume; as measured by vMEMRI ($F_{1,49} = 3.0$, $p = 0.089$; figure 25E left). Furthermore, a main effect of housing conditions could be found ($F_{1,49} = 16.0$, $p < 0.001$) and no interaction effect between shock application and housing was present ($F_{1,49} = 0.65$, $p = 0.422$; figure 25E left), indicating that environmental enrichment led to a significant increase in left hippocampal volume independently of prior shock application. As One-way ANOVA showed a significant difference between groups, ($F_{3,49} = 6.571$, $p = 0.001$) therefore post-hoc analyses were performed, confirming a significant increase in left hippocampal volume between enriched and non enriched animals in both shocked and non shocked mice ($p < 0.05$; Fisher LSD). The housing effect ($F_{1,49} = 7.7$, $p = 0.008$) and differences between enriched and non enriched groups in

Results

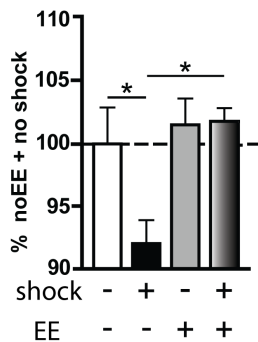
Experiment 1

Behavior



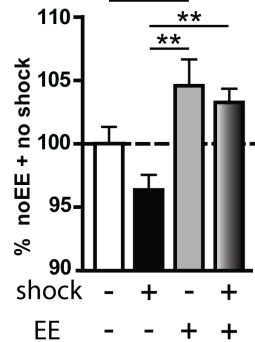
Ultramicroscopy

(D) total hippocampus



vMEMRI

(E) left hippocampus



left hippocampus / whole brain

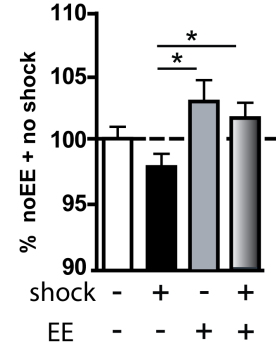


Figure 25: Consequences of environmental enrichment on the development of PTSD-like symptoms and trauma-related volume changes. (A) Contextual fear measured as freezing response to the shock context, (B) fear generalization measured as freezing response to the grid context and (C) hyperarousal measured as acoustic startle responses to noise pulses of different intensities. All measurements taken one month after shock. (D) hippocampal volume measured by ultramicroscopy. (E) Absolute left hippocampal volume (left) and relative left hippocampal volume normalized to whole brain volume (right) measured by vMEMRI. Volumetric measurements were performed 74-88 days after shock. Note that data of standard-housed mice are similar to those shown in figure 24. * $p < 0.05$, ** $p < 0.01$. (Fisher LSD)

shocked mice ($p < 0.05$; Fisher LSD) were still significant following normalization to total brain volume (figure 25E right). A similar effect of housing for right ($F_{1,49} = 6.4$, $p = 0.015$) and total hippocampal volume ($F_{1,49} = 17.1$, $p = 0.001$) was found. However a two-way

ANOVA showed no effect of shock ($F_{1,49} < 2.7$, $p > 0.1$) on right and total hippocampal volume, indicating a higher volume reduction specifically in the left hippocampus after shock application.

3.1.3. Trauma-related changes in other brain structures

The potential of vMEMRI to assess volumetric changes in other brain structures, was further explored. The effects of trauma and environmental enrichment on the central amygdala, the lateral ventricles and total brain volume was examined. Shock experience had a significant impact on the volume of the right central amygdala ($F_{1,49} = 4.5$, $p = 0.038$), as measured by two-way ANOVA, with no effect of housing conditions ($F_{1,49} = 0.15$, $p = 0.695$) and no interaction effect between shock application and housing conditions ($F_{1,47} = 0.19$, $p = 0.669$; figure 26A). The effect of shock was preserved, when right central amygdala volume was normalized to the total brain volume ($F_{1,49} = 3.9$, $p = 0.053$; figure 26 B). No effect was found for the left central amygdala ($F < 0.5$, $p > 0.4$). Housing had a significant effect on lateral ventricle volume ($F_{1,49} = 5.3$, $p = 0.025$; figure 26C) and whole brain volume ($F_{1,49} = 7.1$, $p = 0.010$; figure 26D), with increased volumes seen in mice housed under enriched conditions. There was no significant effect of shock application on lateral ventricle volume ($F_{1,49} = 1.3$, $p = 0.254$) or whole brain volume ($F_{1,49} = 0.60$, $p = 0.443$) and no interaction effect between shock application and housing conditions in either region (lateral ventricles : $F_{1,47} = 0.51$, $p = 0.470$; whole brain: $F_{1,47} = 0.89$, $p = 0.350$) could be observed, indicating an increase in these regions independent of shock application. Post-hoc analysis following one-way ANOVA for whole brain volume ($F_{3,49} = 2.9$, $p = 0.044$) revealed a significant increase in whole brain volume in the environmental enriched groups.

Results

Experiment 1

vMEMRI

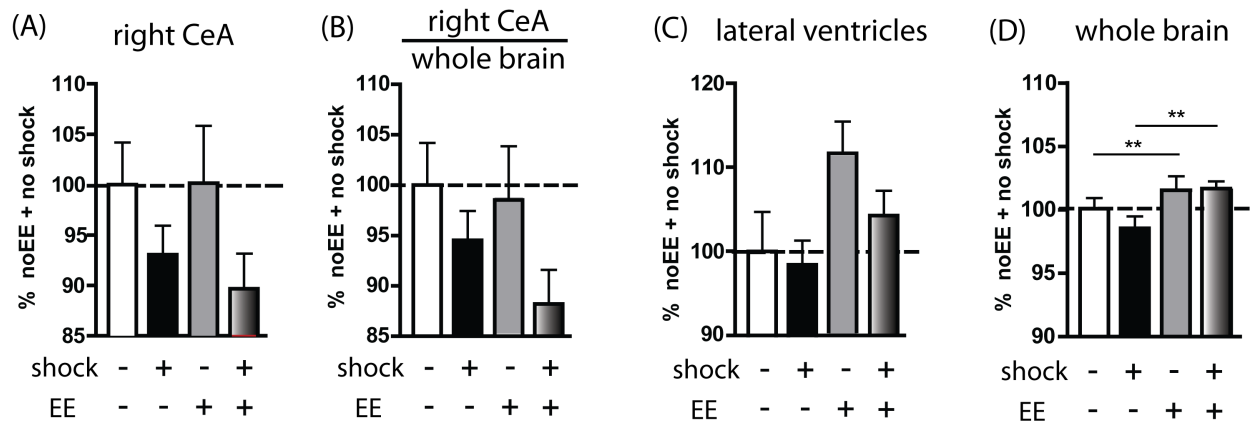


Figure 26. Consequences of trauma and enriched housing on the volume of other brain structures. vMEMRI measurements of the right central amygdala (A), the right central amygdala normalized to the whole brain volume (B), the lateral ventricles (C) and the whole brain (D). All data are compared to the mean of the non-shocked standard housed group. Measurements were performed 74-88 days after shock application. ** $p < 0.01$ (Fisher LSD)

3.2. Experiment 2: Effects of pre- and post-shock EE on PTSD-like symptoms and hippocampal volume loss

It was examined whether the beneficial effects of environmental enrichment on trauma-related volume loss of the hippocampus depended on the time point of enriched housing with respect to the trauma. To answer this question we compared behavioral and morphological data of mice housed in an enriched environment either before (resembling preventive interventions) or after foot shock (resembling therapeutic interventions) with those of mice housed either under enriched or under standard conditions throughout the whole experiment (cf. 3.2. Experiment 2). For freezing responses, a significant group effect on contextual fear ($F_{3,59} = 4.2$, $p = 0.009$; figure 27A) and fear response to the grid context ($F_{3,58} = 4.4$, $p = 0.008$, figure 27B), was found as measured by one-way ANOVA. Post-hoc

Results

analysis showed that freezing responses for all groups of animals housed under an enriched environment was significantly decreased compared to the animals housed under standard housing conditions (For all $p < 0.05$; Fisher LSD). This indicates, that environmental enrichment lowers contextual fear, independent of the time point of enrichment.

One-way ANOVA of volumetric ultramicroscopic measurements of total hippocampal volume showed a significant group effect ($F_{3,54} = 2.8$, $p = 0.049$; figure 27C;). Post-hoc analysis revealed that hippocampal volume was significantly increased in mice housed under an enriched environment after the shock or throughout the experiment compared to standard housed animals ($p < 0.05$, Fisher LSD). As there was a significant effect of environmental enrichment on brain volume ($F_{3,47} = 6.11$, $p = 0.001$; data not shown) increases could be due to a general volumetric increase. vMEMRI measurements of the left and total hippocampal volume relative to the whole brain revealed that there was a specific increase in the hippocampus (left hippocampus/whole brain: $F_{3,47} = 3.16$, $p = 0.032$; figure 27D; total hippocampus/whole brain: $F_{3,47} = 2.46$ $p = 0.053$; figure 27F; two-way ANOVA). Post-hoc analysis revealed that hippocampal volume was, as seen with ultramicroscopy, significantly increased in mice housed under an enriched environment after the shock or throughout the experiment compared to standard housed animals ($p < 0.05$, Fisher LSD). There was no significant group effect on volume in the right hippocampus ($F_{3,47} = 1.23$, $p = 0.309$).

Results

Experiment 2

Behavior

Ultramicroscopy

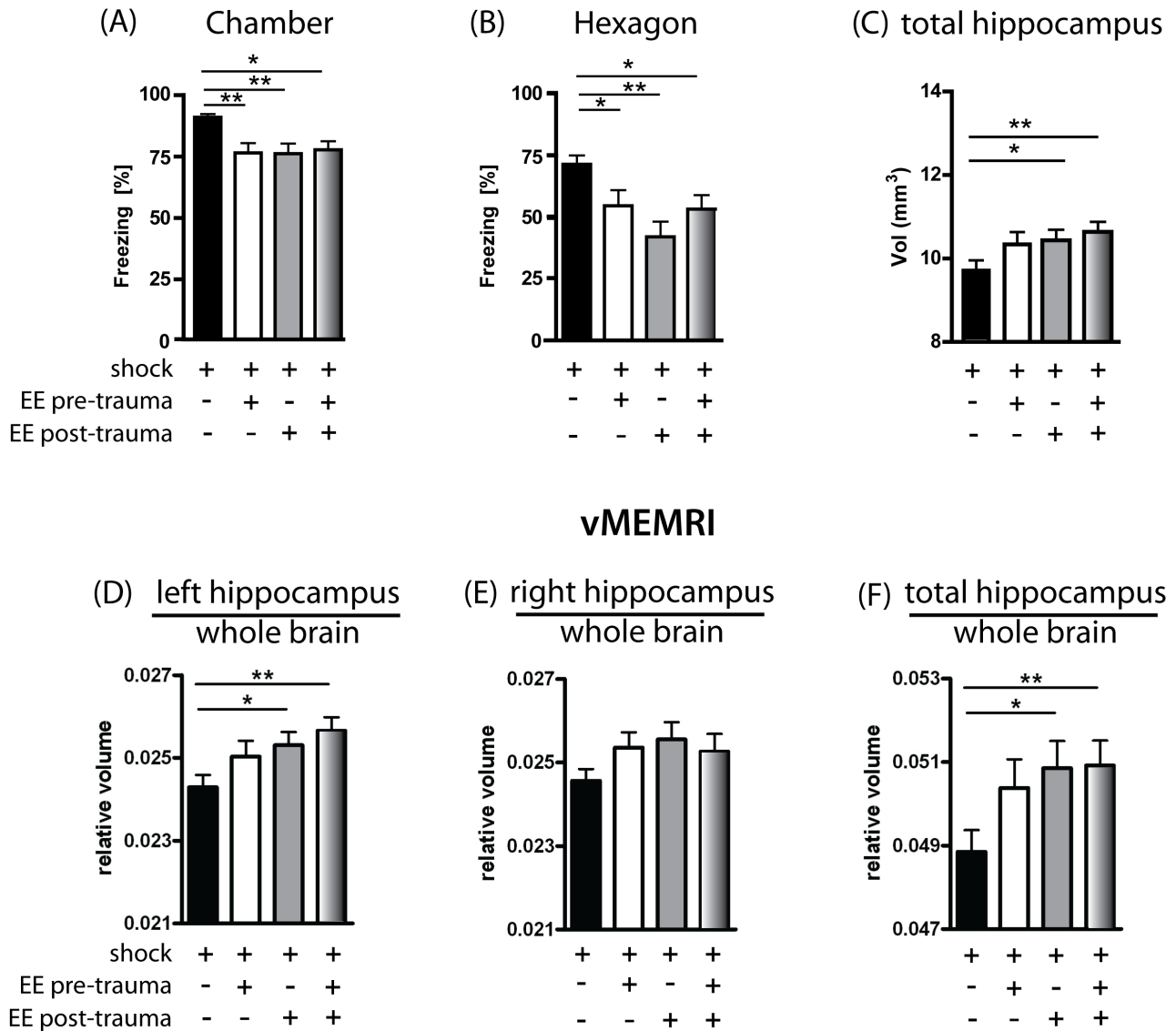


Figure 27. Consequences of pre- and/or post-shock enriched housing on fear and hippocampal volume. (A-B) Contextual fear measured as freezing response to the shock context (A) and fear generalization measured as freezing response to the grid context (B) one month after shock. (C) total hippocampal volume measured by ultramicroscopy (D) Left hippocampal volume (E) right hippocampal volume (F) total hippocampal volume relative to whole brain volume as measured by vMEMRI. Volumetric measurements were performed 74-88 days after shock. * $p < 0.05$, ** $p < 0.01$ (Fisher LSD)

D. Discussion**1. Study 1: Manganese toxicity**

This study investigates short- and long-term effects of MnCl_2 application, in dosages suitable for MEMRI experiments, on health, stress and learning. The single application study shows, that treatment with 99 mg/kg MnCl_2 , although well tolerated in rats, leads to severe health impairment in BL6N mice as shown by significant reduction in body temperature and locomotion. Body temperature and locomotion seem to be reliable, quantifiable markers to measure toxic side effects of MnCl_2 application. Although a dose of 90 mg/kg was reported to be well tolerated by rats even after repeated injection, the presented results are in line with a recent study showing considerable decrease in body weight and voluntary wheel running after single systemic application of 80 mg/kg MnCl_2 in rats (Bock et al., 2008b; Eschenko et al., 2010a). To gain detectable signal changes in MRI contrast and get sufficient contrast in neuroarchitecture, application of dosages between 80 and 160 mg/kg have been reported (Aoki et al., 2004b; Silva et al., 2004; 2008). Taking into consideration the long half-time of manganese in the brain (between 51 and 74 days) it has been proposed to apply MnCl_2 in a fractionated matter (i.e. in smaller dosages more often) to reach a sufficient Mn^{2+} accumulation while minimizing toxic side effects of the acute injection (Takeda et al., 1995; Bock et al., 2008b).

Based on these assumptions, the second study compared the effects of three different fractionated application protocols of MnCl_2 on body temperature and locomotion, behavioral and endocrine measures. The data presented shows that the protocols with doses of 30 mg/kg MnCl_2 showed the least effects on health and on animals' well-being. Hypothermia and hypolocomotion were substantially attenuated in these groups compared to the group injected with 60 mg/kg MnCl_2 . Application of MnCl_2 led to nominally higher

Discussion

corticosterone levels 4 h, and significantly higher corticosterone levels 12 h, after treatment in the 3x60/48 and the pooled 30 group compared to the vehicle group with no significant differences between 60 mg/kg and 30 mg/kg doses. On day 5 of the experiment, however, corticosterone levels of all MnCl_2 groups were comparable to those of the control group. These results denote, that receiving MnCl_2 treatment is a considerable acute stressor, but may readily habituate upon repeated encounter. This implication is supported by the fact that MnCl_2 treatment affects body weight only after the first treatment and that effects were only transient, with recovery after few days. Although the highest total dose of MnCl_2 was delivered with the 8x30/24 application (240 mg/kg) scheme it should be noted, that this led to less severe side effects than the 3x60/48 scheme delivering a total dose of 180 mg/kg. This suggests that the toxic side effects are not just dependent on totally accumulated Mn^{2+} , but rather on the acute toxic side effects on health and hormonal stress of each individual application in a fractionated protocol.

Besides the considerably lower disruption to the animals' well being and hormonal stress response the 8x30 group showed the best contrast enhancement of all tested fractionated application protocols. These findings led to the usage of the 8x30 application protocol in further experiments. Taken together, these findings support the second working hypothesis that a repeated application of MnCl_2 in small dosages minimizes toxic side effects and distress.

The third study deals with short- and long-term effect of MnCl_2 application with the 8x30 protocol on learning and hyperarousal. Significant long-term effects of MnCl_2 application on contextual fear, avoidance of a shock context specific odor and hyperarousal in a mouse model of PTSD more than five weeks after injections were observed. Even though aversive contextual learning took place more than 10 days after

Discussion

MnCl₂ application, contextual fear 4 weeks after shock application is still affected. Additionally, a specific effect of Mn²⁺ accumulation in shocked MnCl₂ treated mice on hyperarousal, as shown by acoustic startle response (ASR) enhancement, was observed. As the injections and MRI scanning took place at least 10 days before shock application, as mentioned before, acute toxic effects of Mn²⁺ can be excluded. Also, a general effect of MRI scanning can be ruled out as all animals, including vehicle treated animals, were scanned. Furthermore, MnCl₂ treatment itself did not cause general hyper- or hypolocomotion, which would have an effect on freezing behavior, as shown by the similarity of freezing behavior of the non-shocked groups. This is also supported by the similar motor-behavior in the CODA task, where MnCl₂ injected mice show no difference in latency to enter a compartment or in the number of compartment entries.

Enhancement of ASR has been shown in people with anxiety disorder and is one of the diagnostic criteria for PTSD (Grillon et al., 1994a; 1996; American Psychiatric Association, 2000). It has been shown in our mouse model of PTSD that enhancement of ASR, after fear incubation, is one of the PTSD-like symptoms that develops following a 1.5 mA footshock (Golub et al., 2009). A sensitization of the ASR as a result of conditioned fear potentiation after footshock application has long been known (Davis, 1989). Although the pathway mediating the ASR in stress and anxiety, as well as in fear related potentiation, is generally described from the auditory nerve across several interstations to the spinal neurons, the caudal pontine reticular nucleus seems to play a key role. The caudal pontine reticular nucleus is influenced by somewhat different neuronal networks that distinguish between anxiety related long-term and fear potentiated short-term effects on ASR (Davis, 1989; Davis et al., 1997). Fear potentiation was shown to be related to the amygdala, parabrachial gray and ventral tegmental area (Davis et al., 1997). Whereas

Discussion

the bed nucleus of the stria terminalis and the hippocampus seem to have an additional pivotal impact on anxiety related ASR enhancement (Walker, 2003). Whether hippocampal impairment in contextual fear due to MnCl_2 application led to the observed potentiation of ASR in shocked mice can only be speculated. Several drugs influencing neuronal transmission were found to enhance, as well as attenuate, ASR. Also a specific effect of drug application on fear- or anxiety-enhanced ASR was observed (Kehne et al., 1981; Grillon et al., 1994b; Fendt et al., 1994; Walker and Davis, 1997). An influence of Mn^{2+} on neuronal transmission which affects ASR seems to be plausible and should be investigated more closely. There are findings that show, that dopaminergic neurons are crucially involved in fear-potentiated and shock-sensitized ASR, which is interesting considering the influence of manganese on dopamine metabolism (Bird et al., 1984; Borowski and Kokkinidis, 1996; Lamont and Kokkinidis, 1998).

It has been shown in the applied mouse model of PTSD, that the development of PTSD-like symptoms becomes noticeable in a dissociation between trauma related associative (i.e. contextual fear) and non-associative fear (i.e. hyperarousal (Siegmund and Wotjak, 2007; Golub et al., 2009; Pamplona et al., 2010)). The selective effect of MnCl_2 application on hyperarousal and contextual fear in shocked animals points to an impairment of associative learning in these animals. Therefore the experiments of the third chapter were designed to determine, whether the observed impairments in associative learning can be specifically ascribed to hippocampus dependent learning processes.

Application of MnCl_2 took place at least 12 h before training in the WCM, but still resulted in significant effects on accuracy in spatial learning during repeated training. However, accuracy in the response or free choice learning protocol was unaffected. Numerous manganese toxicity studies reported a large accumulation of Mn^{2+} in the basal

Discussion

ganglia which could indicate effects on locomotion (Yamada et al., 1986; Newland and Weiss, 1992). Nevertheless, a general effect of MnCl_2 application on motor activity, and in consequence on swimming behavior, can be objected, as there was no difference in accuracy between the groups in the response and free-choice protocols. Furthermore, latency to reach the escape platform was unaffected in every learning protocol by MnCl_2 application (data not shown). The selective impairment of spatial learning due to Mn^{2+} accumulation became even more apparent when MnCl_2 injected animals were divided into animals showing high and low Mn^{2+} accumulation in the hippocampus. Spatial learning was specifically altered in animals showing high Mn^{2+} accumulation in the hippocampus compared to control animals, which emphasized that MnCl_2 application seems to selectively impair hippocampus dependent learning.

Only few studies examined electrophysiological changes after MnCl_2 treatment. It was shown, that a single application of 80 mg/kg MnCl_2 acutely decreases local population postsynaptic response in the dentate gyrus (Eschenko et al., 2010b). This effect can be explained by the great accumulation of Mn^{2+} in the hippocampal structure after systemic MnCl_2 application and Mn^{2+} competition for voltage gated Ca^{2+} channels (Drapeau and Nachshen, 1984; Narita et al., 1990; Bock et al., 2008a). Although it was argued by the same authors, that this single MnCl_2 application did not lead to differences in neuronal excitability and hippocampal plasticity, as shown by choice accuracy in a T-maze delayed alteration task, MnCl_2 was only applied once after the hippocampal task was already learned. Therefore the study merely shows that memory retention 24h after injection was not affected (Eschenko et al., 2010b). Additionally, impairment of spatial learning in the WCM and the long-lasting effects of MnCl_2 application on contextual fear after MnCl_2 application, indicate that Mn^{2+} application seems to rather have an effect on encoding than

Discussion

recall of the memory. A recent study systemically injected one dosage of 40 mg/kg MnCl_2 in rats and tested them 1 and 24 h after application in a morris water maze task. The authors claimed, that hippocampal learning was not disrupted by Mn^{2+} accumulation since MnCl_2 injected rats showed no difference in the time it took to find a hidden platform in a new position compared to vehicle injected rats on two consecutive days (Jackson et al., 2011). Considering the long half-time of Mn^{2+} in the brain the impact on hippocampal learning would only become more apparent on the long run as Mn^{2+} accumulates with successive treatments.

Overall, the first working hypothesis that systemic application of MnCl_2 in standard dosages applied in MEMRI experiments leads to toxic side effects quantifiable with measures of locomotion and body temperature and behavioral and endocrine functioning could be confirmed. Repeated application of Mn^{2+} in small dosages minimized measured toxic side effects and distress and provided adequate MEMRI contrast, which verified the second working hypothesis. The third working hypothesis, that learning and memory processes stay unaffected by fractionated application of MnCl_2 , has to be partially rejected. Associative and spatial learning was shown to be altered by Mn^{2+} accumulation indicating a specific effect of MnCl_2 application, even at small dosages, on contextual learning. Habitual learning processes seem to be unaffected by Mn^{2+} accumulation. Because of the potential side effects MnCl_2 further MEMRI experiments in chapter II and II were conducted as final experiments.

2. Study 2: Validation of vMEMRI

The first part of the results of study 2 demonstrated that the 8x30/24 application protocol not only resulted in the highest signal intensities in T1w-images of the brain, but

Discussion

also provided the best differential contrast among brain structures. Studies using rats have shown that fine structures of the olfactory bulb and cerebellum could be distinguished after Mn^{2+} application (Chuang et al., 2009; 2010). The presented results confirm these findings in mice, who have much smaller brain volumes. The layers of the retrosplenial granular cortex became distinguishable only on images acquired from mice treated with the 8x30/24 protocol. This is supported by a study from Lee and colleagues who also showed that MEMRI is able to resolve fine structures of the mouse cortex (Lee et al., 2005). Despite using single high doses of Mn^{2+} of 88 mg/kg or greater, as it was done by Lee and colleagues, it was shown that visualizing fine brain structures is also possible by applying smaller dosages of Mn^{2+} in a fractionated manner. Furthermore it was shown that Mn^{2+} labeling of laminar structures correlates with standard histological neuronal staining methods (Silva et al., 2008). The high signal intensity in hippocampal substructures which was observed has also been shown by Bock and colleagues (Bock et al., 2008a). This is especially favorable to the currently presented semi-automatic vMEMRI method for determining hippocampal volume; a high signal contrast of the assessed structure improves normalization procedures because structural borders are better detected and aligned.

The contrast differences between brain regions, obtained after administration of a low total dosage of Mn^{2+} (number of pair wise differences for 3x60/48 and 6x30/48 are 3 and 5, respectively), was substantially enhanced by a higher total dosages of Mn^{2+} (number of pair wise differences for 8x30/24 is 12). The coefficient of variation showed that this effect was more dependent on the total dosage than on the fractionated treatment, with the vehicle treated group showing lowest variation followed by the groups that received a total dosage of 180 mg/kg (3x60/48 and 6x30/48). The 8x30/24 group, which

Discussion

received 240 mg/kg showed the highest coefficients of variation. Further extending the low-dosage application protocol beyond the maximally tested 8 treatments might lead to even better contrast enhancement. However, the shown side effects produced by Mn²⁺ accumulation will probably increase with higher total dosages.

It can not be ruled out that the higher regional and overall contrast of the 8x30/24 group was influenced by the shorter inter-injection interval. Previous studies have shown that an increase in MRI signal directly relates to tissue concentration of Mn²⁺, reflecting Ca²⁺ influx into the tissue (Hu et al., 2001; Daire et al., 2008). Furthermore, a correlation between signal intensity and neuronal activation, as measured by cytochrome c staining, and axonal density, as confirmed by histological methods, emphasizes the functional relevance of measured differences in signal intensities (Immonen et al., 2008; Bock et al., 2009). However it can not be assumed that signal enhancement after systemic application of Mn²⁺ leads to a general overview of the most dense and active regions of the brain, since Mn²⁺ favors regions close to the pituitary and lateral ventricles (Bock et al., 2008a).

A newly established method to automatically determine whole brain and hippocampal volumes *in-vivo* is introduced. All previous studies using MEMRI determine volumes manually (cf. appendix table 2). The presented method, based on the normalization tool of SPM2, takes advantage of the tissue contrast introduced by Mn²⁺ application. The specific signal enhancement of the hippocampus alleviates morphing of the outlines of this structure to a template which allows single manual determination of the hippocampus, which excessively reduces time investment for volumetric analysis.

Artificially induced signal gradients caused in T1w images by the surface coil can be efficiently reduced by application of the right bias correction without reducing contrast between tissues. Manual determination of hippocampal volume was shown to be a reliable

Discussion

measure based on the high inter-rater correlations for the data obtained and could be used to verify the semi-automatic vMEMRI method. It was shown that brain and hippocampal volumes obtained by semi-automatic vMEMRI method highly correlated with manually obtained volumes. Manual determination of the brain and the hippocampus of one animal takes a trained rater between 3 – 4 h. Semi-automatic determination of any number of animals can be achieved in a few days.

Previously reported decreases of brain volumes of about 25 % and significant hippocampal volumes changes in Cyclin D2 KO animals (Kowalczyk et al., 2004) have been confirmed by means of vMEMRI. Additionally it could be shown, that differences in hippocampal volume between KO and WT animals are not merely related to overall brain volume decrease, but that hippocampal volume was specifically reduced in KO animals in relation to whole brain volumes. This underlines the great advantage of vMEMRI, namely having an overview of the whole brain structure and the relationship of specific volumetric changes compared to other structures and the whole brain.

Despite the fact that ibotenic acid lesions induce great changes in hippocampal volume the semi-automatic vMEMRI detection could reliably reproduce manually obtained measures. The application of vMEMRI not only reduces time which would be spent to histologically determine lesion induced changes, but also opens the possibility to confirm lesions *in-vivo* and thereby reducing time spent for further experiments.

Previous studies using Mn^{2+} for tissue enhancement on T1w-images and subsequent volumetric analysis of organs have shown, that the obtained volumes of the whole structure and substructures highly correlated with volumes found with other methods (Hu et al., 2004; Berkowitz et al., 2007). Furthermore, a study in birds that

Discussion

determined volume of the area x¹, using MEMRI, found a high correlation of the obtained values with volumes obtained by classical histological methods (Van der Linden et al., 2002). Such finding support the notion that the vMEMRI results that were observed are reflective of true volumetric values. It should be noted however, that higher signal intensities could affect determination of the volume. Due to the insularity of the hippocampal structure within the brain and high contrast between the hippocampus and the surrounding tissue it is unlikely that signal intensity would disrupt volumetric measurements. Moreover, in all currently presented studies no correlation between the signal intensity and the volume was observed (data not shown).

In conclusion, it could be shown for the first time that *in-vivo* semi-automatic detection of hippocampal volume is possible in mice with the newly established method of vMEMRI. The first working hypothesis that semi-automatic detection of hippocampal volume correlates with manually obtained volumes could be confirmed. The high correlation with manually obtained values and the experimental validation in cyclin D2 and ibotenic acid lesioned animals, indicates the high reliability of this method. Also the second and third working hypotheses, that Cyclin D2 and hippocampal lesioned animals show smaller hippocampal volumes could be confirmed. The findings are in agreement with previously reported histological findings and even highly variable differences in hippocampal volume can be detected by means of vMEMRI.

3. Study 3: Application of vMEMRI in a mouse model of PTSD

The third study shows that vMEMRI is capable of measuring small bidirectional differences in hippocampal volume in mice, between 1 and 5 %, altered by enriched

1 Part of the vocal learning pathway in birds

Discussion

housing or a brief exposure to an inescapable footshock. Both volumetric ultramicroscopic measurements and vMEMRI detected a decrease in hippocampal volume in groups exposed to a traumatic event. In line with this, previous data from our group have shown a decrease in the expression levels of GAP43, an axonal marker implied in neurite outgrowth within the hippocampus, after trauma (Golub et al., 2010; data not presented here). Volumetric measurements by means of vMEMRI were able to extend the findings of volumetric ultramicroscopy by demonstrating a laterality effect of hippocampal volume reduction after trauma exposure specific to the left hippocampus. Both ultramicroscopic and vMEMRI measurements revealed that environmental enrichment counteracted the posttraumatic hippocampal volume reduction. Environmental enrichment also led to a decrease in contextual and generalized fear, but not hyperarousal. vMEMRI and Ultramicroscopical analyses indicated that post-shock and continuous enriched housing appeared to be similarly efficient, whereas they did not see the effect for pre-shock housed mice. Furthermore, images obtained by means of vMEMRI allowed for extension of the volumetric analysis to other brain regions. A smaller central amygdala volume in shocked animals, which was specific to the right side, was found in this analysis.

It should be noted, that there was only a weak correlation between volumetric ultramicroscopy and vMEMRI measurements of $r = 0.22$ $p = 0.15$ (Pearson correlation). Differences in ultramicroscopic and vMEMRI data probably result from alterations in tissue volume induced by the processing necessary for ultramicroscopic visualization. In contrast to an *in vivo* visualization of the mouse brain with vMEMRI, *ex vivo* preparation of tissue for ultramicroscopy includes several dehydration steps (see methods section) leading to a shrinkage of hippocampal volume of over 50 % (cf. Ultramicroscopic and vMEMRI data in figure 24). This may explain why effects of environmental enrichment on volumetric

Discussion

changes were found to be less pronounced with ultramicroscopic measurements; particularly because vMEMRI measurements of the lateral ventricles indicated highly significant effects of environmental enrichment on brain fluid content. Nevertheless, hippocampal volume loss arising from the shock exposure and the effects of environmental enrichment were large enough to be detected by both *in vivo* and *ex vivo* approaches.

Volumetric differences of the hippocampus in PTSD patients have been widely detected and hippocampal volume has been inversely related to memory disturbance, trauma severity and severity of PTSD symptoms (Bremner et al., 2008). A recent meta-analysis also found a laterality effect of hippocampal volume reduction in PTSD patients (Woon et al., 2010). In contrast to the study presented here, Woon and colleagues found a volumetric reduction in PTSD patient which is more pronounced for the right hippocampus. The authors also found that the right hippocampus is larger in 'normal' human controls. Interestingly, this is also true for untreated C57Bl/6N mice, with average left hippocampal volume at 12.29 mm³ and average right hippocampal volume 12.49 mm³. Additionally, the present study supports the finding by Woon and colleagues, that hippocampal volume reduction seems to be more dependent on trauma exposure rather than the development of PTSD-symptoms (Woon et al., 2010). No correlation between severity of PTSD-like symptoms and hippocampal volume reduction could be found. Also when animals were grouped by median split into high and low freezers depending on the magnitude of contextual or generalized fear no correlation between symptom severity and hippocampal volume changes was found (data not shown). However, the present data do not rule out the possibility that a smaller hippocampus could increase the individual's vulnerability for developing PTSD in the aftermath of a trauma, as suggested by Gilbertson and colleagues

Discussion

(Gilbertson et al., 2002). It has been previously shown using the same mouse model of PTSD, that hippocampal N-acetylaspartate (NAA) levels, a marker of neuronal integrity, before trauma could predict the severity of PTSD-like symptoms developed up to 9 months after trauma (Siegmund et al., 2009). There are some studies showing an age dependent correlation between hippocampal volume and NAA levels; however, there are also some studies, especially in the field of psychiatric disorders, which did not see any such correlation (Deicken et al., 1999; Schuff et al., 1999; Neylan et al., 2003). Simultaneous *in-vivo* longitudinal measurements of hippocampal volume and NAA levels before and after a trauma could help to resolve this issue.

The current study also found volumetric shrinkage of the right amygdala following trauma exposure. It should be noted, however, that increases in signal intensity due to activity-dependent manganese accumulation in certain areas could compromise volumetric detection. However, no correlation between right amygdalar volume and signal intensity was found ($r = -0.15$, $p = 0.27$; Pearson correlation). This finding supports several studies on amygdalar volume in PTSD patients (Schmahl, 2003; Matsuoka, 2003).

Theoretical models extrapolating from animal research have proposed a neurocircuitry model of anxiety disorder connecting the prefrontal cortex, the hippocampus and the amygdala (McNaughton and Gray, 2000; Rauch et al., 2006; Bast, 2007). These models hypothesize a hyperresponsivity of the amygdala to threat-related stimuli, with inadequate top-down control over the amygdala due to a hyporesponsive prefrontal cortex and/or hippocampus. Hippocampal interaction with the amygdala was shown to be crucially involved in encoding emotional memories and, in consequence, structural and functional changes of the hippocampus such as diminished volume, neuronal or functional integrity are thought to underlie disturbed processing of threat-related stimuli in PTSD

Discussion

(McGaugh, 2004; Dolcos et al., 2004; Shin et al., 2006). Structural changes of the hippocampus and amygdala have also been detected in animals models of depression and chronic stress (Campbell et al., 2004; Lange and Irle, 2004).

Structural changes of the hippocampus have been mainly ascribed to prolonged glucocorticoid exposure (Sapolsky et al., 1985). Prolonged stress experienced in form of chronically enhanced glucocorticoid levels was found to alter neuronal excitability, neurochemistry and plasticity, which were consequentially found to alter overall brain functioning (Joëls, 2010). Nevertheless, hypercortisolism has not been found in patients with PTSD; on the contrary, they even show lower levels of plasma cortisol levels in comparison to controls (de Kloet et al., 2006). Several studies report a positive correlation between blood flow in the hippocampus and parahippocampal regions at rest and symptom severity PTSD patients, which indicates increased activity in these areas (Sachinvala et al., 2000; Chung et al., 2006). A higher basal activity of the hippocampus, in the form of excessive neurotransmission leading to cell death (Kim et al., 1996), could lead to the observed alterations in hippocampal volume .

It has been previously shown that housing rodents in an enriched environment to increases neurogenesis and the survival rate of newborn cells in the hippocampus (Kempermann et al., 1997; van Praag et al., 1999). An enhancement of neurogenesis could partly explain the hippocampal volume increases observed. As stress reduces hippocampal neurogenesis and leads in consequence to hippocampal dysfunction, enhanced neurogenesis could explain the observed beneficial effects of environmental enrichment on ameliorating contextual and generalized fear (Gould and Gross, 2002; Sapolsky, 2003). On the other hand, it is still unclear whether changes in neurogenesis are sufficient to alter learning and memory (Shors et al., 2001). The enlarged lateral ventricles

Discussion

and the increased hippocampal volume by environmental indicate that fluid content and/or vasculature volume could be greatly enhanced by environmental enrichment. An interesting concept was introduced by Czéh and Lucassen (2007) in their review on hippocampal volume decreases in depression; clinical studies show lower fluid content and size of several brain structures together with enlarged ventricles in patients with mood disorders (Manji, 2003) and the authors speculated that a shift in fluid balance could be responsible for hippocampal shrinkage and thereby underlie the disturbances on learning and memory. In line with this reasoning, an enhancement in ventricle volume together with an enhancement in brain fluid content and structure size as seen by enlarged hippocampi and whole brain volume after environmental enrichment could be beneficial to the organism. Additionally, changes in extracellular space and vasculature should also be taken into account (Syková and Chvátal, 2000). These changes could enhance molecular transmission and, in consequence, information processing.

In conclusion, the first working hypothesis can be confirmed: application of a shock leads to a volume reduction of the hippocampus measurable with vMEMRI. Both techniques, ultramicroscopic measurements and vMEMRI could detect this small but significant effect. However, the hippocampal shrinkage induced by trauma exposure was no longer significant, when hippocampal volume was normalized to individual brain volume. The second working hypothesis, that hippocampal volume changes and PTSD-like symptoms are modifiable by environmental conditions, could also be confirmed. The third working hypothesis that vMEMRI can mirror volumetric alterations of the hippocampus obtained via ultramicroscopy can partly be confirmed. Both methods detected reductions in response to the shock, however vMEMRI only detected these changes for the left hippocampus. The enhancement of hippocampal volume due to

Discussion

environmental enrichment could also be detected with both methods, vMEMRI detected great changes, whereas ultramicroscopy only indicated small changes. There was no direct correlation found between the methods, which can probably be ascribed to the measurement of differently processed tissues.

4. Conclusion and outlook

The first two aims of this PhD thesis had been the establishment of a MEMRI protocol in mice and the optimization of a Mn^{2+} application procedure to reduce toxic side effects. They had been addressed in chapter I. The third and fourth aim of this thesis, to develop an automatized method to determine hippocampal volume and to validate the vMEMRI analysis has been subject of chapter II. Chapter II showed an application of vMEMRI in a mouse model of psychopathology.

Study 1 shows that the toxicological side effects of Mn^{2+} , as applied for MEMRI studies, can be substantially reduced by injecting $MnCl_2$ in smaller dosages. Good MRI contrast can be ensured by repeated applications of $MnCl_2$, taking advantage of the long half-life of Mn^{2+} in neuronal tissue. Application of $MnCl_2$ in small dosages of 30 mg/kg, in a repeated manner, reduced hypothermia and hypolocomotion induced by higher dosages of 60 or 99 mg/kg. Additionally, injection stress, seen as corticosterone peaks especially after first injection could be reduced by injecting smaller dosages. Further reducing applied dosages and prolonging the Mn^{2+} application protocol could be proven to be even more beneficial. However, it should be considered that simple intraperitoneal injections can lead to severe stress and alterations in gene expression and brain activity in animals (Sharp et al., 1991). A promising method for a continuous slow Mn^{2+} application could be the delivery of $MnCl_2$ via small osmotic minipumps chronically implanted into the peritoneum

(Eschenko et al., 2010a).

Furthermore, it was also shown in this chapter that increased Mn^{2+} accumulation in the hippocampus seems to selectively disturb functionality of the hippocampus. Lower freezing responses to the shock context and a context reminder, as well as an increased startle response and lack of avoidance in the conditioned odor avoidance task of the shocked Mn^{2+} injected group pointed to altered associative learning in these mice. The impairments in contextual fear and fear conditioning of Mn^{2+} injected mice suggested a disturbance of hippocampal functioning. The idea, that Mn^{2+} specifically confounds hippocampus-dependent learning processes was further strengthened by findings in the water cross maze task. Manganese injected mice were specifically impaired in the spatial learning protocol, but not in the response or free-choice learning protocols, which allowed for the use of hippocampus-independent habitual learning. Although some studies suggest that systemic application of Mn^{2+} in the ranges applied in this study do not lead to functional deficits of the hippocampus (Eschenko et al., 2010b; Jackson et al., 2011), studies should focus on minimizing total applied dosages, while gaining sufficient contrast for morphological analysis. This is further supported by the finding that mice with the highest signal intensity and therefore, increased Mn^{2+} accumulation in the hippocampus showed the lowest spatial learning abilities. Overall, the goal of establishing the vMEMRI method has been to enable longitudinal studies *in-vivo* allowing for repeated analysis of brain morphology without disturbing regional functionality. This requires further detailed investigation of Mn^{2+} toxicology in terms of behavior and neurophysiological consequences in order to allow for the study of developmental morphological effects in particular of the hippocampal in animal models undisturbed by the methodological approach.

The first part of study 2 revealed that an excellent tissue contrast can be achieved

Discussion

with the presented protocol for fractionated application of Mn^{2+} . With the repeated application of small dosages of $MnCl_2$, laminar structures of the olfactory bulb and the cerebellum became visible. Specific layers of the cortex only became visible after 8 injections of 30 mg/kg with an inter-injection interval of 24 hours. Increasing the totally applied dosage of $MnCl_2$ could further enhance visualization of fine structures. However, this would not be advisable for application in experimental animals that should show undisturbed behavior due to the negative effect of Mn^{2+} accumulation in the hippocampus on hippocampal-dependent learning (cf. chapter I). Sampling at higher resolutions should improve visualization of fine structures, such as differentiation of cortical layers for example, which could reduce total applied dosages of Mn^{2+} and scanning artifacts. However, sampling at higher resolutions also means prolonging scanning time and hence extended anesthesia of the animal. Thus the advantages of a higher resolution and the disadvantages of a prolonged anesthesia have to be counterbalanced and adjusted to the experimental demands. Furthermore, technical advances in the field of imaging sequences for small animal MRI over the last decade, the combination of different acquisition techniques, such as T1 mapping, and the adjusted scanning parameters for MEMRI should lead to a considerable improvement of images (Natt et al., 2002; Lee et al., 2005; Chuang and Koretsky, 2006). The importance of post-processing was also shown in Chapter II. Post processing of the image significantly reduces signal gradients introduced by the signal receiving coil while maintaining image contrast. Alignment of artificially induced signal intensity gradients while keeping tissue contrast is important for the precision of the analysis of signal intensity and the improvement of morphing accuracy to other images.

The second part of study 2 introduces a method to semi-automatically determine

Discussion

hippocampal volume. It is shown that the semi-automatic vMEMRI method reliably detects whole brain and hippocampal volume compared to manually determined volumes. The semi-automatic vMEMRI method enables, for the first time, an *in vivo* detection of volumes. Furthermore, in the third part of chapter II, the method of vMEMRI is experimentally validated in animals with genetically and chemically altered hippocampi. Structural plasticity of the hippocampus, especially following the discovery of neurogenesis, became increasingly central in the study of cognitive and behavioral adaptive processes (Kempermann et al., 1997). Structural changes of the hippocampus not only include the addition of new cells, but also cellular mechanisms which alter neuronal plasticity, such as numeric changes in dendritic spines and axonal branches and volumetric changes of the soma, as well as circuit reorganization, such as altered connectivity and excitability of networks, which may have substantial influence on learning and memory (Engert and Bonhoeffer, 1999; Holtmaat et al., 2005; De Paola et al., 2006; Haber et al., 2006). Microscopical and histological methodologies are predominantly applied for the analysis of structural changes (see also general introduction subsection 3). However, these methods are limited by numerous factors, including the examination of pre-selected brain regions, tissue alteration by the fixation method, depiction of neuroanatomical structures at one distinct time point per animal, and the sheer effort needed to examine the whole brain. The vMEMRI method enables a quick overview of the whole brain *in vivo* to identify regions that undergo structural plasticity. This could also directed attention to regions for further investigation that may otherwise be overlooked. Furthermore, repeated analysis of brain structure within one animal is possible. The method of MEMRI does not only allow structural research but also identification of activation differences of certain brain areas. Numerous studies have shown that systemic

Discussion

administration of MnCl_2 leads to an activation dependent accumulation of Mn^{2+} (cf. appendix table2). These studies also show that the differences in activity reliably correlate with other analysis methods of determining neuronal activity (cf. for example Bock et al., 2009). This implies that the method of vMEMRI could not only be applied for volumetric, but also for activation analysis of different brain regions.

The method of vMEMRI could detect volume alterations induced by ablation of neurogenesis in mice lacking cyclin D2. Reported alterations found with histological methods could be reliably detected. vMEMRI could be a valuable tool to indicate volumetric differences in the numerous genetic mouse models of altered structural plasticity and give an overview of structural abnormalities within the brain of the genetically modified mice. The possibility of detecting even highly variable volumetric differences in mice with lesioned hippocampi and thereby confirm the lesions themselves *in vivo* can reduce the time invested in further experimentation. The position, structure and extent of lesions can also be reconstructed in three dimensions. vMEMRI also allowed to normalize the hippocampus to the whole brain, which provided information about the structural specificity of volumetric changes.

Study 3 shows that vMEMRI is also able to reliably detect small differences (between 1 and 5 %) in hippocampal volume induced by a brief footshock and by housing the animals under an enriched environment. It is shown that the differences detected by vMEMRI are mirrored by ultramicroscopical analysis and in line with Western blot analysis. Furthermore, structural alterations of the hippocampus indicate differential processing of the trauma shown by behavioral markers of PTSD-like symptoms including contextual fear and hyperarousal. Increasing evidence supports the notion that neuroanatomy closely relates to cognitive performance. This includes alterations in cognitive performance, such

Discussion

as memory impairment, cognitive processing and attentional deficits in psychiatric diseases which are characterized by structural differences in the hippocampus, amygdala and prefrontal cortex (Burt et al., 1995; Brandes et al., 2002; Campbell et al., 2004; Kieseppä et al., 2005; Woon et al., 2010; see also general introduction subsection 2). Along with the negative effect of distress on volume of neuroanatomical structures positive effects were also found, such as the detected beneficial effects of environmental enrichment detected in Chapter III. Most interesting learning itself has been found to induce volume changes; for example, an alteration of hippocampal and striatal volumes could be seen in humans challenged daily by repeated spatial orientation and learning as well as in mice trained for spatial learning in the Morris water maze (Engert and Bonhoeffer, 1999; Maguire et al., 2000; Bohbot et al., 2007; Lerch et al., 2011). The data on the beneficial results of spatial learning in mice shown by Lerch and colleagues mirrors the beneficial effects on neuroanatomy by housing the animals under an enriched environment shown in the study presented in chapter III. The applied method by Lerch and colleagues, MRI microscopy, lacks the great advantage of vMEMRI to measure structural neuroanatomy *in vivo* with the possibility to execute longitudinal studies which could give more detailed insight into the effects of training and learning on neuroanatomy.

There are extensive possibilities for the future applications of vMEMRI, including: determination of general neuroanatomical structure, especially for identification of differences in cytoarchitecture between different mouse strains and between WT and KO animals; validation and determination of the extend of lesions; studying neuroanatomical plasticity induced by external cues; or even recognizing activation differences of different neuronal regions. The present study provides some of the basic tools and validation procedures necessary for a broader application of vMEMRI in preclinical studies with mice.

Discussion

Further experiments are necessary to determine how observed functional disturbances of the hippocampus can be abolished leading to an improvement of the application protocol for longitudinal studies in learning and memory.

References

- Agency for Toxic Substances and Disease Registry (2008) Draft toxicological profile for manganese. Atlanta, Georgia.
- Albert MS, Butters N, Brandt J (1981) Development of remote memory loss in patients with Huntington's disease. *Journal of clinical neuropsychology* 3:1-12
- Altman J (1962) Are new neurons formed in the brains of adult mammals? *Science* 135:1127
- Amaral D, Witter M (1989) The three-dimensional organization of the hippocampal formation: a review of anatomical data. *Neuroscience* 31:571-591
- American Psychiatric Association (2000) Diagnostic and Statistical Manual of Mental Disorders, Fourth Edition, Text Revision.
- Andersen P, Morris R, Amaral D, Bliss T, O'Keefe J (2007) *The hippocampus book*. Oxford University Press.
- Aoki I, Naruse S, Tanaka C (2004)(a) Manganese-enhanced magnetic resonance imaging (MEMRI) of brain activity and applications to early detection of brain ischemia. *NMR in biomedicine* 17:569-80
- Aoki I, Wu Y-JL, Silva AC, Lynch RM, Koretsky AP (2004)(b) In vivo detection of neuroarchitecture in the rodent brain using manganese-enhanced MRI. *NeuroImage* 22:1046-59
- Apgar J (1968) Comparison of the effect of copper, manganese, and zinc deficiencies on parturition in the rat. *American Journal of Physiology* 215:1478
- Archibald FS, Tyree C (1987) Manganese poisoning and the attack of trivalent manganese upon catecholamines. *Archives of Biochemistry and Biophysics* 256:638-50
- Aschner M, Gannon M (1994) Manganese (Mn) transport across the rat blood-brain barrier: saturable and transferrin-dependent transport mechanisms. *Brain research bulletin* 33:345-9
- Aschner M, Erikson KM, Dorman DC (2005) Manganese Dosimetry: Species Differences and Implications for Neurotoxicity. *Critical Reviews in Toxicology* 35:1-32
- Ashe KH (2001) Learning and memory in transgenic mice modeling Alzheimer's disease. *Learning & memory (Cold Spring Harbor, N.Y.)* 8:301-8
- Badea A, Ali-Sharief a a, Johnson G a (2007) Morphometric analysis of the C57BL/6J mouse brain. *NeuroImage* 37:683-93
- Baly DL, Schneiderman JS, Garcia-Welsh AL (1990) Effect of manganese deficiency on insulin binding, glucose transport and metabolism in rat adipocytes. *Journal of Nutrition* 120:1075
- Bannerman DM, Rawlins JNP, McHugh SB, Deacon RMJ, Yee BK, Bast T, Zhang W-N, Pothuizen HHJ, Feldon J (2004) Regional dissociations within the hippocampus--memory and anxiety. *Neuroscience and biobehavioral reviews* 28:273-83
- Barbeau A, Inoué N, Cloutier T (1976) Role of manganese in dystonia. *Advances in Neurology* 14:339-52

References

- Barceloux DG (1999) Manganese. *Journal of toxicology. Clinical toxicology* 37:293-307
- Bard P (1929) The central representation of the sympathetic system as indicated by certain physiologic observations. *Archives of Neurology and Psychiatry* 22:230
- Barnes CA, McNaughton BL (1985) An age comparison of the rates of acquisition and forgetting of spatial information in relation to long-term enhancement of hippocampal synapses. *Behavioral neuroscience* 99:1040-8
- Barnes J, Bartlett JW, Pol L a van de, Loy CT, Scahill RI, Frost C, Thompson P, Fox NC (2009) A meta-analysis of hippocampal atrophy rates in Alzheimer's disease. *Neurobiology of aging* 30:1711-23
- Bast T (2003) Hippocampal modulation of sensorimotor processes. *Progress in Neurobiology* 70:319-345
- Bast T (2007) Toward an integrative perspective on hippocampal function: from the rapid encoding of experience to adaptive behavior. *Reviews in the Neurosciences* 18:253
- Bayer SA, Yackel JW, Puri PS (1982) Neurons in the rat dentate gyrus granular layer substantially increase during juvenile and adult life. *Science* 216:890
- Bayer S (1982) Changes in the total number of dentate granule cells in juvenile and adult rats: a correlated volumetric and 3 H-thymidine autoradiographic study. *Experimental Brain Research* 46:315-323
- Bell LT, Hurley LS (1973) Ultrastructural effects of manganese deficiency in liver, heart, kidney, and pancreas of mice. *Laboratory investigation; a journal of technical methods and pathology* 29:732-36
- Ben Abdallah NM-B, Slomianka L, Vyssotski AL, Lipp H-P (2010) Early age-related changes in adult hippocampal neurogenesis in C57 mice. *Neurobiology of aging* 31:151-61
- Benninger F, Beck H, Wernig M, Tucker KL, Brüstle O, Scheffler B (2003) Functional integration of embryonic stem cell-derived neurons in hippocampal slice cultures. *The Journal of neuroscience : the official journal of the Society for Neuroscience* 23:7075-83
- Berkowitz B a, Roberts R, Goebel DJ, Luan H (2006) Noninvasive and simultaneous imaging of layer-specific retinal functional adaptation by manganese-enhanced MRI. *Investigative ophthalmology & visual science* 47:2668-74
- Berkowitz B a, Roberts R, Penn JS, Gadianu M (2007) High-resolution manganese-enhanced MRI of experimental retinopathy of prematurity. *Investigative ophthalmology & visual science* 48:4733-40
- Bernheimer H, Birkmayer W, Hornykiewicz O, Jellinger K, Seitelberger F (1973) Brain dopamine and the syndromes of Parkinson and Huntington. Clinical, morphological and neurochemical correlations. *Journal of the neurological sciences* 20:415-55
- Biebl M, Cooper CM, Winkler J, Kuhn HG (2000) Analysis of neurogenesis and programmed cell death reveals a self-renewing capacity in the adult rat brain. *Neuroscience letters* 291:17-20
- Bird ED, Anton AH, Bullock B (1984) The effect of manganese inhalation on basal ganglia dopamine concentrations in rhesus monkey. *Neurotoxicology* 5:59-65

References

- Bloch F (1946) Nuclear induction. *Physical Review* 70:460-474
- Bock NA, Paiva FF, Nascimento GC, Newman JD, Silva AC (2008)(a) Cerebrospinal fluid to brain transport of manganese in a non-human primate revealed by MRI. *Brain research* 1198:160–170
- Bock NA, Paiva FF, Silva AC (2008)(b) Fractionated manganese-enhanced MRI. *NMR in Biomedicine* 21:473–478
- Bock NA, Kocharyan A, Silva AC (2009) Manganese-enhanced MRI visualizes V1 in the non-human primate visual cortex. *NMR in biomedicine* 22:730-6
- Bohbot VD, Lerch J, Thorndycraft B, Iaria G, Zijdenbos AP (2007) Gray matter differences correlate with spontaneous strategies in a human virtual navigation task. *The Journal of neuroscience : the official journal of the Society for Neuroscience* 27:10078-83
- Bonne O, Brandes D, Gilboa a, Gomori JM, Shenton ME, Pitman RK, Shalev a Y (2001) Longitudinal MRI study of hippocampal volume in trauma survivors with PTSD. *The American journal of psychiatry* 158:1248-51
- Borowski TB, Kokkinidis L (1996) Contribution of ventral tegmental area dopamine neurons to expression of conditional fear: effects of electrical stimulation, excitotoxin lesions, and quinpirole infusion on potentiated startle in rats. *Behavioral Neuroscience* 110:1349-64
- Brandes D, Ben-Schachar G, Gilboa A, Bonne O, Freedman S, Shalev AY (2002) PTSD symptoms and cognitive performance in recent trauma survivors. *Psychiatry research* 110:231-8
- Bremner JD, Elzinga B, Schmahl C, Vermetten E (2008) Structural and functional plasticity of the human brain in posttraumatic stress disorder. *Progress in brain research* 167:171-86
- Breslau N, Davis GC, Schultz LR (2003) Posttraumatic stress disorder and the incidence of nicotine, alcohol, and other drug disorders in persons who have experienced trauma. *Archives of general psychiatry* 60:289-94
- Brewin CR (2001) A cognitive neuroscience account of posttraumatic stress disorder and its treatment. *Behaviour research and therapy* 39:373-93
- Brewin CR, Kleiner JS, Vasterling JJ, Field AP (2007) Memory for emotionally neutral information in posttraumatic stress disorder: A meta-analytic investigation. *Journal of abnormal psychology* 116:448-63
- Buckmaster PS, Schwartzkroin PA (1995) Interneurons and inhibition in the dentate gyrus of the rat in vivo. *The Journal of neuroscience* 15:774
- Burt DB, Zembor MJ, Niederehe G (1995) Depression and memory impairment: a meta-analysis of the association, its pattern, and specificity. *Psychological bulletin* 117:285-305
- Burwell RD (2000) The Parahippocampal Region : Corticocortical Connectivity. *Annals of the New York Academy of Sciences* 911
- Bush VJ, Moyer TP, Batts KP, Parisi JE (1995) Essential and toxic element concentrations in fresh and formalin-fixed human autopsy tissues. *Clinical chemistry* 41:284-94

References

- Buzsáki G (1986) Hippocampal sharp waves: their origin and significance. *Brain research* 398:242-52
- Caine ED, Hunt RD, Weingartner H, Ebert MH (1978) Huntington's dementia: Clinical and neuropsychological features. *Archives of General Psychiatry* 35:377
- Calhoun ME, Kurth D, Phinney a L, Long JM, Hengemihle J, Mouton PR, Ingram DK, Jucker M (1999) Hippocampal neuron and synaptophysin-positive bouton number in aging C57BL/6 mice. *Neurobiology of aging* 19:599-606
- Calhoun ME, Wiederhold KH, Abramowski D, Phinney a L, Probst a, Sturchler-Pierrat C, Staufenbiel M, Sommer B, Jucker M (1998) Neuron loss in APP transgenic mice. *Nature* 395:755-6
- Campbell S, Marriott M, Nahmias C, MacQueen GM (2004) Lower hippocampal volume in patients suffering from depression: a meta-analysis. *American Journal of Psychiatry* 161:598
- Cannon WB (1927) The James-Lange theory of emotions: A critical examination and an alternative theory. *The American Journal of Psychology* 39:106–124
- Chapman P (2001) Genes, models and Alzheimer's disease. *Trends in Genetics* 17:254-261
- Chauveau F, Célérier A, Ognard R, Pierard C, Béracochéa D (2005) Effects of ibotenic acid lesions of the mediodorsal thalamus on memory: relationship with emotional processes in mice. *Behavioural brain research* 156:215-23
- Chuang K-H, Belluscio L, Koretsky AP (2010) In vivo detection of individual glomeruli in the rodent olfactory bulb using manganese enhanced MRI. *NeuroImage* 49:1350-6
- Chuang K-H, Koretsky A (2006) Improved neuronal tract tracing using manganese enhanced magnetic resonance imaging with fast T(1) mapping. *Magnetic resonance in medicine : official journal of the Society of Magnetic Resonance in Medicine / Society of Magnetic Resonance in Medicine* 55:604-11
- Chuang K-H, Lee JH, Silva AC, Belluscio L, Koretsky AP (2009) Manganese enhanced MRI reveals functional circuitry in response to odorant stimuli. *NeuroImage* 44:363-72
- Chung YA, Kim SH, Chung SK, Chae J-H, Yang DW, Sohn HS, Jeong J (2006) Alterations in cerebral perfusion in posttraumatic stress disorder patients without re-exposure to accident-related stimuli. *Clinical neurophysiology* 117:637-42
- Cleland TA (1996) Inhibitory glutamate receptor channels. *Molecular Neurobiology* 13:97–136
- Cohen G, Heikkila RE (1974) The Generation of Hydrogen Peroxide, Superoxide Radical, and Hydroxyl Radical by 6-Hydroxidopamine, Dialuric Acid, and Related Cytotoxic Agents. *Journal of Biological Chemistry* 249:2447-2452
- Commission on Life Science (CLS) (1989) Recommended dietary allowances 10th ed. Washington, D.C. National Academy Press.
- Connick RE, Poulson RE (1959) Effect of Paramagnetic Ions on the Nuclear Magnetic Resonance of O17 in Water and the Rate of Elimination of Water Molecules from the First Coordination Sphere of Cations. *The Journal of Chemical Physics* 30:759

References

- Cooper DC, Klipec WD, Fowler M a, Ozkan ED (2006) A role for the subiculum in the brain motivation/reward circuitry. *Behavioural Brain Research* 174:225-31
- Cotzias GC, Horiuchi K, Fuenzalida S, Mena I (1968) Chronic manganese poisoning. Clearance of tissue manganese concentrations with persistence of the neurological picture. *Neurology* 18:376-82
- Cotzias GC, Papavasiliou PS, Ginos J, Steck A, Düby S (1971) Metabolic modification of Parkinson's disease and of chronic manganese poisoning. *Annual Review of Medicine* 22:305-26
- Couper J (1837) On the effects of black oxide of manganese when inhaled into the lungs. *Br. Ann. Med. Pharmacol.* 1:41-42
- Czéh B, Lucassen PJ (2007) What causes the hippocampal volume decrease in depression? Are neurogenesis, glial changes and apoptosis implicated? *European archives of psychiatry and clinical neuroscience* 257:250-60
- Célérier A, Pierard C, Beracochea D (2004) Effects of ibotenic acid lesions of the dorsal hippocampus on contextual fear conditioning in mice: comparison with mammillary body lesions. *Behavioural brain research* 151:65-72
- Daire JL, Hyacinthe JN, Tatar I, Montet-Abou K, Ivancevic MK, Masterson K, Jorge-Costa M, Morel DR, Vallée JP (2008) In vivo myocardial infarct area at risk assessment in the rat using manganese enhanced magnetic resonance imaging (MEMRI) at 1.5T. *Magnetic resonance in medicine* 59:1422-30
- Davis M (1989) Sensitization of the acoustic startle reflex by footshock. *Behavioral Neuroscience* 103:495-503
- Davis M, Walker DL, Lee Y (1997) Amygdala and bed nucleus of the stria terminalis: differential roles in fear and anxiety measured with the acoustic startle reflex. *Philosophical transactions of the Royal Society of London. Series B, Biological sciences* 352:1675-87
- De Bellis MD, Hall J, Boring AM, Frustaci K, Moritz G (2001) A pilot longitudinal study of hippocampal volumes in pediatric maltreatment-related posttraumatic stress disorder. *Biological Psychiatry* 50:305–309
- De Paola V, Holtmaat A, Knott G, Song S, Wilbrecht L, Caroni P, Svoboda K (2006) Cell type-specific structural plasticity of axonal branches and boutons in the adult neocortex. *Neuron* 49:861-75
- Deans AE, Wadghiri YZ, Berrios-Otero C a, Turnbull DH (2008) Mn enhancement and respiratory gating for in utero MRI of the embryonic mouse central nervous system. *Magnetic resonance in medicine : official journal of the Society of Magnetic Resonance in Medicine* 59:1320-8
- Dedovic K, Duchesne A, Andrews J, Engert V, Pruessner JC (2009) The brain and the stress axis: the neural correlates of cortisol regulation in response to stress. *NeuroImage* 47:864-71
- Deicken RF, Pegues M, Amend D (1999) Reduced hippocampal N-acetylaspartate without volume loss in schizophrenia. *Schizophrenia research* 37:217-23
- Dodt HU, Leischner U, Schierloh A, Jährling N, Mauch CP, Deininger K, Deussing JM,

References

- Eder M, Zieglgänsberger W, Becker K (2007) Ultramicroscopy: three-dimensional visualization of neuronal networks in the whole mouse brain. *Nature Methods* 4:331–336
- Dolcos F, LaBar KS, Cabeza R (2004) Interaction between the amygdala and the medial temporal lobe memory system predicts better memory for emotional events. *Neuron* 42:855-63
- Dorman DC, McManus BE, Parkinson CU, Manuel C a, McElveen AM, Everitt JI (2004) Nasal toxicity of manganese sulfate and manganese phosphate in young male rats following subchronic (13-week) inhalation exposure. *Inhalation toxicology* 16:481-8
- Dorman DC, Struve MF, Marshall MW, Parkinson CU, James RA, Wong B a (2006) Tissue manganese concentrations in young male rhesus monkeys following subchronic manganese sulfate inhalation. *Toxicological sciences* 92:201-10
- Dragoi G, Buzsáki G (2006) Temporal encoding of place sequences by hippocampal cell assemblies. *Neuron* 50:145-57
- Drapeau P, Nachshen D (1984) Manganese fluxes and manganese-dependent neurotransmitter release in presynaptic nerve endings isolated from rat brain. *The Journal of Physiology* 348:493
- Eichenbaum H (1997) How Does the Brain Organize Memories? *Science* 277:330-332
- Elder A, Gelein R, Silva V, Feikert T, Opanashuk L, Carter J, Potter R, Maynard A, Ito Y, Finkelstein J, Oberdörster G (2006) Translocation of Inhaled Ultrafine Manganese Oxide Particles to the Central Nervous System. *Environmental Health Perspectives* 114:1172-1178
- Engert F, Bonhoeffer T (1999) Dendritic spine changes associated with hippocampal long-term synaptic plasticity. *Nature* 399:66-70
- Eriksson H, Tedroff J, Thuomas K-Å, Aquilonius S-M, Hartvig P, Fasth K-J, Bjurling P, Långström B, Hedström K-G, Heilbronn E (1992) Manganese induced brain lesions in *Macaca fascicularis* as revealed by positron emission tomography and magnetic resonance imaging. *Archives of Toxicology* 66:403-407
- Eschenko O, Canals S, Simanova I, Beyerlein M, Murayama Y, Logothetis NK (2010)(a) Mapping of functional brain activity in freely behaving rats during voluntary running using manganese-enhanced MRI: implication for longitudinal studies. *NeuroImage* 49:2544-55
- Eschenko O, Canals S, Simanova I, Logothetis NK (2010)(b) Behavioral, electrophysiological and histopathological consequences of systemic manganese administration in MEMRI. *Magnetic resonance imaging* 28:1165-1174
- Etchamendy N, Desmedt A, Cortes-Torrea C, Marighetto A, Jaffard R (2003) Hippocampal lesions and discrimination performance of mice in the radial maze: sparing or impairment depending on the representational demands of the task. *Hippocampus* 13:197-211
- Fairén a (2005) Pioneering a golden age of cerebral microcircuits: the births of the combined Golgi-electron microscope methods. *Neuroscience* 136:607-14
- Fanselow MS, Dong HW (2010) Are the Dorsal and Ventral Hippocampus Functionally

References

Distinct Structures? *Neuron* 65:7–19

- Fendt M, Koch M, Schnitzler HU (1994) Amygdaloid noradrenaline is involved in the sensitization of the acoustic startle response in rats. *Pharmacology, Biochemistry, and Behavior* 48:307-14
- Fennema-Notestine C, Stein MB, Kennedy CM, Archibald SL, Jernigan TL (2002) Brain morphometry in female victims of intimate partner violence with and without posttraumatic stress disorder. *Biological Psychiatry* 52:1089-101
- Fisher RS, Boas WE, Blume W, Elger C, Genton P, Lee P, Engel Jr J (2005) Epileptic seizures and epilepsy: definitions proposed by the International League Against Epilepsy (ILAE) and the International Bureau for Epilepsy (IBE). *Epilepsia* 46:470–472
- Fraga CG (2005) Relevance, essentiality and toxicity of trace elements in human health. *Molecular aspects of medicine* 26:235-44
- Frey BN, Andreatza AC, Nery FG, Martins MR, Quevedo J, Soares JC, Kapczinski F (2007) The role of hippocampus in the pathophysiology of bipolar disorder. *Behavioural Pharmacology* 18:419-30
- Frost G, Asling CW, Nelson MM (1959) Skeletal deformities in manganese-deficient rats. *The Anatomical Record* 134:37-53
- Fulton JF (1953) The limbic system: a study of the visceral brain in primates and man. *Journal of Biology and Medicine* 26
- Gage FH, Kelly P, Bjorklund A (1984) Regional changes in brain glucose metabolism reflect cognitive impairments in aged rats. *The Journal of Neuroscience* 4:2856
- Gallup W, Norris L (1938) The essentialness of manganese for the normal development of bone. *Science* 87:18
- Games D, Adams D, Alessandrini R, Barbour R, Berthelette P, Blackwell C, Carr T, Clemens J, Donaldson T, Gillespie F (1995) Alzheimer-type neuropathology in transgenic mice overexpressing V717F beta-amyloid precursor protein. *Nature* 373:523-7
- Garner CD, Nachtman JP (1989) Manganese catalyzed auto-oxidation of dopamine to 6-Hydroxydopamine in vitro. *Chemico-Biological Interactions* 69:345-351
- Gerdes HH, Kaether C (1996) Green fluorescent protein: applications in cell biology. *FEBS Letters* 389:44-7
- Gibbons R a, Dixon SN, Hallis K, Russell a M, Sansom BF, Symonds HW (1976) Manganese metabolism in cows and goats. *Biochimica et Biophysica Acta* 444:1-10
- Gilbertson MW, Shenton ME, Ciszewski A, Kasai K, Lasko NB, Orr SP, Pitman RK (2002) Smaller hippocampal volume predicts pathologic vulnerability to psychological trauma. *Nature Neuroscience* 5:1242–1247
- Gillies ME, Birkbeck J a (1983) Tea and coffee as sources of some minerals in the New Zealand diet. *The American Journal of Clinical Nutrition* 38:936-42
- Giovagnoli a R, Avanzini G (1999) Learning and memory impairment in patients with temporal lobe epilepsy: relation to the presence, type, and location of brain lesion.

References

- Epilepsia 40:904-11
- Glowinsky H (1973) Cognitive deficits in temporal lobe epilepsy: an investigation of memory functioning. *The Journal of Nervous and Mental Disease* 157:129
- Goldapple K, Segal Z, Garson C, Lau M, Bieling P, Kennedy S, Mayberg H (2004) Modulation of cortical-limbic pathways in major depression: treatment-specific effects of cognitive behavior therapy. *Archives of General Psychiatry* 61:34-41
- Golier JA, Yehuda R, Lupien SJ, Harvey PD, Grossman R, Elkin A (2002) Memory performance in Holocaust survivors with posttraumatic stress disorder. *American Journal of Psychiatry* 159:1682
- Golier J a, Harvey PD, Legge J, Yehuda R (2006) Memory performance in older trauma survivors: implications for the longitudinal course of PTSD. *Annals of the New York Academy of Sciences* 1071:54-66
- Golub Y, Kaltwasser SF, Mauch CP, Herrmann L, Schmidt U, Holsboer F, Czisch M, Wotjak CT (2010) Reduced hippocampus volume in the mouse model of Posttraumatic Stress Disorder. *Journal of Psychiatric Research* i:1-10
- Golub Y, Mauch CP, Dahloff M, Wotjak CT (2009) Consequences of extinction training on associative and non-associative fear in a mouse model of Posttraumatic Stress Disorder (PTSD). *Behavioural Brain Research* 205:544-9
- Gould E, Beylin a, Tanapat P, Reeves a, Shors TJ (1999) Learning enhances adult neurogenesis in the hippocampal formation. *Nature Neuroscience* 2:260-5
- Gould E, Gross CG (2002) Neurogenesis in adult mammals: some progress and problems. *The Journal of Neuroscience* 22:619-23
- Gould E, Westlind-Danielsson A, Frankfurt M, McEwen BS (1990) Sex differences and thyroid hormone sensitivity of hippocampal pyramidal cells. *Journal of Neuroscience* 10:996
- Grillon C, Ameli R, Goddard A, Woods SW, Davis M (1994)(a) Baseline and fear-potentiated startle in panic disorder patients. *Biological Psychiatry* 35:431-9
- Grillon C, Morgan C a, Southwick SM, Davis M, Charney DS (1996) Baseline startle amplitude and prepulse inhibition in Vietnam veterans with posttraumatic stress disorder. *Psychiatry Research* 64:169-78
- Grillon C, Sinha R, Malley SSO (1994)(b) Psychopharmacology Effects of ethanol on the acoustic startle reflex in humans. *Psychopharmacology* 1:167-171
- Gross CG (2000) Neurogenesis in the adult brain: death of a dogma. *Nature reviews. Neuroscience* 1:67-73
- Grünecker B, Kaltwasser SF, Peterse Y, Sämann PG, Schmidt MV, Wotjak CT, Czisch M (2010) Fractionated manganese injections: effects on MRI contrast enhancement and physiological measures in C57BL/6 mice. *NMR in Biomedicine* 23:913-21
- Haber M, Zhou L, Murai KK (2006) Cooperative astrocyte and dendritic spine dynamics at hippocampal excitatory synapses. *The Journal of Neuroscience* 26:8881-91
- Hansen SL, Spears JW, Lloyd KE, Whisnant CS (2006) Feeding a low manganese diet to heifers during gestation impairs fetal growth and development. *Journal of Dairy*

References

Science 89:4305-11

- Heckers S (2001) Neuroimaging studies of the hippocampus in schizophrenia. *Hippocampus* 11:520-8
- Holtmaat AJGD, Trachtenberg JT, Wilbrecht L, Shepherd GM, Zhang X, Knott GW, Svoboda K (2005) Transient and persistent dendritic spines in the neocortex in vivo. *Neuron* 45:279-91
- Hu TCC, Bao W, Lenhard SC, Schaeffer TR, Yue T-li, Willette RN, Jucker BM (2004) Simultaneous assessment of left-ventricular infarction size, function and tissue viability in a murine model of myocardial infarction by cardiac manganese-enhanced magnetic resonance imaging (MEMRI). *NMR in Biomedicine* 17:620-6
- Hu TCC, Pautler RG, MacGowan G a, Koretsky AP (2001) Manganese enhanced MRI of mouse heart during changes in inotropy. *Magnetic Resonance in Medicine* 46:884-890
- Hulse GK, Lautenschlager NT, Tait RJ, Almeida OP (2005) Dementia associated with alcohol and other drug use. *International Psychogeriatrics* 17:S109
- Hurley LS (1981) Tetragenic aspects of manganese, zinc, and copper nutrition. *The American Physiological Society* 61
- Hurley LS, Keen CL (1987) Trace Elements in Human and Animal Nutrition W. Mertz, ed. San Diego, California: Academic Press.
- Hutton M et al. (1998) Association of missense and 5'-splice-site mutations in tau with the inherited dementia FTDP-17. *Nature* 393:702-5
- Imayoshi I, Sakamoto M, Ohtsuka T, Takao K, Miyakawa T, Yamaguchi M, Mori K, Ikeda T, Itohara S, Kageyama R (2008) Roles of continuous neurogenesis in the structural and functional integrity of the adult forebrain. *Nature Neuroscience* 11:1153-61
- Immonen RJ, Kharatishvili I, Sierra A, Einula C, Pitkänen A, Gröhn OHJ (2008) Manganese enhanced MRI detects mossy fiber sprouting rather than neurodegeneration, gliosis or seizure-activity in the epileptic rat hippocampus. *NeuroImage* 40:1718-30
- Institute of Medicine (IOM) (2001) Dietary reference intakes for Vitamin A, Vitamin K, Arsenic, Boron, Chromium, Copper, Iodine, Iron, Manganese, Molybdenum, Nickel, Silicon, Vanadium, and Zinc. Washington, D.C. National Academy Press.
- Jackson SJ, Hussey R, Jansen M a, Merrifield GD, Marshall I, MacLulich A, Yau JLW, Bast T (2011) Manganese-enhanced magnetic resonance imaging (MEMRI) of rat brain after systemic administration of MnCl₂: hippocampal signal enhancement without disruption of hippocampus-dependent behavior. *Behavioural Brain Research* 216:293-300
- Jarrard LE (1989) On the use of ibotenic acid to lesion selectively different components of the hippocampal formation. *Journal of Neuroscience Methods* 29:251-9
- Joëls M (2010) Impact of glucocorticoids on brain function: Relevance for mood disorders. *Psychoneuroendocrinology*:406-414
- Kamprath K, Wotjak CT (2004) Nonassociative learning processes determine expression and extinction of conditioned fear in mice. *Learning & Memory* (Cold Spring Harbor,

References

- N.Y.) 11:770-86
- Kang YS, Gore JC (1984) Studies of Tissue NMR Relaxation Enhancement by Manganese. *Investigative Radiology* 19:399-407
- Karl A, Werner A (2010) The use of proton magnetic resonance spectroscopy in PTSD research--meta-analyses of findings and methodological review. *Neuroscience and Biobehavioral Reviews* 34:7-22
- Kehne JH, Gallager DW, Davis M (1981) Strychnine: brainstem and spinal mediation of excitatory effects on acoustic startle. *European Journal of Pharmacology* 76:177-186
- Kemmerer A, Elvehjem C, Hart E (1931) Studies on the relation of manganese to the nutrition of the mouse. *Journal of Biological Chemistry* 92:623
- Kempermann G, Kuhn HG, Gage FH (1997) More hippocampal neurons in adult mice living in an enriched environment. *Nature* 386:493-5
- Kempermann G (2003) Early determination and long-term persistence of adult-generated new neurons in the hippocampus of mice. *Development* 130:391-399
- Kennedy SH, Evans KR, Krüger S, Mayberg HS, Meyer JH, McCann S, Arifuzzman a I, Houle S, Vaccarino FJ (2001) Changes in regional brain glucose metabolism measured with positron emission tomography after paroxetine treatment of major depression. *The American Journal of Psychiatry* 158:899-905
- Kessler RC, Sonnega A, Bromet E, Hughes M, Nelson CB (1995) Posttraumatic stress disorder in the National Comorbidity Survey. *Archives of general psychiatry* 52:1048
- Kieseppä T, Tuulio-Henriksson A, Haukka J, Van Erp T, Glahn D, Cannon TD, Partonen T, Kaprio J, Lönqvist J (2005) Memory and verbal learning functions in twins with bipolar-I disorder, and the role of information-processing speed. *Psychological Medicine* 35:205-15
- Kim JJ, Foy MR, Thompson RF (1996) Behavioral stress modifies hippocampal plasticity through N-methyl-D-aspartate receptor activation. *Proceedings of the National Academy of Sciences of the United States of America* 93:4750
- Kim JJ, Song EY, Kosten T a (2006) Stress effects in the hippocampus: synaptic plasticity and memory. *Stress (Amsterdam, Netherlands)* 9:1-11
- Klimis-Tavantzis D, Leach Jr R, Kris-Etherton P (1983) The effect of dietary manganese deficiency on cholesterol and lipid metabolism in the Wistar rat and in the genetically hypercholesterolemic RICO rat. *Journal of Nutrition* 113:328
- Kloet CS de, Vermetten E, Geuze E, Kavelaars a, Heijnen CJ, Westenberg HGM (2006) Assessment of HPA-axis function in posttraumatic stress disorder: pharmacological and non-pharmacological challenge tests, a review. *Journal of Psychiatric Research* 40:550-67
- Kloet ER de (2000) Stress in the brain. *European journal of pharmacology* 405:187-98
- Knoth R, Singec I, Ditter M, Pantazis G, Capetian P, Meyer RP, Horvat V, Volk B, Kempermann G (2010) Murine features of neurogenesis in the human hippocampus across the lifespan from 0 to 100 years. *PloS one* 5:e8809

References

- Konrad C, Ukas T, Nebel C, Arolt V, Toga a W, Narr KL (2009) Defining the human hippocampus in cerebral magnetic resonance images--an overview of current segmentation protocols. *NeuroImage* 47:1185-95
- Koretsky AP, Silva AC (2004) Manganese-enhanced magnetic resonance imaging (MEMRI). *NMR in Biomedicine* 17:527-31
- Kowalczyk A, Filipkowski RK, Rylski M, Wilczynski GM, Konopacki F a, Jaworski J, Ciemerych M a, Sicinski P, Kaczmarek L (2004) The critical role of cyclin D2 in adult neurogenesis. *The Journal of Cell Biology* 167:209-13
- Kuhn HG, Dickinson-Anson H, Gage FH (1996) Neurogenesis in the dentate gyrus of the adult rat: age-related decrease of neuronal progenitor proliferation. *The Journal of Neuroscience* 16:2027
- Ladouceur CD, Almeida JRC, Birmaher B, Axelson D a, Nau S, Kalas C, Monk K, Kupfer DJ, Phillips ML (2008) Subcortical gray matter volume abnormalities in healthy bipolar offspring: potential neuroanatomical risk marker for bipolar disorder? *Journal of the American Academy of Child and Adolescent Psychiatry* 47:532-9
- Lamont EW, Kokkinidis L (1998) Infusion of the dopamine D1 receptor antagonist SCH 23390 into the amygdala blocks fear expression in a potentiated startle paradigm. *Brain Research* 795:128-36
- Lange C, Irle E (2004) Enlarged amygdala volume and reduced hippocampal volume in young women with major depression. *Psychological Medicine* 34:1059-64
- Larrabee GJ, Crook TH (1994) Estimated prevalence of age-associated memory impairment derived from standardized tests of memory function. *International Psychogeriatrics / IPA* 6:95-104
- Larrabee GJ, Crook TH (1989) Dimensions of everyday memory in age-associated memory impairment. *Psychological Assessment* 1:92-97
- Lauterbur PC (1973) Image formation by induced local interactions: examples employing nuclear magnetic resonance. *Nature* 242:190-191
- Lavenex P, Lavenex PB, Bennett JL, Amaral DG (2009) Postmortem changes in the neuroanatomical characteristics of the primate brain: hippocampal formation. *The Journal of Comparative Neurology* 512:27-51
- Leach RM (1971) Role of manganese in mucopolysaccharide metabolism. *Federation Proceedings* 30:991-4
- Leach RM, Muenster A-M (1962) Studies on the role of manganese in bone formation. I. Effect upon the mucopolysaccharide content of chick bone. *The Journal of nutrition* 78:51-6
- Leach R, Muenster A-M, Wien E (1969) Studies on the role of manganese in bone formation: II. Effect upon chondroitin sulfate synthesis in chick epiphyseal cartilage. *Archives of Biochemistry and Biophysics* 133:22-28
- Lee J-W (2000) Manganese Intoxication. *Archives of Neurology* 57:597-599
- Lee JH, Silva AC, Merkle H, Koretsky AP (2005) Manganese-enhanced magnetic resonance imaging of mouse brain after systemic administration of MnCl₂: dose-dependent and temporal evolution of T1 contrast. *Magnetic Resonance in Medicine*

References

53:640-8

- Lerch JP, Yiu AP, Martinez-Canabal A, Pekar T, Bohbot VD, Frankland PW, Henkelman RM, Josselyn S a, Sled JG (2011) Maze training in mice induces MRI-detectable brain shape changes specific to the type of learning. *NeuroImage* 54:2086-95
- Levin BE, Tomer R, Rey GJ (1992) Cognitive impairments in Parkinson's disease. *Neurologic Clinics* 10:471-85
- Litvan I (1994) Cognitive disturbances in progressive supranuclear palsy. *Journal of neural transmission. Supplementum* 42:69-78
- Lobo A, Launer L, Fratiglioni L, Andersen K (2000) Prevalence of dementia and major subtypes in Europe: a collaborative study of population-based cohorts. *Neurology*
- Lucassen PJ, Müller MB, Holsboer F, Bauer J, Holtrop a, Wouda J, Hoogendijk WJ, De Kloet ER, Swaab DF (2001) Hippocampal apoptosis in major depression is a minor event and absent from subareas at risk for glucocorticoid overexposure. *The American Journal of Pathology* 158:453-68
- Lucchini R, Albin E, Placidi D, Gasparotti R, Pigozzi MG, Montani G, Alessio L (2000) Brain magnetic resonance imaging and manganese exposure. *Neurotoxicology* 21:769-75
- MacLean PD (1949) Psychosomatic disease and the visceral brain; recent developments bearing on the Papez theory of emotion. *Psychosomatic Medicine* 11:338-53
- Maguire E a, Gadian DG, Johnsrude IS, Good CD, Ashburner J, Frackowiak RS, Frith CD (2000) Navigation-related structural change in the hippocampi of taxi drivers. *Proceedings of the National Academy of Sciences of the United States of America* 97:4398-403
- Maheswaran S, Barjat H, Rueckert D, Bate ST, Howlett DR, Tilling L, Smart SC, Pohlmann A, Richardson JC, Hartkens T, Hill DLG, Upton N, Hajnal JV, James MF (2009) Longitudinal regional brain volume changes quantified in normal aging and Alzheimer's APP x PS1 mice using MRI. *Brain Research* 1270:19-32
- Malecki E, Lo H, Yang H, Davis C, Ney D, Greger J (1995) Tissue manganese concentrations and antioxidant enzyme activities in rats given total parenteral nutrition with and without supplemental manganese. *Journal of Parenteral and Enteral Nutrition* 19:222-226
- Manji H (2003) Enhancing neuronal plasticity and cellular resilience to develop novel, improved therapeutics for Difficult-to-Treat depression. *Biological Psychiatry* 53:707-742
- Mansfield P (1977) Multi-planar image formation using NMR spin echoes. *Journal of Physics C: Solid State Physics* 10:L55
- Matsuoka Y (2003) A volumetric study of amygdala in cancer survivors with intrusive recollections. *Biological Psychiatry* 54:736-743
- McEwen BS (1999) Stress and hippocampal plasticity. *Annual Review of Neuroscience* 22:105-22
- McEwen BS (2001) Plasticity of the hippocampus: adaptation to chronic stress and allostatic load. *Annals of the New York Academy of Sciences* 933:265-77

References

- McGaugh JL (2004) The amygdala modulates the consolidation of memories of emotionally arousing experiences. *Annual Review of Neuroscience* 27:1-28
- McNally RJ, Lasko NB, Macklin ML, Pitman RK (1995) Autobiographical memory disturbance in combat-related posttraumatic stress disorder. *Behaviour Research and Therapy* 33:619–630
- McNaughton N, Gray J a (2000) Anxiolytic action on the behavioural inhibition system implies multiple types of arousal contribute to anxiety. *Journal of Affective Disorders* 61:161-76
- Mendonça-Dias MH, Gaggelli E, Lauterbur PC (1983) Paramagnetic contrast agents in nuclear magnetic resonance medical imaging. *Seminars in Nuclear Medicine* 13:364-376
- Mertz W (1995) Risk assessment of essential trace elements: new approaches to setting recommended dietary allowances and safety limits. *Nutrition Reviews* 53:179–185
- Meshi D, Drew MR, Saxe M, Ansorge MS, David D, Santarelli L, Malapani C, Moore H, Hen R (2006) Hippocampal neurogenesis is not required for behavioral effects of environmental enrichment. *Nature Neuroscience* 9:729-31
- Michelot D (2003) *Amanita muscaria*: chemistry, biology, toxicology, and ethnomycology. *Mycological Research* 107:131-146
- Morello M, Zatta P, Zambenedetti P, Martorana a, D'Angelo V, Melchiorri G, Bernardi G, Sancesario G (2007) Manganese intoxication decreases the expression of manganoproteins in the rat basal ganglia: an immunohistochemical study. *Brain Research Bulletin* 74:406-15
- Moser EI, Kropff E, Moser M-B (2008) Place cells, grid cells, and the brain's spatial representation system. *Annual Review of Neuroscience* 31:69-89
- Moser MB, Moser EI (1998) Functional differentiation in the hippocampus. *Hippocampus* 8:608-19
- Narita K, Kawasaki F, Kita H (1990) Mn and Mg influxes through Ca channels of motor nerve terminals are prevented by verapamil in frogs. *Brain Research* 510:289-95
- Natt O, Watanabe T, Boretius S, Radulovic J, Frahm J, Michaelis T (2002) High-resolution 3D MRI of mouse brain reveals small cerebral structures in vivo. *Journal of Neuroscience Methods* 120:203-9
- Ndode-Ekane XE, Hayward N, Gröhn O, Pitkänen a (2010) Vascular changes in epilepsy: functional consequences and association with network plasticity in pilocarpine-induced experimental epilepsy. *Neuroscience* 166:312-32
- Neumeister A, Wood S, Bonne O, Nugent AC, Luckenbaugh D a, Young T, Bain EE, Charney DS, Drevets WC (2005) Reduced hippocampal volume in unmedicated, remitted patients with major depression versus control subjects. *Biological Psychiatry* 57:935-7
- Newland MC, Weiss B (1992) Persistent effects of manganese on effortful responding and their relationship to manganese accumulation in the primate globus pallidus. *Toxicology and Applied Pharmacology* 113:87-97
- Neylan TC, Schuff N, Lenoci M, Yehuda R, Weiner MW, Marmar CR (2003) Cortisol levels

References

- are positively correlated with hippocampal N-acetylaspartate. *Biological Psychiatry* 54:1118–1121
- Nielsen FH (2006) Boron, manganese, molybdenum, nickel, silicon, and vanadium. Book Chapter
- Normandin L, Hazell AS (2002) Manganese neurotoxicity: an update of pathophysiologic mechanisms. *Metabolic Brain Disease* 17:375-87
- Oberley LW, Buettner GR (1979) Role of Superoxide Dismutase in Cancer : A Review. *Cancer Research* 39:1141-1149
- Olpe H-R (1978) The action of muscimol on neurones of the substantia nigra of the rat. *Experientia* 124:185-235
- Orent ER, McCollum E (1931) Effects of deprivation of manganese in the rat. *Journal of Biological Chemistry* 92:651
- O'Keefe J, Dostrovsky J (1971) The hippocampus as a spatial map. Preliminary evidence from unit activity in the freely-moving rat. *Brain Research* 34:171
- O'Neill J, Senior T, Csicsvari J (2006) Place-selective firing of CA1 pyramidal cells during sharp wave/ripple network patterns in exploratory behavior. *Neuron* 49:143-55
- Pamplona F a, Henes K, Micale V, Mauch CP, Takahashi RN, Wotjak CT (2010) Prolonged fear incubation leads to generalized avoidance behavior in mice. *Journal of Psychiatric Research* 45:354-360
- Panegyres PK (2004) The contribution of the study of neurodegenerative disorders to the understanding of human memory. *QJM : monthly journal of the Association of Physicians* 97:555-67
- Papez J (1937) A proposed mechanism of emotion. *Archives of Neurology and Psychiatry*
- Patil CG, Lad SP, Katznelson L, Laws ER (2007) Brain atrophy and cognitive deficits in Cushing's disease. *Neurosurgical FOCUS* 23:1-4
- Pautler RG, Silva a C, Koretsky a P (1998) In vivo neuronal tract tracing using manganese-enhanced magnetic resonance imaging. *Magnetic Resonance in Medicine* 40:740-8
- Pautler RG (2004) In vivo, trans-synaptic tract-tracing utilizing manganese-enhanced magnetic resonance imaging (MEMRI). *NMR in Biomedicine* 17:595-601
- Pautler RG, Koretsky AP (2002) Tracing odor-induced activation in the olfactory bulbs of mice using manganese-enhanced magnetic resonance imaging. *NeuroImage* 16:441-8
- Pautler RG, Mongeau R, Jacobs RE (2003) In vivo trans-synaptic tract tracing from the murine striatum and amygdala utilizing manganese enhanced MRI (MEMRI). *Magnetic resonance in medicine : official journal of the Society of Magnetic Resonance in Medicine / Society of Magnetic Resonance in Medicine* 50:33-9
- Paxinos G, Franklin KBJ (2004) *The mouse brain in stereotaxic coordinates*. Academic Press.
- Pennington JA, Young BE, Wilson DB, Johnson RD, Vanderveen JE (1986) Mineral content of foods and total diets: the Selected Minerals in Foods Survey, 1982 to

References

1984. *Journal of the American Dietetic Association* 86:876-91
- Picot M-C, Baldy-Moulinier M, Daurès J-P, Dujols P, Crespel A (2008) The prevalence of epilepsy and pharmaco-resistant epilepsy in adults: a population-based study in a Western European country. *Epilepsia* 49:1230-8
- Pillon B, Deweer B, Michon A, Malapani C, Agid Y, Dubois B (1994) Are explicit memory disorders of progressive supranuclear palsy related to damage to striatofrontal circuits? Comparison with Alzheimer's, Parkinson's, and Huntington's diseases. *Neurology* 44:1264-70
- Plumlee M, Thrasher D, Beeson W, Andrews F, Parker H (1956) The effects of a manganese deficiency upon the growth, development, and reproduction of swine. *Journal of Animal Science* 15:352
- Poorkaj P, Bird TD, Wijsman E, Nemens E, Garruto RM, Anderson L, Andreadis a, Wiederholt WC, Raskind M, Schellenberg GD (1998) Tau is a candidate gene for chromosome 17 frontotemporal dementia. *Annals of Neurology* 43:815-25
- Popov VI, Bocharova LS (1992) Hibernation-induced structural changes in synaptic contacts between mossy fibres and hippocampal pyramidal neurons. *Neuroscience* 48:53-62
- Popov VI, Bocharova LS, Bragin a G (1992) Repeated changes of dendritic morphology in the hippocampus of ground squirrels in the course of hibernation. *Neuroscience* 48:45-51
- Praag H van, Kempermann G, Gage FH (1999) Running increases cell proliferation and neurogenesis in the adult mouse dentate gyrus. *Nature Neuroscience* 2:266–270
- Prohaska JR (1987) Functions of trace elements in brain metabolism. *Physiological Reviews* 67:858-901
- Purcell EM, Torrey HC, Pound RV (1946) Resonance absorption by nuclear magnetic moments in a solid. *Physical Review* 69:37–38
- Rabinovitch M, DeStefano MJ (1973) Manganese stimulates adhesion and spreading of mouse sarcoma I ascites cells. *The Journal of cell biology* 59:165-76
- Radyushkin K, El-Kordi a, Boretius S, Castaneda S, Ronnenberg a, Reim K, Bickeböller H, Frahm J, Brose N, Ehrenreich H (2010) Complexin2 null mutation requires a “second hit” for induction of phenotypic changes relevant to schizophrenia. *Genes, Brain, and Behavior* 9:592-602
- Rapp PR, Gallagher M (1996) Preserved neuron number in the hippocampus of aged rats with spatial learning deficits. *Proceedings of the National Academy of Sciences of the United States of America* 93:9926-30
- Rasmussen T, Schliemann T, Sørensen JC, Zimmer J, West MJ (1996) Memory impaired aged rats: no loss of principal hippocampal and subicular neurons. *Neurobiology of Aging* 17:143-7
- Rauch SL, Shin LM, Phelps E a (2006) Neurocircuitry models of posttraumatic stress disorder and extinction: human neuroimaging research--past, present, and future. *Biological Psychiatry* 60:376-82
- Reynolds N, Blumsohn a, Baxter JP, Houston G, Pennington CR (1998) Manganese

References

- requirement and toxicity in patients on home parenteral nutrition. *Clinical nutrition* (Edinburgh, Scotland) 17:227-30
- Risold PY, Swanson LW (1996) Structural evidence for functional domains in the rat hippocampus. *Science* 272:1484-6
- Rodríguez VM, Dufour L, Carrizales L, Díaz-Barriga F, Jiménez-Capdeville ME (1998) Effects of oral exposure to mining waste on in vivo dopamine release from rat striatum. *Environmental Health Perspectives* 106:487-91
- Roth J a (2009) Are there common biochemical and molecular mechanisms controlling manganism and parkinsonism. *Neuromolecular Medicine* 11:281-96
- Rucker D, Thadhani R, Tonelli M (2010) Trace element status in hemodialysis patients. *Seminars in Dialysis* 23:389-95
- Sachinvala CN, Kling A, Suffin S, Lake R, Cohen M (2000) Increased regional cerebral perfusion by 99mTc hexamethyl propylene amine oxime single photon emission computed tomography in post-traumatic stress disorder. *Military medicine* 165:473-479
- Sapolsky RM (1996) Why stress is bad for your brain. *Science* 273:749-50
- Sapolsky RM (2000) Glucocorticoids and hippocampal atrophy in neuropsychiatric disorders. *Archives of General Psychiatry* 57:925-35
- Sapolsky RM, Krey LC, McEwen BS (1985) Prolonged glucocorticoid exposure reduces hippocampal neuron number: implications for aging. *The Journal of Neuroscience* 5:1222
- Sapolsky RM (2003) Stress and plasticity in the limbic system. *Neurochemical Research* 28:1735-42
- Savitz J, Drevets WC (2009) Bipolar and major depressive disorder: neuroimaging the developmental-degenerative divide. *Neuroscience and Biobehavioral Reviews* 33:699-771
- Schmahl C (2003) Magnetic resonance imaging of hippocampal and amygdala volume in women with childhood abuse and borderline personality disorder. *Psychiatry Research: Neuroimaging* 122:193-198
- Schuff N, Amend DL, Knowlton R, Norman D, Fein G, Weiner MW (1999) Age-related metabolite changes and volume loss in the hippocampus by magnetic resonance spectroscopy and imaging. *Neurobiology of aging* 20:279–285
- Scoville WB, Milner B (1957) Loss of recent memory after bilateral hippocampal lesions. *Journal of Neurology, Neurosurgery & Psychiatry* 20:11-21
- Scoville W (1954) The Limbic Lobe in Man. *Journal of Neurosurgery* 11:64–66
- Selkoe DJ (2001) Alzheimer's disease: genes, proteins, and therapy. *Physiological Reviews* 81:741
- Sharp F, Sagar S, Hicks K, Lowenstein D, Hisanaga K (1991) c-fos mRNA, Fos, and Fos-related antigen induction by hypertonic saline and stress. *The Journal of Neuroscience* 11:2321
- Sheline YI, Sanghavi M, Mintun M a, Gado MH (1999) Depression duration but not age

References

- predicts hippocampal volume loss in medically healthy women with recurrent major depression. *The Journal of Neuroscience* 19:5034-43
- Shin LM, Rauch SL, Pitman RK (2006) Amygdala, medial prefrontal cortex, and hippocampal function in PTSD. *Annals of the New York Academy of Sciences* 1071:67-79
- Shors TJ, Miesegaes G, Beylin a, Zhao M, Rydel T, Gould E (2001) Neurogenesis in the adult is involved in the formation of trace memories. *Nature* 410:372-6
- Shors TJ, Townsend D a, Zhao M, Kozorovitskiy Y, Gould E (2002) Neurogenesis may relate to some but not all types of hippocampal-dependent learning. *Hippocampus* 12:578-84
- Sicinska E, Aifantis I, Le Cam L, Swat W, Borowski C, Yu Q, Ferrando A a, Levin SD, Geng Y, Boehmer H von, Sicinski P (2003) Requirement for cyclin D3 in lymphocyte development and T cell leukemias. *Cancer cell* 4:451-61
- Sicinski P, Donaher JL, Geng Y, Parker SB, Gardner H, Park MY, Robker RL, Richards JS, McGinnis LK, Biggers JD, Eppig JJ, Bronson RT, Elledge SJ, Weinberg R a (1996) Cyclin D2 is an FSH-responsive gene involved in gonadal cell proliferation and oncogenesis. *Nature* 384:470-4
- Sicinski P, Donaher JL, Parker SB, Li T, Fazeli a, Gardner H, Haslam SZ, Bronson RT, Elledge SJ, Weinberg R a (1995) Cyclin D1 provides a link between development and oncogenesis in the retina and breast. *Cell* 82:621-30
- Siegmund A, Kaltwasser SF, Holsboer F, Czisch M, Wotjak CT (2009) Hippocampal N-acetylaspartate levels before trauma predict the development of long-lasting posttraumatic stress disorder-like symptoms in mice. *Biological Psychiatry* 65:258-62
- Siegmund A, Wotjak CT (2007) A mouse model of posttraumatic stress disorder that distinguishes between conditioned and sensitised fear. *Journal of Psychiatric Research* 41:848-60
- Silva AC, Lee JH, Aoki I, Koretsky AP (2004) Manganese-enhanced magnetic resonance imaging (MEMRI): methodological and practical considerations. *NMR in Biomedicine* 17:532-43
- Silva AC, Lee JH, Wu CW-H, Tucciarone J, Pelled G, Aoki I, Koretsky AP (2008) Detection of cortical laminar architecture using manganese-enhanced MRI. *Journal of Neuroscience Methods* 167:246-57
- Simić G, Kostović I, Winblad B, Bogdanović N (1997) Volume and number of neurons of the human hippocampal formation in normal aging and Alzheimer's disease. *The Journal of Comparative Neurology* 379:482-94
- Simmons ML, Frondoza CG, Coyle JT (1991) Immunocytochemical localization of N-acetyl-aspartate with monoclonal antibodies. *Neuroscience* 45:37-45
- Simpson PB, Challiss R a, Nahorski SR (1995) Divalent cation entry in cultured rat cerebellar granule cells measured using Mn²⁺ quench of fura 2 fluorescence. *The European Journal of Neuroscience* 7:831-40
- Sloot WN, Gramsbergen JB (1994) Axonal transport of manganese and its relevance to

References

- selective neurotoxicity in the rat basal ganglia. *Brain Research* 657:124-32
- Sloot WN, Korf J, Koster JF, De Wit LE, Gramsbergen JB (1996) Manganese-induced hydroxyl radical formation in rat striatum is not attenuated by dopamine depletion or iron chelation in vivo. *Experimental Neurology* 138:236-45
- Smith LE, Smallwood R, Macneil S (2010) A comparison of imaging methodologies for 3D tissue engineering. *Microscopy Research and Technique* 73:1123-33
- Smith RA, Alexander RB, Wolman MG (1987) Water-quality trends in the nation's rivers. *Science* 235:1607
- Song H-jun, Stevens CF, Gage FH (2002) Neural stem cells from adult hippocampus develop essential properties of functional CNS neurons. *Nature Neuroscience* 5:438-45
- Soria G, Wiedermann D, Justicia C, Ramos-Cabrer P, Hoehn M (2008) Reproducible imaging of rat corticothalamic pathway by longitudinal manganese-enhanced MRI (L-MEMRI). *NeuroImage* 41:668-74
- Squire LR (1992) Memory and the hippocampus: a synthesis from findings with rats, monkeys, and humans. *Psychological Review* 99:195-231
- St-Pierre A, Normandin L, Carrier G, Kennedy G, Butterworth R, Zayed J (2001) Bioaccumulation and locomotor effect of manganese dust in rats. *Inhalation Toxicology* 13:623-632
- Strause LG, Hegenauer J, Saltman P, Cone R, Resnick D (1986) Effects of long-term dietary manganese and copper deficiency on rat skeleton. *The Journal of Nutrition* 116:135-41
- Sullivan EV, Pfefferbaum A (2009) Neuroimaging of the Wernicke-Korsakoff syndrome. *Alcohol & Alcoholism* 44:155-65
- Suzuki DA, Yamada T, Hoedema R, Yee RD (2011) Smooth-Pursuit Eye-Movement Deficits With Chemical Lesions in Macaque Nucleus Reticularis Tegmenti Pontis. *Journal of Neurophysiology*:1178-1186
- Swanson LW, Cowan WM (1977) An autoradiographic study of the organization of the efferent connections of the hippocampal formation in the rat. *The Journal of Comparative Neurology* 172:49-84
- Syková E, Chvátal a (2000) Glial cells and volume transmission in the CNS. *Neurochemistry International* 36:397-409
- Takeda A, Sawashita J, Okada S (1995) Biological half-lives of zinc and manganese in rat brain. *Brain Research* 695:53-58
- Takeuchi A, Irizarry MC, Duff K, Saido TC, Ashe KH, Hasegawa M, Mann DMA, Hyman BT, Iwatsubo T (2000) Age-related amyloid β deposition in transgenic mice overexpressing both Alzheimer mutant presenilin 1 and amyloid β precursor protein Swedish mutant is not associated with global neuronal loss. *The American Journal of Pathology* 157:331
- Tenaud I, Sainte-Marie I, Jumbou O, Litoux P, Dréno B (1999) In vitro modulation of keratinocyte wound healing integrins by zinc, copper and manganese. *The British*

References

Journal of Dermatology 140:26-34

- Tindemans I, Boumans T, Verhoye M, Van der Linden A (2006) IR-SE and IR-MEMRI allow in vivo visualization of oscine neuroarchitecture including the main forebrain regions of the song control system. *NMR in Biomedicine* 19:18-29
- Tjälve H, Mejåre C, Borg-Neczak K (1995) Uptake and transport of manganese in primary and secondary olfactory neurones in pike. *Pharmacology & Toxicology* 77:23-31
- Tombaugh GC, Rowe WB, Chow AR, Michael TH, Rose GM (2002) Theta-frequency synaptic potentiation in CA1 in vitro distinguishes cognitively impaired from unimpaired aged Fischer 344 rats. *The Journal of Neuroscience* 22:9932-40
- U.S. EPA (2009) Health assessment document for manganese: final report (Report No. EPA/600/8-83/013F). Cincinnati, OH.
- Van der Linden a, Verhoye M, Van Meir V, Tindemans I, Eens M, Absil P, Balthazart J (2002) In vivo manganese-enhanced magnetic resonance imaging reveals connections and functional properties of the songbird vocal control system. *Neuroscience* 112:467-74
- Van der Linden A, Van Meir V, Tindemans I, Verhoye M, Balthazart J (2004) Applications of manganese-enhanced magnetic resonance imaging (MEMRI) to image brain plasticity in song birds. *NMR in Biomedicine* 17:602-12
- Vasterling JJ, Duke LM, Brailey K, Constans JI, Allain AN, Sutker PB (2002) Attention, Learning, and Memory Performances and Intellectual Resources in Vietnam Veterans: PTSD and No Disorder Comparisons. *Neuropsychology* 16:5-14
- Vermetten E (2003) Long-term treatment with paroxetine increases verbal declarative memory and hippocampal volume in posttraumatic stress disorder. *Biological Psychiatry* 54:693-702
- Vermetten E, Schmahl C, Lindner S, Loewenstein RJ, Bremner JD (2006) Hippocampal and amygdalar volumes in dissociative identity disorder. *American Journal of Psychiatry* 163:630
- Walker D (2003) Role of the bed nucleus of the stria terminalis versus the amygdala in fear, stress, and anxiety. *European Journal of Pharmacology* 463:199-216
- Walker DL, Davis M (1997) Double dissociation between the involvement of the bed nucleus of the stria terminalis and the central nucleus of the amygdala in startle increases produced by conditioned versus unconditioned fear. *The Journal of Neuroscience* 17:9375-83
- Walker R, Woodruff G, Kerkut G (1971) The effect of ibotenic acid and muscimol on single neurons of the snail, *Helix aspersa*. *Comparative and General Pharmacology* 2:168-174
- Watanabe T, Natt O, Boretius S, Frahm J, Michaelis T (2002) In vivo 3D MRI staining of mouse brain after subcutaneous application of MnCl₂. *Magnetic Resonance in* 48:852-9
- Wendland MF (2004) Applications of manganese-enhanced magnetic resonance imaging (MEMRI) to imaging of the heart. *NMR in Biomedicine* 17:581-94
- Wenlock RW, Buss DH (1979) Trace nutrients. 2. Manganese in British food. *The British*

References

Journal of Nutrition 41:153-261

- Winner B, Cooper-Kuhn CM, Aigner R, Winkler J, Kuhn HG (2002) Long-term survival and cell death of newly generated neurons in the adult rat olfactory bulb. *European Journal of Neuroscience* 16:1681-1689
- Witter MP (1986) A survey of the anatomy of the hippocampal formation, with emphasis on the septotemporal organization of its intrinsic and extrinsic connections. *Advances in Experimental Medicine and Biology* 203:67-82
- Woermann FG, Vollmar C (2009) Clinical MRI in children and adults with focal epilepsy: a critical review. *Epilepsy & Behavior : E&B* 15:40-9
- Woolley CS, Weiland NG, McEwen BS, Schwartzkroin P a (1997) Estradiol increases the sensitivity of hippocampal CA1 pyramidal cells to NMDA receptor-mediated synaptic input: correlation with dendritic spine density. *The Journal of Neuroscience* 17:1848-59
- Woon FL, Sood S, Hedges DW (2010) Hippocampal volume deficits associated with exposure to psychological trauma and posttraumatic stress disorder in adults: a meta-analysis. *Progress in Neuropsychopharmacology & Biological Psychiatry* 34:1181-8
- Yamada M, Ohno S, Okayasu I, Okeda R, Hatakeyama S, Watanabe H, Ushio K, Tsukagoshi H (1986) Chronic manganese poisoning: a neuropathological study with determination of manganese distribution in the brain. *Acta Neuropathologica* 70:273-8
- Yang T, Zhou D, Stefan H (2010) Why mesial temporal lobe epilepsy with hippocampal sclerosis is progressive: uncontrolled inflammation drives disease progression? *Journal of the Neurological Sciences* 296:1-6
- Yehuda R, Golier J a, Tischler L, Harvey PD, Newmark R, Yang RK, Buchsbaum MS (2007) Hippocampal volume in aging combat veterans with and without post-traumatic stress disorder: relation to risk and resilience factors. *Journal of Psychiatric Research* 41:435-45
- Zheng W, Ren S, Graziano JH (1998) Manganese inhibits mitochondrial aconitase: a mechanism of manganese neurotoxicity. *Brain Research* 799:334-42
- Zheng W, Fu SX, Dydak U, Cowan DM (2011) Biomarkers of manganese intoxication. *Neurotoxicology* 32:1-8

Appendix

Table1: List of studies on aging and hippocampal plasticity. ↓ decreases ↑ increases ↔ does not change

Authors	Animals	↓	↑	↔	comments
(Sapolsky et al., 1985)	F344 (8 vs. 28 months)	cort. receptors; cell bodies >140μm ² (CA3+CA1) (CA1 only in 'normal' aged)	cell bodies <70μm ² (CA3+CA1) (CA1 only in 'normal' aged)		stereological; 3 months of (5mg/day) cort. exposure appropriate model for aging
(Curcio and Hinds, 1983)	Sprague Dawley (6 vs. 24 and 30 months)			Dendritic spine volume; synapses; granule cells (DG)	stereological
(Cotman and Scheff, 1979)	F344 (3 vs. 24 months)	synapse growth (as response to lesioned DG)		synapses (DG)	stereological; Holmes-staining
(Sánchez et al., 2011)	Wistar-Kioto (2;4 and 8 months; hypertensive)	Dendritic spines (pyramidal neurons in hippocampus)			Golgi-cox staining; hypertensive rats;
(Genisman and Bondareff, 1976)	F344 (3 vs. 24 months)	synapses (DG)		granule cells; volume granule cell layer (DG)	stereological
(Adams et al., 2010)	F344 + brown norway (10 vs. 29 months)	synapses (Stratum lacunosum moleculare CA3)		Synapses; synapse size; spine size (complete CA3)	3-D electron microscopy
(Landfield et al., 1981b)	F344 (4-7 vs. 3-15 vs. 25-28 months)	pyramidal neurons (CA3)	dark glia (CA3)	astrocytes (CA3)	electron microscopy
(Landfield et al., 1981a)	F344 (5 vs. 27 months)	neurons; nucleus „roundness“ (CA1+DG)	Glia; astrocytes (CA1+DG)		stereological; adrenal ectomized (ACTH↑) animals do not show this

Appendix

(Rapp and Gallagher, 1996)	Long-Evans (6 vs. 27-28 months)			Total neurons (DG; CA1-2; CA3)	stereological; no correlation with spatial learning;
(Rasmussen et al., 1996)	Male Wistar (2.5 vs. 24 months)			Total neurons (DG; CA1-2; CA3; Hilius; Subiculum)	stereological; no correlation with spatial learning;
(Gage et al., 1984)	Rats (3 vs. 22-24 months)	Glucose metabolism (CA1; CA3; DG)			Decrease in hippocampal (and PFC) glucose metabolism positively correlated with impairment in hippocampal tasks
(Barnes and McNaughton, 1985)	F 344 (12 vs. 24 months)	maximum: long-term synaptic enhancement (parahippocampal region)	decay: long-term synaptic enhancement (parahippocampal region)		electrophysiology
(Tombaugh et al., 2002)	F344 rats (4-6 vs. 24-26 months)	<i>in-vitro</i> LTP (5Hz) (CA1) only in rats with impaired learning			electrophysiology
(Gallagher et al., 1990)	Long-Evans (7-8 vs. 27-28 months)			Choline acetyl transferase (hippocampus)	Markers for biogenic amines differed in basal forebrain, striatum, and frontal cortex
(Tanaka and Mizoguchi, 2009)	F344 (5 vs. 24 months)	Chondroitin sulfate (Glycoprotein crucially modulating synaptic plasticity) (CA3 but not in DG)			also in PFC

- Adams MM, Donohue HS, Linville MC, Iversen E a, Newton IG, Brunso-Bechtold JK (2010) Age-related synapse loss in hippocampal CA3 is not reversed by caloric restriction. *Neuroscience* 171:373-82
- Barnes CA, McNaughton BL (1985) An age comparison of the rates of acquisition and forgetting of spatial information in relation to long-term enhancement of hippocampal synapses. *Behavioral Neuroscience* 99:1040-8
- Cotman CW, Scheff SW (1979) Compensatory synapse growth in aged animals after neuronal death. *Mechanisms of Aging and Development* 9:103–117
- Curcio C a, Hinds JW (1983) Stability of synaptic density and spine volume in dentate gyrus of aged rats. *Neurobiology of Aging* 4:77-87
- Gage FH, Kelly P, Bjorklund A (1984) Regional changes in brain glucose metabolism reflect cognitive impairments in aged rats. *The Journal of Neuroscience* 4:2856
- Gallagher M, Burwell RD, Kodosi MH, McKinney M, Southerland S, Vella-Rountree L, Lewis MH (1990) Markers for biogenic amines in the aged rat brain: relationship to decline in spatial learning ability. *Neurobiology of Aging* 11:507-14
- Genisman Y, Bondareff W (1976) Decrease in the number of synapses in the senescent brain: a quantitative electron microscopic analysis of the dentate gyrus molecular layer in the rat. *Mechanisms of Aging and Development* 5:11-23
- Landfield PW, Baskin RK, Pitler T a (1981)(a) Brain aging correlates: retardation by hormonal-pharmacological treatments. *Science (New York, N.Y.)* 214:581-4
- Landfield PW, Braun LD, Pitler T a, Lindsey JD, Lynch G (1981)(b) Hippocampal aging in rats: a morphometric study of multiple variables in semithin sections. *Neurobiology of Aging* 2:265-75
- Rapp PR, Gallagher M (1996) Preserved neuron number in the hippocampus of aged rats with spatial learning deficits. *Proceedings of the National Academy of Sciences of the United States of America* 93:9926-30
- Rasmussen T, Schliemann T, Sørensen JC, Zimmer J, West MJ (1996) Memory impaired aged rats: no loss of principal hippocampal and subicular neurons. *Neurobiology of Aging* 17:143-7
- Sapolsky RM, Krey LC, McEwen BS (1985) Prolonged glucocorticoid exposure reduces hippocampal neuron number: implications for aging. *The Journal of Neuroscience* 5:1222
- Sánchez F, Gómez-Villalobos M de J, Juárez I, Quevedo L, Flores G (2011) Dendritic morphology of neurons in medial prefrontal cortex, hippocampus, and nucleus accumbens in adult SH rats. *Synapse (New York, N.Y.)* 65:198-206
- Tanaka Y, Mizoguchi K (2009) Influence of aging on chondroitin sulfate proteoglycan expression and neural stem/progenitor cells in rat brain and improving effects of a herbal medicine, yokukansan. *Neuroscience* 164:1224-34
- Tombaugh GC, Rowe WB, Chow AR, Michael TH, Rose GM (2002) Theta-frequency synaptic potentiation in CA1 in vitro distinguishes cognitively impaired from unimpaired aged Fischer 344 rats. *The Journal of Neuroscience* 22:9932-40

Appendix

Table2: List of all MEMRI studies with rodents. Studies are sorted by : studies on neuroarchitecture (Mn²⁺ as tissue contrast enhancer), studies using Mn²⁺ as an activity marker and studies using Mn²⁺ for neuronal tract tracing

Mn ²⁺ as tissue contrast enhancer						
Author-date	Animal	Application Mn ²⁺ concentration (time of scan)	Regions of interest	Correlation of MEMRI with other measurements	Findings related to MEMRI	Analytical method
(Aoki et al., 2004)	Rats (Sprague Dawley)	intravenous 141.5 mg/kg (5,10,100 min; 2 h 1,4,14 days)	Whole brain	-	Enhancement of neuroarchitecture	manual ROIs absolute intensity; signal normalized to noise/cortex
(Banerjee et al., 2007)	Mice (Nf1flox/mut GFAP-Cre)	intraperitoneal 140 mg/kg (16–48 h)	tumor	-	detection of optic glioma	visual
(Bock et al., 2008a)	monkeys (marmosets) Rats (Sprague Dawley)	intravenous (tail) 4*30 mg/kg/48h (48h)	neuro- architecture	-	enhanced uptake of Mn ²⁺ with larger ventricles; determination of structures showing great enhancement	manual ROIs 3D reconstruction of enhanced sites
(Bock et al., 2008b)	Rats (Sprague Dawley)	intraperitoneal 6*30 mg/kg 3*60 mg/kg (48h) intravenous (tail) 2*90 mg/kg 1*180 mg/kg (48h)	Whole brain	-	dose-response of Mn ²⁺ , fractionation of dosages decrease toxicity and increase signal intensity	manual ROIs signal normalized to surrounding muscle
(Bock et al., 2009)	monkeys (marmosets)	intravenous (tail) 4*30 mg/kg/48 h (48h)	Visual cortex	Cytochrome oxidase	detailed structure of visual cortex	manual ROIs signal normalized to surrounding muscle
(Bouilleret et al., 2009)	Rats (Wistar)	intraperitoneal 3*100mg/kg/d1,1.6 months) (25h)	Different regions	-	traumatic brain injury → decreased cortex and hippocampus volume (not thalamic or amygdala volumes); focal signal changes post-injury → prediction of severity of neuro- degenerative changes.	manual ROIs signal normalized to baseline manual volume;
(Chan et al., 2008a)	Rats (Sprague Dawley) Mice (C57BL/6N)	intraperitoneal 45 mg/kg (24 h)	Damaged cortex	SOD	cortical injury leads to signal intensity enhancement (SOD)	visual
(Chen et al., 2007)	Rats (Sprague Dawley)	Intravenous (femoralis) 80 mg/kg (300g rat) 120 mg/kg (200g rat) (0 h) BBB disruption (mannitol)	Different regions	-	alterations in signal intensity of PFC, cingulate and thalamus due to scent (novel/fear- inducing)	manual ROI signal normalized to contra-lateral side
(Chuang et al., 2009a)	Rats (Sprague Dawley)	intravenous (tail) 176 mg/kg (0,1,7,28,35 d)	Whole brain	Mn ²⁺ concentration (mass spectroscopy)	half time of Mn ²⁺ , relaxation times correlate with Mn ²⁺ concentration	T1 mapping

Appendix

(Chuang et al., 2010)	Rats (Sprague Dawley)	intravenous (tail) 176 mg/kg (24h)	Olfactory bulb	-	detection of individual glomeruli in olfactory bulb	manual ROI signal normalized to background noise
(Daire et al., 2008)	Rats (Sprague Dawley)	Intravenous (tail) 4.95 mg/kg (30 min)	heart	-	Hypoenhanced volume detected with MEMRI represents area at risk, correlation with heart function	manual ROI manual volume (wall thickness)
(Deans et al., 2008)	Mice (ICR)	intraperitoneal 20, 40, and 80 mg/kg (24 h)	Whole brain	-	application of different concentrations at different times of pregnancy, visualization of embryonal brain development	manual ROI manual volume
(Delattre et al., 2010)	Mice (C57BL/6J)	intraperitoneal 0,5,6,11,2,16,24,32,40,51,62,77 mg/kg best: 32 mg/kg (0 h)	heart	-	heart function and signal enhancement after application of different concentrations of Mn ²⁺ , intensity for infarct volume determination	segmentation manual volume
(de Sousa et al., 2007)	Rats (Wistar)	intravenous (tail) 175 mg/kg (24 h)	Whole brain	-	no age-dependent differences in Mn ²⁺ uptake	manual ROIs
(Golub et al., 2010)	Mice (C57Bl/6N)	intraperitoneal 3*60 mg/kg/48h (24 h)	Hippocampus Amygdala	-	Differences in hippocampal volumes after footshock (decrease) and environmental enrichment (increase)	normalization and backdeformation of ROIs to native space semi-automatic volume
(Grünecker et al., 2010)	Mice (C57Bl/6N)	intraperitoneal 3*60 mg/kg/48h 6*30 mg/kg/48h 8*30 mg/kg/24h (24 h)	Different structures	-	toxicity + intensity after different systemic applications of Mn ²⁺	normalization and backdeformation of ROIs to native space; signal normalized to muscle
(Haapanen et al., 2007)	Mice (C57Bl/6 cathepsinD ko)	subcutaneous 40mg/kg (48 h)	lesions	Microglial activation	Mn as a lesion marker	Apparent diffusion coefficient
(Henning et al., 2005)	Rats (Sprague Dawley)	intravenous (femoral vein) 20 mg (0 h)	lesions	-	cortical spreading depression leads to differences in cortical and subcortical regions	manual ROIs signal normalized to contralateral side
(Hu et al., 2004)	Mice (CD1-ICR)	intravenous (tail or jugularis) 1.5 or 0.4 mg/kg (0 h)	Heart	Histological staining	signal decrease after heart infarct (coronal occlusion)	manual ROI manual volume signal normalized to baseline
(Hyacinthe et al., 2008)	Rats (Sprague Dawley)	intraperitoneal 2.8 mg/kg (0,15 min)	Heart	-	MEMRI facilitates magnetization tagging of coronal walls after heart infarct	automatic MR tagging (coronal walls)

Appendix

(Immonen et al., 2008)	Rats (Wistar)	intraperitoneal 45 mg/kg (15,37 h)	Hippocampus	Axonal density	MEMRI is not related to seizure activity, neurodegeneration, astrogliosis or microgliosis	manual ROIs signal normalized to control
(Jackson et al., 2011)	Rats (Lister hooded)	intraperitoneal 40 mg/kg (24 h)	Hippocampus	-	no alteration of hippocampus dependent task after Mn ²⁺ application	Visual
(Kawai et al., 2010)	Rats (Sprague Dawley)	intravenous (tail) 175 mg/kg (24 h)	Stroke region	astrogliosis	signal intensity after stroke (artery occlusion) correlates with reactive astrogliosis	manual ROI signal normalized to background noise
(Kuo et al., 2005)	Mice (C57BI/6N)	Intravenous (tail) 99 mg/kg intraperitoneal 99 mg/kg subcutaneous 198 mg/kg (0,15,45min;24,72 h)	Whole brain	-	signal intensity comparison after different application modes → signal enhancement without destroying BBB	manual ROI signal normalized to probe T1 relaxation
(Kuo et al., 2006)	Mice (C57BI/6N)	Intravenous (tail) 60 mg/kg (0,2 h)	Whole brain	-	time course of signal enhancement after intravenous injection, fasting increases signal enhancement	manual ROI signal normalized to probe T1 relaxation
(Kuo et al., 2010)	Mice (C57BI/6N)	Intravenous (tail) 60 mg/kg (0 h)	Whole brain	-	intensity alterations as an indicator for BBB permeability, increase with age and higher saturated fat diet, lower after lower saturated fat diet	manual ROI signal normalized to probe increase relative to baseline
(Lee et al., 2005)	Mice (FVB)	Intravenous (tail) 9,18,44,88,131,175 mg/kg (1,2,4,6,8,10,24 h)	Whole brain	-	dose-response, Mn ²⁺ application-T1 relaxation, largest changes 44-88 mg/kg, layer specificity at certain time points	manual ROI T1 relaxation
(Lee et al., 2010)	Mice (C57BI/6N)	Intravenous (tail) 4,10,20,40,80 mg/kg (0 h)	Non CNS organs	-	correlation signal intensity (T1 _{eff}) and Mn ²⁺ concentration in non CNS tissue	manual ROI T1 relaxation
(Martirosyan et al., 2010)	Rats (Sprague Dawley)	stereotactic (lateral ventricle) 80 µg (60 h)	Spinal chord	Mn ²⁺ concentration (mass spectroscopy)	signal intensity decrease after spinal chord injury, correlation between Mn concentration and signal intensity	manual ROI signal normalized to surrounding muscle
(Silva et al., 2008)	Rats (Sprague Dawley) Mice (Reeler)	Intravenous (tail) 175 mg/kg stereotactic (3rd Ventricle) 88 µg (24 h)	Whole brain	Nissl and BDA labelling	enhancement of neurocytoarchitecture and neuronal tract tracing, visual comparison to histological labeling	visual

Appendix

(Stieltjes et al., 2006)	Mice (?)	intravenous 197 mg/kg subcutaneous 40 mg/kg stereotactic (cisterna magna) 80 µg stereotactic (lateral ventricle) 40 µg (24 h)	Spinal chord	-	signal intensity indicated treatment success after spinal chord injury	manual ROI signal normalized to noise
(Van der Linden et al., 2002)	Birds (Starlings)	stereotactic (high vocal center) 3µg (2,4,6,8 h)	High vocal center	-	volume determination of the bird's song center	manual ROI intensity slope corrected
(Wadghiri et al., 2004)	Mice (Swiss-Webster, Gbx2-CKO)	intraperitoneal 40 mg/kg (variable time points after injection, peak at 24 h)	Cerebellum	Granule cell layer density (cresyl violett)	signal intensity difference in cerebellum in KO and WT	manual ROI signal normalized to noise
(Walder et al., 2008)	Rats (?)	stereotactic (cisterna magna) 12,6 mg (ex vivo!)	Spinal chord	-	intensity correlated with motor function after spinal chord injury	manual ROI signal intensity normalized to noise
(Watanabe et al., 2002)	Mice (NMRI)	subcutaneous 20 mg/kg (0, 6, 24, 48 h)	Whole brain		determination of signal enhancing structures after subcutaneous application	manual ROI signal intensity normalized to noise
(Widerøe et al., 2009)	Rats (Wistar)	intraperitoneal 40 mg/kg (24 h)	Whole brain		intensity in hypoxic-ischemia is more dependent on microglia activation	manual ROI signal normalized to contralateral side
(Yang and Wu, 2008)	Rats (Sprague Dawley)	intraperitoneal (anesthetized) 88 mg/kg (repeated up to 7 times 2 times on first day until d21)	Gray matter lesions		signal intensity differences after hypoxic ischemic injury, MEMRI detects injury until late phase	visual
(Yang et al., 2008)	Rats (Sprague Dawley)	intraperitoneal (anesthetized) 88 mg/kg (repeated up to 9 times 2 times on first day until d49)	lesions	superoxide dismutase and glutamine sythetase	hypoxic ischemic injury, correlation of Mn signal intensity and histologic determination of superoxide dismutase and glutamine sythetase	manual ROI signal intensity normalized to contralateral side
Mn²⁺ as activity marker						
(Berkowitz et al., 2006)	Rats (Sprague Dawley)	intraperitoneal 44 mg/kg (3.5 h)	Retinal layers	-	different accumulation of Mn ²⁺ in inner and outer retina due to light	manual ROIs absolute intensity; manual volume
(Berkowitz et al., 2007a)	Rats (Sprague Dawley)	intraperitoneal 44 mg/kg (4 h)	Damaged retinal tissue	-	altered retinal Mn ²⁺ intensity after ocular injury	manual ROIs absolute intensity; manual volume
(Berkowitz et al., 2007b)	Rats (50/10)	intraperitoneal 44 mg/kg (4 h)	Damaged retinal tissue	-	altered retinal volume and Mn ²⁺ intensity in experimental retinopathy of prematurity	manual ROIs absolute intensity; manual volume

Appendix

(Berkowitz et al., 2007c)	Rats (Sprague Dawley)	intraperitoneal 44 mg/kg (4 h)	Retinal layers	-	accumulation of Mn ²⁺ and retinal thickness differ in diabetes animals, normalized by α-lipoic acid	manual ROIs absolute intensity; manual volume
(Berkowitz et al., 2008)	Rats (Sprague Dawley + albino Royal College of Surgeons)	intraperitoneal 44 mg/kg (4 h)	Retinal layers	-	altered retinal Mn intensity in pathological, but not developmental, retinal thinning, normalized by repetitive hypoxic preconditioning protocol	manual ROIs absolute intensity; manual volume
(Berkowitz et al., 2009a)	Mice (C57BL/6 + SOD over-expressing)	intraperitoneal 66 mg/kg (3.5-4 h)	Retinal layers	-	altered retinal volume and Mn ²⁺ intensity in diabetes, not in diabetic SOD overexpressing mice, but retinal and vascular degeneration	manual ROIs absolute intensity; manual volume
(Berkowitz et al., 2009b)	Mice (C57BL/6 + nonsense mutation in exon 3 of the RPE65 gene)	intraperitoneal 66 mg/kg (3.5-4 h)	Retinal layers	intensity of background light	no differences in study in mice with mutation	manual ROIs absolute intensity; manual volume
(Bissig and Berkowitz, 2009)	Rats (Sprague Dawley)	intraperitoneal 66 mg/kg (8h)	Visual cortex Superior colliculus	-	layer specific enhancement due to visual stimulation	voxel wise comparison
(Brozoski et al., 2007)	Rats (Long Evans)	intraperitoneal 20 mg/kg (24-28 h)	Auditory brainstem forebrain structures	-	tinnitus or sound leads to enhancement in auditory brainstem and decrease in forebrain structures	manual ROIs signal normalized to baseline
(Eschenko et al., 2010a)	Rats (Sprague Dawley)	subcutaneous 16 mg/kg 32 mg/kg 80 mg/kg minipumps 80 mg/kg/7 days (12 h minipumps: after d6 of wheel running)	motor and sensory cortex, dorsal raphe; PAG	-	wheel running and food intake affected by higher systemic applications of Mn, intensity enhancement due to wheel running	Voxel wise comparison
(Eschenko et al., 2010b)	Rats (Sprague Dawley)	subcutaneous 16 or 80 mg/kg (24 h)	-	-	no electrophysiological and functional impact of Mn ²⁺ on the hippocampus	-
(Hankir et al., 2011)	Mice (C57Bl/6)	subcutaneous 99 mg/kg (0 h)	ARC, ventromedial hypothalamus, paraventricular nucleus	-	intensity differences in fasted mice and mice treated with different appetite suppressing peptides	manual ROI signal normalized to probe
(Hu et al., 2001)	Mice (FVB)	intravenous (tail) 6, 12.6, 25 mg/kg (0-120 min)	Heart	Ca ²⁺ influx	signal intensity measures Ca ²⁺ influx into heart	manual ROIs serial images, signal normalized to probe

Appendix

(Inui-Yamamoto et al., 2010)	Rats (Wistar)	intraperitoneal 3*20 mg/kg (24 h)	Different brain regions	-	intensity differences to presentation of conditioned stimuli (conditioned taste aversion)	manual ROIs absolute intensity
(Itoh et al., 2008)	Rats (Wistar)	intraperitoneal 12.5 and 50 mg/kg (1,2,3 ...h)	Whole brain	Glutamatergic activation	signal intensity after treatment with different anesthetics, intensity higher after glutamatergic NMDA activation	manual ROI signal normalized to probe
(Ivanova et al., 2010)	Mice (rd1/rd1)	intraperitoneal 66 mg/kg (4 h)	Retinal layers	-	signal enhancement due to higher uptake in response to Channelrhodopsin activation	manual ROI signal normalized to muscle
(Lin and Koretsky, 1997)	Rats (Sprague Dawley)	intravenous 0.6 mg/min (0 h)	Whole brain	-	signal intensity = neuronal activation	manual ROI signal normalized to baseline
(Lu et al., 2007)	Rats (Sprague Dawley)	intravenous 30 mg/kg BBB disruption (Manitol)	Whole brain	Ca ²⁺ dependent (antagonized)	signal intensity after cocaine and forepaw stimulation	activation maps manual ROI signal normalized to baseline
(Lu et al., 2008)	Rats (Sprague Dawley)	intravenous 50 mg/kg BBB disruption (Manitol)	Whole brain	-	real-time MRI of signal enhancement after cocaine application	real time activation maps (fMRI)
(Morita et al., 2002)	Rats (Wistar-Hamamu)	intravenous 70 mg/kg BBB disruption (Manitol)	Hypothalamus, supraoptic nucleus, preoptic area	FOS	signal enhancement in areas of central osmotic regulation, signal intensity correlates with FOS expression	manual ROI absolute signal intensity
(Parkinson et al., 2009)	Mice (C57Bl/6)	intraperitoneal 99 mg/kg (0 h)	Hypothalamus, brainstem	-	signal intensity differences in fasted mice after different anorexigenic agents	manual ROI signal intensity normalized to baseline
(So et al., 2007)	Mice (?)	intravenous 60 mg/kg (0 h)	Hypothalamus	-	signal intensity increase in hypothalamic nuclei after feeding with different diet	manual ROI signal normalized to baseline
(Waghorn et al., 2009)	Mice (C57Bl/6)	intravenous (tail) 38 mg/kg (1h)	Heart	Ca ²⁺ efflux	T1 maps quantify heart Ca ²⁺ efflux	T1 maps
(Watanabe et al., 2008)	Mice (NMRI)	subcutaneous 99 mg/kg (48 h)	Auditory pathway		signal intensity increase in auditory circuit due to tone presentation	manual ROI signal intensity normalized to noise
(Weng et al., 2007)	Rats (Wistar)	intraperitoneal 50 mg/kg BBB disruption (Manitol) (3 h ex vivo!)	Somatosensory cortex		specific signal increase in somatosensory cortex after whisker stimulation	subtraction of group mean images after normalization and co-registration

Appendix

(Yu et al., 2005)	Mice (Swiss Webster female)	intraperitoneal 80 mg/kg (24 h)	Inferior culliculus	-	signal intensity differences after tone presentation in normal mice and mice with conductive hearing loss	all images co-registration, segmentation of IC on mean, analysis of voxels with signal >15% above Cpu
(Yu et al., 2008)	Mice (ICR)	intraperitoneal 80 mg/kg (24 h)	Inferior culliculus	-	signal intensity differences after tone presentation of different frequency, tonotopic accumulation	all images co-registration and segmentation, mean intensity and SD normalisation, IC extraction
(Yu et al., 2011)	Mice (WT, KO and HET, fibroblast growth factor)	intraperitoneal 80 mg/kg (24 h)	IC (intensity), PFC and cerebellum, smaller OB (morphology)	-	signal intensity and accumulation differences after tone presentation in normal and mutant mice Fibroblast growth factor	all images co-registration and segmentation, mean intensity and SD normalisation, IC extraction
Mn²⁺ for neuronal tract tracing						
(Bearer et al., 2007)	Mice (C57BL/6 + CBA/J)	intravitreal (eye) 200 mM, 2 µL (30 min for 2h/6min)	Optical nerves	-	uptake and transport but not trans synaptic transmission of Mn ²⁺ without electrical activity	manual ROIs signal normalised to baseline
(Canals et al., 2008)	Rats (Sprague Dawley)	stereotactic 16 ng - 2560 ng (0 h)	Cortical connectivity	-	toxicological comparison of different Mn concentrations and injection volumes	connectivity maps manual ROIs signal normalized to probe
(Chan et al., 2007)	Rats (Sprague Dawley)	intravitreal (eye) 3 mg (2,3,4,5,8, 24 h)	Damaged optical nerves	-	glaucoma leads to alterations in Mn ²⁺ intensity in visual system	manual ROIs signal normalized to baseline
(Chan et al., 2008b)	Rats (Sprague Dawley)	intravitreal (eye) 3 mg (2,3,4,5 h)	Damaged optical nerves	-	glaucoma leads to alterations in Mn ²⁺ intensity in visual system	manual ROIs signal normalized to baseline
(Chan et al., 2010)	Rats (Sprague Dawley)	intravitreal (eye) 3 mg (24 h)	Superior culliculus	-	retinotopic organization of superior colliculus; volumes of signal enhancement comparison of damaged to control pathway	volume included pixels > mean + 2*SD control region
(Chen et al., 2008)	Rats (Lewis)	stereotactic (visual cortex) 60 mg/kg (1,2,4,7,15 h)	Corpus callosum	ion dys-homeostasis	alterations of intensity in corpus callosum after experimentally induced immune reaction (encephalomyelitis)	manual ROIs serial T1 weighted images signal normalized to control
(Chuang and Koretsky, 2006)	Rats (Sprague Dawley)	intranasal 95 µg (0 h)	Whole brain	-	introduction of T1 mapping for MEMRI	T1 mapping

Appendix

(Chuang and Koretsky, 2009)	Rats (Sprague Dawley)	intranasal 1.9 mg intravenous (tail) 10 mg/kg 44 mg/kg (0,1,12,24,36,48 h)	Hippocampus Pituitary	-	unspecific signal enhancement in hippocampus and pituitary in neuronal tract studies	manual ROIs signal normalized to background noise
(Chuang et al., 2009b)	Mice (C57Bl/6)	intranasal 1.4 mg (20 min)	Olfactory bulb	-	topological enhancement in olfactory bulb in response to different odors	time series of realigned images signal normalized to baseline
(Doron and Goelman, 2010)	Rats (Sprague Dawley)	stereotactic (right Cpu) 1.59 µg (0,3,24,48,72 h)	Connections of caudate putamen	-	principal component analysis of signal intensity to determine projections	principal component analysis
(Fa et al., 2010)	Rats (Wistar)	intranasal 6 mg (?)	visual cortex Deep brain structures	-	intensity differences due to visual stimulation	Coregistration group mean comparison of ROIs
(Hsu et al., 2008)	Rats (Sprague Dawley)	stereotactic (habenular nucleus) 4 µg (50-300,450 - 600min, 24,32,48 h)	VTA, dorsomedial part of the striatum, PFC	-	methamphetamine application leads to differences in signal increase in some regions (pathway alterations)	manual ROIs time series of manually realigned images
(Kivity et al., 2010)	Mice (C3H)	intranasal 4 mg	Olfactory bulb	-	intensity alteration in olfactory bulb after anti-ribosomal-P application	manual ROIs signal normalized to pituitary
(Li et al., 2009)	Rats (Sprague Dawley)	stereotactic (VTA) 8 µg (24 h)	Connections of ventral tegmental area	-	neuronal tract tracing from ventral tegmental area + neurotoxicity	manual ROIs signal normalized to contralateral side
(Liang et al., 2010)	Hamsters (Syrian golden)	intravitreal (eye) 3 mg (24 h)	Whole brain		signal intensity indicates CNS regeneration (chronic injury)	visual
(Madsen et al., 2008)	Rats (Sprague Dawley)	intravitreal (eye) 3 mg (24 h)	Superior colliculi	MRS	no correlation between signal intensity and MRS, Mn application does not disturb MRS	T1-relaxation
(Matsuda et al., 2010)	Rats (Sprague Dawley)	injection (into nerve) 40, 80 mg (72 h)	Damaged nerve	-	retrograde axonal tracing after nerve damage, signal decrease and increase after nerve damage and regeneration	manual ROI signal normalized to muscle
(Nairismägi et al., 2006)	Rats (Wistar)	stereotactic (entorhinal cortex) 8 µg (3, 5d)	hippocampus	Mossy fiber sprouting (histological)	neuronal-tract tracing, correlation signal intensity and neuronal sprouting	manual ROI, volume voxels > 1.2*mean+SD
(Obenaus and Jacobs, 2007)	Mice (C57Bl/6)	stereotactic (posterior hippocampus) 0.4 µg (n/a)	Lesioned regions	Diffusion tensor imaging	application in epilepsy	visual

Appendix

(Pautler et al., 1998)	Mice (?)	Intranasal 3 mg intravitreal (eye) 0,3 mg (10,20,30,40,50,60 h)	Connections of naris and eye	-	First neuronal tract tracing study after intravitreal and intranasal application	manual ROI absolute signal intensity
(Pautler and Koretsky, 2002)	Mice (FVB)	humidifier (Mn + Odor) 15 g/50 ml (1.5 h) intranasal 3 mg (24 h)	Connections of naris	Microtubule transportation and Ca ²⁺ dependent (blocked and antagonized)	neuronal tract tracing, Mn ²⁺ -transportation Ca ²⁺ -channel and microtubule associated, odor pathway activation	manual ROIs absolute signal intensity
(Pautler et al., 2003)	Mice (C57/Bl6)	stereotactic (dorsal striatum; BLA) 9 µg (24 h (striatum) 48 h (amygdala) 10d)	Connections of basolateral amygdala and dorsal striatum	-	neuronal tract tracing from basolateral amygdala and dorsal striatum	visual
(Pelled et al., 2007)	Rats (Sprague Dawley)	stereotactic (entopeduncular nucleus; substantia nigra pars compacta; Habenula) 9 µg (0, 3, 24, 28 h)	Connections of entopeduncular nucleus, substantia nigra pars compacta and Habenula	-	alteration of neuronal tract tracing in Parkinsons disease model	manual ROIs signal intensity normalized to baseline
(Serrano et al., 2008)	Mice (C57Bl/6 ko:Hexb; APP; Kv4.2)	intranasal 3 mg (24h)	Olfactory bulb and olfactory cortex	-	comparison of ROI in olfactory cortex to ROI in olfactory bulb as indication of synaptic transport of Mn, disruption by pharmacological agents	manual ROIs signal intensity normalized to other ROI
(Sharma et al., 2010)	Mice (C57/Bl6)	intranasal 3 mg (1 h)	Olfactory system	-	decrease in signal enhancement over time with oxidative stress (Hyperglycemia induction)	manual ROI signal intensity normalized to surrounding muscle
(Smith et al., 2007)	Mice (C57Bl/6 + Tg2576)	intranasal 3 mg (? h)	Axonal transport	-	Decrease in axonal transport in Alzheimer's disease (Tg2576)	manual ROI signal intensity normalized to surrounding muscle
(Smith and Paylor, 2010)	Mice (Tg2576 and C57Bl6/SJL)	intranasal 3 mg (25 min)	Axonal transport		Deficits of axonal transport in Alzheimer's disease before plaque development	manual ROI signal intensity normalized to surrounding muscle
(Soria et al., 2008)	Rats (Wistar)	stereotactic (S1fl) 3*16 µg on d2,d15,d29 (0, 15, 24h + 7d)	S1	-	intensity accumulation after repeated injection, no toxicity effects after repeated injection, no disturbance of fMRI	visual

Appendix

(Thuen et al., 2008)	Rats (Sprague Dawley)	intravitreal (eye) 0, 6, 29, 58, 290, 580 µg (48 h)	Visual pathway	-	dose-response for application in the visual pathway	manual ROI signal intensity normalized to noise
(Thuen et al., 2009)	Rats (Fisher)	intravitreal (eye) 29 µg (48 h)	Retinal ganglion cells	Diffusion tensor imaging	signal intensity indicates cell regeneration, comparison to DTI	manual ROI signal intensity normalized to noise
(Tindemans et al., 2003)	Birds (canaries)	stereotactic (high vocal center) 3µg	High vocal center	-	signal intensity differences after conspecific song stimulation	manual ROI signal intensity slope corrected
(Tindemans et al., 2006)	Birds (zebra finches canaries)	stereotactic (high vocal center) 20 ng (7h)	High vocal center	-	neural tract tracing in birds, signal enhancement by inversion recovery sequence, adjustment of injection parameters	manual ROI inversion recovery
(Tucciarone et al., 2009)	Rats (Sprague Dawley)	stereotactic (S1, Thalamus) 11µg (6, 12, 24 h)	Somatosensory connections	-	neuronal tract tracing of somatosensory connections (S1, Thalamus)	T1 mapping voxel wise comparison after normalisation, group statistics
(van der Zijden et al., 2007)	Rats (Wistar)	stereotactic (sensori motorcortex) 40 µg (6, 24h and 2, 4, 6, 8 d9)	Connections of motor cortex	-	neuronal tract tracing after stroke	manual ROI (volume) signal intensity > mean+2*SD
(Watanabe et al., 2001)	Rats (albino Wistar)	intravitreal (eye) 20 mg (24 h)	Visual pathway		neuronal tract tracing of visual pathway	manual ROI signal intensity normalized to noise
(Yang et al., 2011)	Rats (?)	stereotactic (Thalamus) ? 120 mM solution for 15 min (5.5 h)	Different specific brain regions		differences in signal intensity after pain (mild, strong) + morphine	co-registration, pixel intensity normalization; volume of interest analysis, F-contrast statistical maps
(Zhang et al., 2010)	Mice (DAT KO and WT)	stereotactic (PFC) 0,6 mg	Whole brain	-	neuronal tract tracing in Parkinson mice	all images co-registered and voxelwise comparison

Aoki I, Wu Y-JL, Silva AC, Lynch RM, Koretsky AP (2004) In vivo detection of neuroarchitecture in the rodent brain using manganese-enhanced MRI. *NeuroImage* 22:1046-59

Banerjee D, Hegedus B, Gutmann DH, Garbow JR (2007) Detection and measurement of neurofibromatosis-1 mouse optic glioma in vivo. *NeuroImage* 35:1434-7

Bearer EL, Falzone TL, Zhang X, Biris O, Rasin A, Jacobs RE (2007) Role of neuronal activity and kinesin on tract tracing by manganese-enhanced MRI (MEMRI). *NeuroImage* 37 Suppl 1:S37-46

Appendix

- Berkowitz BA, Gadianu M, Schafer S, Jin Y, Porchia A, Iezzi R, Roberts R (2008) Ionic dysregulatory phenotyping of pathologic retinal thinning with manganese-enhanced MRI. *Investigative Ophthalmology & Visual Science* 49:3178
- Berkowitz BA, Gadianu M, Bissig D, Kern TS, Roberts R (2009)(a) Retinal ion regulation in a mouse model of diabetic retinopathy: natural history and the effect of Cu/Zn superoxide dismutase overexpression. *Investigative Ophthalmology & Visual Science* 50:2351
- Berkowitz BA, Roberts R, Luan H, Bissig D, Bui BV, Gadianu M, Calkins DJ, Vingrys AJ (2007)(a) Manganese-enhanced MRI studies of alterations of intraretinal ion demand in models of ocular injury. *Investigative Ophthalmology & Visual Science* 48:3796
- Berkowitz BA, Roberts R, Oleske DA, Chang M, Schafer S, Bissig D, Gadianu M (2009) (b) Quantitative mapping of ion channel regulation by visual cycle activity in rodent photoreceptors in vivo. *Investigative Ophthalmology & Visual Science* 50:1880
- Berkowitz B a, Roberts R, Goebel DJ, Luan H (2006) Noninvasive and simultaneous imaging of layer-specific retinal functional adaptation by manganese-enhanced MRI. *Investigative Ophthalmology & Visual Science* 47:2668-74
- Berkowitz B a, Roberts R, Penn JS, Gadianu M (2007)(b) High-resolution manganese-enhanced MRI of experimental retinopathy of prematurity. *Investigative Ophthalmology & Visual Science* 48:4733-40
- Berkowitz B a, Roberts R, Stemmler A, Luan H, Gadianu M (2007)(c) Impaired apparent ion demand in experimental diabetic retinopathy: correction by lipoic Acid. *Investigative Ophthalmology & Visual Science* 48:4753-8
- Bissig D, Berkowitz B a (2009) Manganese-enhanced MRI of layer-specific activity in the visual cortex from awake and free-moving rats. *NeuroImage* 44:627-35
- Bock NA, Paiva FF, Nascimento GC, Newman JD, Silva AC (2008)(a) Cerebrospinal fluid to brain transport of manganese in a non-human primate revealed by MRI. *Brain Research* 1198:160–170
- Bock NA, Paiva FF, Silva AC (2008)(b) Fractionated manganese-enhanced MRI. *NMR in Biomedicine* 21:473–478
- Bock NA, Kocharyan A, Silva AC (2009) Manganese-enhanced MRI visualizes V1 in the non-human primate visual cortex. *NMR in Biomedicine* 22:730-6
- Boulleret V, Cardamone L, Liu YR, Fang K, Myers DE, O'Brien TJ (2009) Progressive brain changes on serial manganese-enhanced MRI following traumatic brain injury in the rat. *Journal of Neurotrauma* 26:1999-2013
- Brozoski TJ, Ciobanu L, Bauer C a (2007) Central neural activity in rats with tinnitus evaluated with manganese-enhanced magnetic resonance imaging (MEMRI). *Hearing Research* 228:168-79
- Canals S, Beyerlein M, Keller a L, Murayama Y, Logothetis NK (2008) Magnetic resonance imaging of cortical connectivity in vivo. *NeuroImage* 40:458-72
- Chan KC, Cai K-xia, Su H-xing, Hung VK, Cheung MM, Chiu C-tat, Guo H, Jian Y, Chung SK, Wu W-tian, Wu EX (2008)(a) Early detection of neurodegeneration in brain

- ischemia by manganese-enhanced MRI. Conference proceedings : Annual International Conference of the IEEE Engineering in Medicine and Biology Society. IEEE Engineering in Medicine and Biology Society. Conference 2008:3884-7
- Chan KC, Fu Q-ling, Hui ES, So K-fai, Wu EX (2008)(b) Evaluation of the retina and optic nerve in a rat model of chronic glaucoma using in vivo manganese-enhanced magnetic resonance imaging. *NeuroImage* 40:1166-74
- Chan KC, Fu Q-L, So K-fai, Wu EX (2007) Evaluation of the visual system in a rat model of chronic glaucoma using manganese-enhanced magnetic resonance imaging. Conference proceedings : Annual International Conference of the IEEE Engineering in Medicine and Biology Society. IEEE Engineering in Medicine and Biology Society. Conference 2007:67-70
- Chan KC, Li J, Kau P, Zhou IY, Cheung MM, So K-F, Wu EX (2010) In vivo retinotopic mapping of superior colliculus using manganese-enhanced magnetic resonance imaging. *NeuroImage* 54:389-395
- Chen C-CV, Zechariah A, Hsu Y-H, Chen H-W, Yang L-C, Chang C (2008) Neuroaxonal ion dyshomeostasis of the normal-appearing corpus callosum in experimental autoimmune encephalomyelitis. *Experimental Neurology* 210:322-30
- Chen W, Tenney J, Kulkarni P, King J a (2007) Imaging unconditioned fear response with manganese-enhanced MRI (MEMRI). *NeuroImage* 37:221-9
- Chuang K-H, Belluscio L, Koretsky AP (2010) In vivo detection of individual glomeruli in the rodent olfactory bulb using manganese enhanced MRI. *NeuroImage* 49:1350-6
- Chuang K-H, Koretsky A (2006) Improved neuronal tract tracing using manganese enhanced magnetic resonance imaging with fast T(1) mapping. *Magnetic Resonance in Medicine* 55:604-11
- Chuang K-H, Koretsky AP (2009) Accounting for nonspecific enhancement in neuronal tract tracing using manganese enhanced magnetic resonance imaging. *Magnetic Resonance Imaging* 27:594-600
- Chuang K-H, Koretsky AP, Sotak CH (2009)(a) Temporal changes in the T1 and T2 relaxation rates (ΔR_1 and ΔR_2) in the rat brain are consistent with the tissue-clearance rates of elemental manganese. *Magnetic Resonance in Medicine* 61:1528-32
- Chuang K-H, Lee JH, Silva AC, Belluscio L, Koretsky AP (2009)(b) Manganese enhanced MRI reveals functional circuitry in response to odorant stimuli. *NeuroImage* 44:363-72
- Daire JL, Hyacinthe JN, Tatar I, Montet-Abou K, Ivancevic MK, Masterson K, Jorge-Costa M, Morel DR, Vallée JP (2008) In vivo myocardial infarct area at risk assessment in the rat using manganese enhanced magnetic resonance imaging (MEMRI) at 1.5T. *Magnetic Resonance in Medicine* 59:1422-30
- Deans AE, Wadghiri YZ, Berrios-Otero C a, Turnbull DH (2008) Mn enhancement and respiratory gating for in utero MRI of the embryonic mouse central nervous system. *Magnetic Resonance in Medicine* 59:1320-8
- Delattre BM a, Braunersreuther V, Hyacinthe J-N, Crowe L a, Mach F, Vallée J-P (2010) Myocardial infarction quantification with Manganese-Enhanced MRI (MEMRI) in

Appendix

- mice using a 3T clinical scanner. *NMR in Biomedicine* 23:503-13
- Doron O, Goelman G (2010) Evidence for asymmetric intra substantia nigra functional connectivity-application to basal ganglia processing. *NeuroImage* 49:2940-6
- Eschenko O, Canals S, Simanova I, Beyerlein M, Murayama Y, Logothetis NK (2010)(a) Mapping of functional brain activity in freely behaving rats during voluntary running using manganese-enhanced MRI: implication for longitudinal studies. *NeuroImage* 49:2544-55
- Eschenko O, Canals S, Simanova I, Logothetis NK (2010)(b) Behavioral, electrophysiological and histopathological consequences of systemic manganese administration in MEMRI. *Magnetic Resonance Imaging* 28:1165-1174
- Fa Z, Zhang P, Huang F, Li P, Zhang R, Xu R, Wen Z, Jiang X (2010) Activity-induced manganese-dependent functional MRI of the rat visual cortex following intranasal manganese chloride administration. *Neuroscience letters* 481:110-4
- Golub Y, Kaltwasser SF, Mauch CP, Herrmann L, Schmidt U, Holsboer F, Czisch M, Wotjak CT (2010) Reduced hippocampus volume in the mouse model of Posttraumatic Stress Disorder. *Journal of Psychiatric Research* i:1-10
- Grünecker B, Kaltwasser SF, Peterse Y, Sämann PG, Schmidt MV, Wotjak CT, Czisch M (2010) Fractionated manganese injections: effects on MRI contrast enhancement and physiological measures in C57BL/6 mice. *NMR in Biomedicine* 23:913-21
- Haapanen A, Ramadan UA, Autti T, Joensuu R, Tynnelä J (2007) In vivo MRI reveals the dynamics of pathological changes in the brains of cathepsin D-deficient mice and correlates changes in manganese-enhanced MRI with microglial activation. *Magnetic Resonance Imaging* 25:1024-31
- Hankir MK, Parkinson JRC, Minnion JS, Addison ML, Bloom SR, Bell JD (2011) Peptide YY(3-36) and Pancreatic Polypeptide Differentially Regulate Hypothalamic Neuronal Activity in Mice In Vivo as Measured by Manganese-Enhanced Magnetic Resonance Imaging. *Journal of Neuroendocrinology* 23:371-80
- Henning EC, Meng X, Fisher M, Sotak CH (2005) Visualization of cortical spreading depression using manganese-enhanced magnetic resonance imaging. *Magnetic Resonance in Medicine* 53:851-7
- Hsu Y-H, Chen C-CV, Zechariah A, Yen CC, Yang L-C, Chang C (2008) Neuronal dysfunction of a long projecting multisynaptic pathway in response to methamphetamine using manganese-enhanced MRI. *Psychopharmacology* 196:543-53
- Hu TCC, Bao W, Lenhard SC, Schaeffer TR, Yue T-li, Willette RN, Jucker BM (2004) Simultaneous assessment of left-ventricular infarction size, function and tissue viability in a murine model of myocardial infarction by cardiac manganese-enhanced magnetic resonance imaging (MEMRI). *NMR in Biomedicine* 17:620-6
- Hu TCC, Pautler RG, MacGowan G a, Koretsky AP (2001) Manganese enhanced MRI of mouse heart during changes in inotropy. *Magnetic Resonance in Medicine* 46:884-890
- Hyacinthe JN, Ivancevic M, Daire JL, Vallée JP (2008) Feasibility of complementary spatial modulation of magnetization tagging in the rat heart after manganese injection.

NMR in Biomedicine 21:15–21

- Immonen RJ, Kharatishvili I, Sierra A, Einula C, Pitkänen A, Gröhn OHJ (2008) Manganese enhanced MRI detects mossy fiber sprouting rather than neurodegeneration, gliosis or seizure-activity in the epileptic rat hippocampus. *NeuroImage* 40:1718-30
- Inui-Yamamoto C, Yoshioka Y, Inui T, Sasaki KS, Ooi Y, Ueda K, Seiyama a, Ohzawa I (2010) The brain mapping of the retrieval of conditioned taste aversion memory using manganese-enhanced magnetic resonance imaging in rats. *Neuroscience* 167:199-204
- Itoh K, Sakata M, Watanabe M, Aikawa Y, Fujii H (2008) The entry of manganese ions into the brain is accelerated by the activation of N-methyl-D-aspartate receptors. *Neuroscience* 154:732-40
- Ivanova E, Roberts R, Bissig D, Pan Z-H, Berkowitz B a (2010) Retinal channelrhodopsin-2-mediated activity in vivo evaluated with manganese-enhanced magnetic resonance imaging. *Molecular Vision* 16:1059-67
- Jackson SJ, Hussey R, Jansen M a, Merrifield GD, Marshall I, MacLulich A, Yau JLW, Bast T (2011) Manganese-enhanced magnetic resonance imaging (MEMRI) of rat brain after systemic administration of MnCl₂: hippocampal signal enhancement without disruption of hippocampus-dependent behavior. *Behavioural Brain Research* 216:293-300
- Kawai Y, Aoki I, Umeda M, Higuchi T, Kershaw J, Higuchi M, Silva AC, Tanaka C (2010) In vivo visualization of reactive gliosis using manganese-enhanced magnetic resonance imaging. *NeuroImage* 49:3122-31
- Kivity S, Tsarfaty G, Agmon-Levin N, Blank M, Manor D, Konen E, Chapman J, Reichlin M, Wasson C, Shoenfeld Y, Kushnir T (2010) Abnormal olfactory function demonstrated by manganese-enhanced MRI in mice with experimental neuropsychiatric lupus. *Annals of the New York Academy of Sciences* 1193:70-7
- Kuo YT, Herlihy AH, So PW, Bhakoo KK, Bell JD (2005) In vivo measurements of T1 relaxation times in mouse brain associated with different modes of systemic administration of manganese chloride. *Journal of Magnetic Resonance Imaging* 21:334–339
- Kuo Y, Herlihy A, So P, Bell JD (2006) Manganese-enhanced magnetic resonance imaging (MEMRI) without compromise of the blood–brain barrier detects hypothalamic neuronal activity in vivo. *NMR in Biomedicine* 19:1028–1034
- Kuo Y-T, So P-W, Parkinson JR, Yu WS, Hankir M, Herlihy AH, Goldstone AP, Frost GS, Wasserfall C, Bell JD (2010) The combined effects on neuronal activation and blood-brain barrier permeability of time and n-3 polyunsaturated fatty acids in mice, as measured in vivo using MEMRI. *NeuroImage* 50:1384-91
- Lee JH, Silva AC, Merkle H, Koretsky AP (2005) Manganese-enhanced magnetic resonance imaging of mouse brain after systemic administration of MnCl₂: dose-dependent and temporal evolution of T1 contrast. *Magnetic Magnetic Resonance in Medicine* 53:640-8
- Lee L-W, So P-W, Price AN, Parkinson JRC, Larkman DJ, Halliday J, Poucher SM, Pugh J

Appendix

- a T, Cox AG, McLeod CW, Bell JD (2010) Manganese enhancement in non-CNS organs. *NMR in Biomedicine* 23:931-8
- Li Y, Fang F, Wang X, Lei H (2009) Neuronal projections from ventral tegmental area to forebrain structures in rat studied by manganese-enhanced magnetic resonance imaging. *Magnetic Resonance Imaging* 27:293-9
- Liang Y-X, Cheung SWH, Chan KCW, Wu EX, Tay DKC, Ellis-Behnke RG (2010) CNS regeneration after chronic injury using a self-assembled nanomaterial and MEMRI for real-time in vivo monitoring. *Nanomedicine : Nanotechnology, Biology, and Medicine*:1-9
- Lin YJ, Koretsky a P (1997) Manganese ion enhances T1-weighted MRI during brain activation: an approach to direct imaging of brain function. *Magnetic Resonance in Medicine* 38:378-88
- Lu H, Xi Z-X, Gitajn L, Rea W, Yang Y, Stein E a (2007) Cocaine-induced brain activation detected by dynamic manganese-enhanced magnetic resonance imaging (MEMRI). *Proceedings of the National Academy of Sciences of the United States of America* 104:2489-94
- Lu H, Yang S, Zuo Y, Demny S, Stein E a, Yang Y (2008) Real-time animal functional magnetic resonance imaging and its application to neuropharmacological studies. *Magnetic Resonance Imaging* 26:1266-72
- Madsen KS, Holm DA, Søgaard LV, Rowland IJ (2008) Effect of paramagnetic manganese cations on ¹H MRS of the brain. *NMR in Biomedicine* 21:1087–1093
- Martirosyan NL, Bennett KM, Theodore N, Preul MC (2010) Manganese-enhanced magnetic resonance imaging in experimental spinal cord injury: correlation between T1-weighted changes and Mn(2+) concentrations. *Neurosurgery* 66:131-6
- Matsuda K, Wang HX, Suo C, McCombe D, Horne MK, Morrison W a, Egan GF (2010) Retrograde axonal tracing using manganese enhanced magnetic resonance imaging. *NeuroImage* 50:366-74
- Morita H, Ogino T, Seo Y, Fujiki N, Tanaka K, Takamata A, Nakamura S, Murakami M (2002) Detection of hypothalamic activation by manganese ion contrasted T(1)-weighted magnetic resonance imaging in rats. *Neuroscience Letters* 326:101-4
- Nairismägi J, Pitkänen A, Narkilahti S, Huttunen J, Kauppinen R a, Gröhn OHJ (2006) Manganese-enhanced magnetic resonance imaging of mossy fiber plasticity in vivo. *NeuroImage* 30:130-5
- Obenaus A, Jacobs RE (2007) Magnetic resonance imaging of functional anatomy: use for small animal epilepsy models. *Epilepsia* 48 Suppl 4:11-7
- Parkinson JRC, Chaudhri OB, Kuo Y-T, Field BCT, Herlihy AH, Dhillon WS, Ghatei M a, Bloom SR, Bell JD (2009) Differential patterns of neuronal activation in the brainstem and hypothalamus following peripheral injection of GLP-1, oxyntomodulin and lithium chloride in mice detected by manganese-enhanced magnetic resonance imaging (MEMRI). *NeuroImage* 44:1022-31
- Pautler RG, Silva a C, Koretsky a P (1998) In vivo neuronal tract tracing using manganese-enhanced magnetic resonance imaging. *Magnetic Resonance in Medicine* 40:740-8

- Pautler RG, Koretsky AP (2002) Tracing odor-induced activation in the olfactory bulbs of mice using manganese-enhanced magnetic resonance imaging. *NeuroImage* 16:441-8
- Pautler RG, Mongeau R, Jacobs RE (2003) In vivo trans-synaptic tract tracing from the murine striatum and amygdala utilizing manganese enhanced MRI (MEMRI). *Magnetic Resonance in Medicine* 50:33-9
- Pelled G, Bergman H, Ben-Hur T, Goelman G (2007) Manganese-enhanced MRI in a rat model of Parkinson's disease. *Journal of Magnetic Resonance Imaging : JMRI* 26:863-70
- Serrano F, Deshazer M, Smith KDB, Ananta JS, Wilson LJ, Pautler RG (2008) Assessing transneuronal dysfunction utilizing manganese-enhanced MRI (MEMRI). *Magnetic Resonance in Medicine* 60:169-75
- Sharma R, Buras E, Terashima T, Serrano F, Massaad C a, Hu L, Bitner B, Inoue T, Chan L, Pautler RG (2010) Hyperglycemia induces oxidative stress and impairs axonal transport rates in mice. *PLoS one* 5:e13463
- Silva AC, Lee JH, Wu CW-H, Tucciarone J, Pelled G, Aoki I, Koretsky AP (2008) Detection of cortical laminar architecture using manganese-enhanced MRI. *Journal of Neuroscience Methods* 167:246-57
- Smith KDB, Kallhoff V, Zheng H, Pautler RG (2007) In vivo axonal transport rates decrease in a mouse model of Alzheimer's disease. *NeuroImage* 35:1401-8
- Smith K, Paylor R (2010) R-flurbiprofen improves axonal transport in the Tg2576 mouse model of Alzheimer's Disease as determined by MEMRI. *Magnetic Resonance in Medicine* 000:1-7
- So P-W, Yu W-S, Kuo Y-T, Wasserfall C, Goldstone AP, Bell JD, Frost G (2007) Impact of resistant starch on body fat patterning and central appetite regulation. *PLoS one* 2:e1309
- Soria G, Wiedermann D, Justicia C, Ramos-Cabrer P, Hoehn M (2008) Reproducible imaging of rat corticothalamic pathway by longitudinal manganese-enhanced MRI (L-MEMRI). *NeuroImage* 41:668-74
- Sousa PL de, Souza SL de, Silva AC, Souza RE de, Castro RM de (2007) Manganese-enhanced magnetic resonance imaging (MEMRI) of rat brain after systemic administration of MnCl₂: changes in T1 relaxation times during postnatal development. *Journal of magnetic resonance imaging : JMRI* 25:32-8
- Stieltjes B, Klussmann S, Bock M, Umathum R, Mangalathu J, Letellier E, Rittgen W, Edler L, Krammer PH, Kauczor H-U, Martin-Villalba A, Essig M (2006) Manganese-enhanced magnetic resonance imaging for in vivo assessment of damage and functional improvement following spinal cord injury in mice. *Magnetic Resonance in Medicine* 55:1124-31
- Thuen M, Berry M, Pedersen TB, Goa PE, Summerfield M, Haraldseth O, Sandvig A, Brekken C (2008) Manganese-enhanced MRI of the rat visual pathway: acute neural toxicity, contrast enhancement, axon resolution, axonal transport, and clearance of Mn(2+). *Journal of Magnetic Resonance Imaging : JMRI* 28:855-65
- Thuen M, Olsen O, Berry M, Pedersen TB, Kristoffersen A, Haraldseth O, Sandvig A,

Appendix

- Brekken C (2009) Combination of Mn(2+)-enhanced and diffusion tensor MR imaging gives complementary information about injury and regeneration in the adult rat optic nerve. *Journal of Magnetic Resonance Imaging* : JMRI 29:39-51
- Tindemans I, Verhoye M, Balthazart J, Van der Linden A (2003) In vivo dynamic ME-MRI reveals differential functional responses of RA-and area X-projecting neurons in the HVC of canaries exposed to conspecific song. *European Journal of Neuroscience* 18:3352–3360
- Tindemans I, Boumans T, Verhoye M, Van der Linden A (2006) IR-SE and IR-MEMRI allow in vivo visualization of oscine neuroarchitecture including the main forebrain regions of the song control system. *NMR in Biomedicine* 19:18-29
- Tucciarone J, Chuang K-H, Dodd SJ, Silva A, Pelled G, Koretsky AP (2009) Layer specific tracing of corticocortical and thalamocortical connectivity in the rodent using manganese enhanced MRI. *NeuroImage* 44:923-31
- Van der Linden a, Verhoye M, Van Meir V, Tindemans I, Eens M, Absil P, Balthazart J (2002) In vivo manganese-enhanced magnetic resonance imaging reveals connections and functional properties of the songbird vocal control system. *Neuroscience* 112:467-74
- Wadghiri YZ, Blind J a, Duan X, Moreno C, Yu X, Joyner AL, Turnbull DH (2004) Manganese-enhanced magnetic resonance imaging (MEMRI) of mouse brain development. *NMR in Biomedicine* 17:613-9
- Waghorn B, Yang Y, Baba A, Matsuda T, Schumacher A, Yanasak N, Hu TC-C (2009) Assessing manganese efflux using SEA0400 and cardiac T1-mapping manganese-enhanced MRI in a murine model. *NMR in Biomedicine* 22:874-81
- Walder N, Petter-Puchner AH, Brejnikow M, Redl H, Essig M, Stieltjes B (2008) Manganese enhanced magnetic resonance imaging in a contusion model of spinal cord injury in rats: correlation with motor function. *Investigative Radiology* 43:277-83
- Watanabe T, Frahm J, Michaelis T (2008) Manganese-enhanced MRI of the mouse auditory pathway. *Magnetic Resonance in Medicine* 60:210-2
- Watanabe T, Michaelis T, Frahm J (2001) Mapping of retinal projections in the living rat using high-resolution 3D gradient-echo MRI with Mn²⁺-induced contrast. *Magnetic Resonance in Medicine* 46:424–429
- Watanabe T, Natt O, Boretius S, Frahm J, Michaelis T (2002) In vivo 3D MRI staining of mouse brain after subcutaneous application of MnCl₂. *Magnetic Resonance in Medicine* 48:852-9
- Weng J-C, Chen J-H, Yang P-F, Tseng W-YI (2007) Functional mapping of rat barrel activation following whisker stimulation using activity-induced manganese-dependent contrast. *NeuroImage* 36:1179-88
- Widerøe M, Olsen Ø, Pedersen TB, Goa PE, Kavelaars A, Heijnen C, Skranes J, Brubakk A-M, Brekken C (2009) Manganese-enhanced magnetic resonance imaging of hypoxic-ischemic brain injury in the neonatal rat. *NeuroImage* 45:880-90
- Yang J, Khong P-L, Wang Y, Chu AC-Y, Ho S-L, Cheung P-T, Wu EX (2008) Manganese-enhanced MRI detection of neurodegeneration in neonatal hypoxic-ischemic cerebral injury. *Magnetic Resonance in Medicine* 59:1329-39

- Yang J, Wu EX (2008) Detection of cortical gray matter lesion in the late phase of mild hypoxic-ischemic injury by manganese-enhanced MRI. *NeuroImage* 39:669-79
- Yang P-F, Chen D-Y, Hu JW, Chen J-H, Yen C-T (2011) Functional tracing of medial nociceptive pathways using activity-dependent manganese-enhanced MRI. *Pain* 152:194-203
- Yu X, Nieman BJ, Sudarov A, Szulc KU, Abdollahian DJ, Bhatia N, Lalwani AK, Joyner AL, Turnbull DH (2011) Morphological and functional midbrain phenotypes in Fibroblast Growth Factor 17 mutant mice detected by Mn-enhanced MRI. *NeuroImage*
- Yu X, Wadghiri YZ, Sanes DH, Turnbull DH (2005) In vivo auditory brain mapping in mice with Mn-enhanced MRI. *Nature Neuroscience* 8:961–968
- Yu X, Zou J, Babb JS, Johnson G, Sanes DH, Turnbull DH (2008) Statistical mapping of sound-evoked activity in the mouse auditory midbrain using Mn-enhanced MRI. *NeuroImage* 39:223-30
- Zhang X, Bearer EL, Boulat B, Hall FS, Uhl GR, Jacobs RE (2010) Altered neurocircuitry in the dopamine transporter knockout mouse brain. *PloS one* 5:e11506
- Zijden JP van der, Wu O, Toorn A van der, Roeling TP, Bleys RL a W, Dijkhuizen RM (2007) Changes in neuronal connectivity after stroke in rats as studied by serial manganese-enhanced MRI. *NeuroImage* 34:1650-7

Contributions

Contributions

Sebastian F. Kaltwasser: conceptualized analysis of MEMRI data and designed or partly designed all experiments, conducted and analyzed all experiments of study 1 experiment 1 and 3.1 and study 2 experiment 2.1, did main part of MEMRI measurements of study 2 experiment 2.2 and study 3 and part of the MEMRI measurements of study 1 experiment 2 and 3.2 and study 2 experiment 1. He did all analysis of MEMRI except for study 1 experiment 2 and study 2 experiment 1 where the analysis was assisted by others. He conducted and analyzed telemetric measurements, did all statistical analysis of study 2 experiment 1 and wrote the manuscript.

Carsten T. Wotjak: supervised all experiments and contributed to the design of all experiments as well as interpretation of data.

Michael Czisch: supervised conceptualization and design of the MEMRI experiments, supervised all NMR scanning and conceptualization and analysis of the MEMRI data.

Barabara Grünecker: assisted in conceptualization of the MEMRI data analysis, conducted some of the MEMRI measurements and analysis of chapter I experiment 2 and study 2 experiment 1.

Benedikt Bedenk: assisted with the MEMRI measurements of chapter I experiment 3.2 and study 2 experiment 2.2.

Philipp G. Sämann: helped in the statistical analysis of MEMRI data for study 2 experiment 1.

Armin Mann: gave technical support

Karl Kleinknecht: conducted and analyzed water cross maze experiments.

Anja Mederer: performed surgery for ibotenic acid application.

Contributions

Yulia Golub: conducted behavioral experiments and part of MEMRI measurements of study 3. She analyzed the behavioral data of this study and carried out part of the the statistical analysis.

Christoph P. Mauch: conducted ultramicroscopic measurements and analyzed and interpreted ultramicroscopic data.

Caitlin J. Riebe: corrected and edited the manuscript.

Yorick Peterse: assisted with part of the MEMRI measurements of chapter I experiment 2 and study 2 experiment 1

Mathias V. Schmidt: helped design experiment 2.3 and with interpretation of corticosterone measurements in study 1 experiment 2.3.

Bianca Mayer: performed corticosterone measurements in study 1 experiment 2.3.

Acknowledgments

Acknowledgments

I would like to thank all contributors for their individual efforts.

First, I would like to thank my mentor and supervisor and the head of the research group, Dr. Carsten Wotjak, who inspired me with his great enthusiasm and love for science.

Thank you for the great time and opportunities you gave me.

I want to also especially thank the head of the NMR research group, Dr. Michael Czisch for his great effort to illuminate the complicated world of physics and ability to make NMR techniques understandable. Thank you for letting me assimilate into your group.

Many, many thanks go to the whole research group Wotjak and Czisch, especially to Benedikt Bedenk and Barbara Grünecker, my officemates and friends for sticking it out with me through thick and thin.

I want to thank my wife, Caitlin Riebe, for taking my mind off things when I am stressed and for all her support in every manner. I love you.

Last but not least, I want to thank my family. First of all my twin brother Florian for being the best brother one could wish, taking care of me and being a real friend. I also especially want to thank my grandparents for their great concern about my work and my findings.

Thank you Steffi and Klaus for your constant support and love although I'm mainly not available. Thanks to Matthias, my godfather, for his great support and interest in my well being. Thank you Margot for your support. Last, but definitely not least, thanks to my roots, my Mom, my father, my stepfather, my brothers and sisters for being there for me when I need them.

Lastly, in memory of my father, Tillmann Kaltwasser, I wish you were here. I miss you!

Ehrenwörtliche Versicherung und Erklärung

Hiermit versichere ich ehrenwörtlich, dass ich die vorliegende Dissertation selbständig und ohne unerlaubte Hilfe angefertigt habe. Es wurden nur die in der Arbeit ausdrücklich benannten Quellen und Hilfsmittel benutzt. Wörtlich oder sinngemäß übernommenes Gedankengut habe ich als solches kenntlich gemacht.

Des Weiteren erkläre ich, dass ich nicht anderweitig ohne Erfolg versucht habe, eine Dissertation einzureichen oder mich der Doktorprüfung zu unterziehen. Die vorliegende Dissertation liegt weder ganz noch in wesentlichen Teilen einer anderen Prüfungskommission vor.

München, den 03.05.2011

.....
(Sebastian Kaltwasser)